

A Thesis Submitted for the Degree of PhD at the University of Warwick

Permanent WRAP URL:

<http://wrap.warwick.ac.uk/169413>

Copyright and reuse:

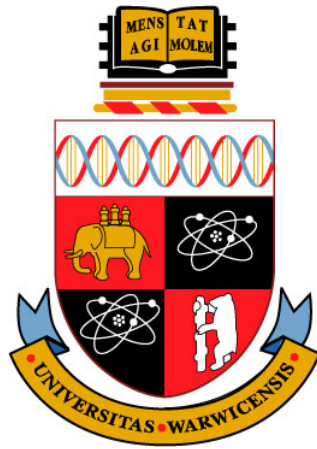
This thesis is made available online and is protected by original copyright.

Please scroll down to view the document itself.

Please refer to the repository record for this item for information to help you to cite it.

Our policy information is available from the repository home page.

For more information, please contact the WRAP Team at: wrap@warwick.ac.uk



Mathematically modelling the deformation of frictional elastic half-spaces in contact with a rolling rigid cylinder

Hanson Bharth¹

Supervisor: Dr. Edward James Brambley^{1,2}

¹ Mathematics Institute

² Warwick Manufacturing Group

University of Warwick

June 13, 2022

Abstract

Keywords: Contact mechanics, elasticity, Wiener–Hopf, spectral methods

In this thesis we derive an analytical model of the deformation of an elastic half-space caused by a cylindrical roller. The roller is considered rigid, and is forced into the half-space and rolls across its surface, with contact modelled by Coulomb friction. In general, portions of the surface of the roller in contact with the half-space may slip across the surface of the half-space, or may stick to it. In this thesis, we consider the contact surface to have a central sticking region as well as a simplifying regime where the entire contact surface is fully slipping. This results in two mixed boundary value problems, which are formulated into a 4×4 matrix Wiener–Hopf problem for the stick-slip regime and a 2×2 matrix Wiener–Hopf problem for the full-slip regime. The exponential factors in the Wiener–Hopf matrix allows a solution by following the iterative method of [Priddin, Kisil, and Ayton](#) (*Phil. Trans. Roy. Soc. A* 378, p. 20190241, 2020) which is implemented numerically by computing Cauchy transforms using a spectral method following [Slevinsky and Olver](#) (*J. Comput. Phys.* 332, pp. 290–315, 2017). The limits of the contact region and stick-slip transitions are located a posteriori by applying a free-boundary method based on the secant method. The solution is illustrated with several examples, and the frictional regimes are analysed.

Acknowledgements

I would like to thank my supervisor Dr. E. J. Brambley for his guidance and friendship throughout my PhD studies. His enthusiasm, experience and patience has made this an enriching and rewarding endeavour. He has provided the mentorship to facilitate my growth as a mathematician and scientist. I would also like to thank Dr. M. J. Priddin, Dr. A. Kisil and Dr. D. O’Kiely for their helpful discussions and advice.

I am extremely grateful to my family, who have provided unconditional support and made selfless sacrifices to help me overcome adversities not just during my PhD but throughout my life. I am also appreciative of my friends, but in particular to *all* of those in “MASDOC House”. Finally, I would like to give thanks to MASDOC, and the University of Warwick for supporting me throughout the PhD.

Declaration

The following constitutes my own work and any work resulting from collaboration is listed below and stated explicitly in the text. This work, nor any part, is substantially the same as any work I have submitted, or is being concurrently submitted, for a degree or diploma or other qualification at the University of Warwick or any other University or similar institution.

The derivation of the governing equations in chapter 2 and the analysis in the full-slip regime in chapter 4 is based on joint work with Dr. E. J. Brambley, due to be submitted for publication.

Contents

Abstract	ii
Acknowledgements	iii
Declaration	iv
List of Figures	ix
1 Introduction	1
1.1 Background	1
1.1.1 Metal forming	3
1.2 Contact mechanics	7
1.3 Thesis outline	9
2 The governing equations	11
2.1 Introduction	11
2.2 Derivation of the boundary conditions	13
2.2.1 Contact boundary condition	13
2.2.2 Stick boundary condition	14

2.2.3	Slip boundary condition	14
2.2.4	Stress-free boundary condition	16
2.3	Linearisation of the governing equations	16
2.3.1	Linearised boundary conditions	18
2.3.2	Full-slip	19
2.3.3	Full-stick	20
2.3.4	Stick-slip	20
2.4	General solution	21
3	The Wiener–Hopf technique	25
3.1	Introduction	25
3.2	Scalar Wiener–Hopf technique	28
3.2.1	Half-range transforms	38
3.2.2	Wiener–Hopf splittings	39
3.3	Matrix Wiener–Hopf technique	41
3.3.1	Iterative method	43
4	Rolling contact in the full-slip regime	48
4.1	Introduction	48
4.2	Mathematical formulation	51
4.2.1	Boundary conditions	52

4.2.2	General solution	53
4.3	Constructing the matrix Wiener–Hopf equation	54
4.3.1	Transformation of the boundary conditions	55
4.3.2	Assembling the matrix Wiener–Hopf equation	57
4.4	Application of the iterative method	59
4.4.1	Wiener–Hopf splittings	63
4.5	Free-boundary problem	70
4.5.1	Example	73
4.5.2	Convergence	75
4.6	Results	77
4.6.1	Parameter study	81
4.6.2	Von Mises yield criterion	88
4.7	Conclusion	89
5	Rolling contact in the stick-slip regime	91
5.1	Introduction	91
5.2	Model formulation	94
5.2.1	Boundary conditions	94
5.2.2	General solution	97
5.3	Constructing the matrix Wiener–Hopf equation	97
5.3.1	Transformation of the boundary conditions	98

5.3.2	Assembling the matrix Wiener–Hopf equation	100
5.4	Application of the iterative method	104
5.4.1	Wiener–Hopf splittings	109
5.5	Free-boundary problem	111
5.5.1	Large k limit	113
5.6	Results	115
5.6.1	Parameters	116
5.6.2	Stick-slip configuration	116
5.6.3	Discussion	122
5.7	Conclusion	123
6	Outlook	127
6.1	Small omega limit	129
6.2	Full-stick	129
6.3	General framework for rolling problems	130
6.4	Plasticity	130
6.5	Closing remarks	131
A	Some useful definitions and theorems	132
B	Matrix Wiener–Hopf for the full-stick regime	134
B.1	Boundary conditions	135

B.2	Matrix Wiener–Hopf equation	136
C	Matrix Wiener–Hopf for two rollers in the full-slip regime	138
C.1	Boundary conditions	138
C.2	Transformation of the boundary conditions	139
C.3	Matrix Wiener–Hopf equation	140
	Bibliography	142

List of Figures

1.1.1	Historic records of atmospheric CO ₂ levels.	2
1.1.2	The development of the flexible asymmetric metal sheet spinning [71].	5
1.1.3	A schematic of three rollers deforming a metal sheet.	6
1.1.4	A schematic of a roller deforming an elastic half-space.	6
2.1.1	A schematic of a rigid cylinder rolling along an elastic half-space.	12
3.2.1	A schematic of a semi-infinite punch (shaded) sliding along an elastic half-space.	28
3.2.2	A diagram of the boundary conditions and their domains for a semi-infinite punch sliding along an elastic half-space.	29
3.2.3	A diagram of the complex k -plane with the upper half-plane, lower half-plane and strip shown.	31
3.2.4	Plots of the solution to the toy problem for Metal parameter values from table 4.1.	37
4.2.1	A schematic of a cylinder rolling along an elastic half-space.	52

4.2.2	A diagram of the full-slip boundary conditions on the half-space.	53
4.3.1	A diagram of the rearranged full-slip boundary conditions on the half-space.	55
4.4.1	A figure of the phase-portrait for $K(k)$ with Metal parameters 4.1 and $\omega = -5i$	60
4.4.2	Plots of the exact error ($\ f(z) - f_+(z)\ _2$) of numerical methods to compute the upper decomposition of the function $f(z) = \frac{1}{(z-8.5-8.5i)\sqrt{z+10i}}$. The figures show the exact error with $z = ri$ in the interval $[0, 20]$ for 500 equidistant points.	69
4.5.1	Plots of the solution and asymptotic behaviour for the Metal parameter values from table 4.1 and backwards slip. The contact points are determined by the continuity of $\tau(x, 0)$, and are found to be $-1.636, 1.4462$	72
4.5.2	Plots of the solution and asymptotic behaviour for Metal parameter values from table 4.1 and backwards slip. The contact points are determined by the continuity of $v(x, 0)$, and are found to be $-1.4395, 1.4386$	73
4.5.3	Plots of the example contact problem with the inversion methods of equations 4.19 and 4.20.	75
4.5.4	A plot of the the error at each iteration for applying the minimisation algorithm to locate the contact points based on the continuity of $\tau_{yy}(\chi^j, 0)$, with Metal parameters taken from table 4.1.	77
4.6.1	Plots of the solution for Metal values from table 4.1 with backwards slip and the contact points found to be $-0.82514, 0.85749$	80

4.6.2 Plots of the solution for Alternative values from table 4.1 with forwards slip and the contact points found to be -0.88374 , 0.87925	82
4.6.3 Plots of the solution for Metal values from table 4.1 with forwards slip and the contact points found to be -0.77637 , 0.92200	84
4.6.4 Plots of the solution for Metal values from table 4.1 with backwards slip and the contact points found to be -0.82514 , 0.85749	84
4.6.5 The number of spectral coefficients required to approximate $K(k)$ to machine precision for $\omega = -2^{-n}i$ with Metal parameters in table 4.1.	86
4.6.6 Contour plots of $\tau_{yy}(x, y)$ under the Metal parameter values from table 4.1 and forward slip with increasing ω	87
4.6.7 Contour plots of $v(x, 0)$ under the Metal parameter values from table 4.1 and forward slip with decreasing ω	88
4.6.8 Contour plots of the magnitude of the Von Mises yield criterion in both directions of slip for the Metal parameter values 4.1.	89
5.2.1 A schematic of a cylinder rolling along an elastic half-space.	95
5.2.2 A diagram of the rearranged stick-slip boundary conditions on the surface of the half-space.	96
5.5.1 A plot of the error for the free-boundary method at each iteration until the solution has converged. The parameter values are those in table 5.1.	113
5.6.1 Plots of the solution for the forward-stick-forward configuration.	118

5.6.2 Plots of the solution for the forward-stick-backward configuration.	119
5.6.3 Plots of the solution for the backward-stick-forward configuration.	120
5.6.4 Plots of the solution for the backward-stick-backward configuration.	121
5.6.5 A plot of the error for the free-boundary method at each iteration until the solution has converged. The parameter values are those in table 5.1, with $\omega = -0.5i$	123
5.6.6 Plots of the solution with $\omega = -0.5i$ and the backward-stick-backward configuration.	124
5.6.7 Plots of the solution of the small ω case with a higher spectral resolution.	125
B.1.1A diagram showing the full-stick boundary conditions and the regions where they hold.	135

Chapter 1

Introduction

1.1 Background

The amount of atmospheric CO₂ has increased from 277.2 parts per million (ppm) in 1763 [64] to 415.86 ppm on the 16th November 2021 [31], with the Industrial Revolution (1760s) coinciding as a turning point in the atmospheric CO₂ levels trend, as seen in figure 1.1.1. Human activities such as burning fossil fuels and deforestation are the drivers of the post-industrial trend, with global efforts currently being implemented to prevent atmospheric CO₂ levels causing an accelerated impact on the climate and the environment. In this section we explain the impact that increasing atmospheric CO₂ levels have on the climate and how a strategy to mitigate its impact provides the inspiration for this thesis.

In the absence of an atmosphere, the electromagnetic radiation that the Earth receives from the Sun alone would lead to a surface temperature below the freezing point of water [69]. Given that water exists in all of its states on Earth, the presence of an atmosphere must exhibit a warming effect on the Earth. This warming effect is known as the greenhouse effect and was first proposed by the Mathematician Joseph Fourier [36]. The Earth receives

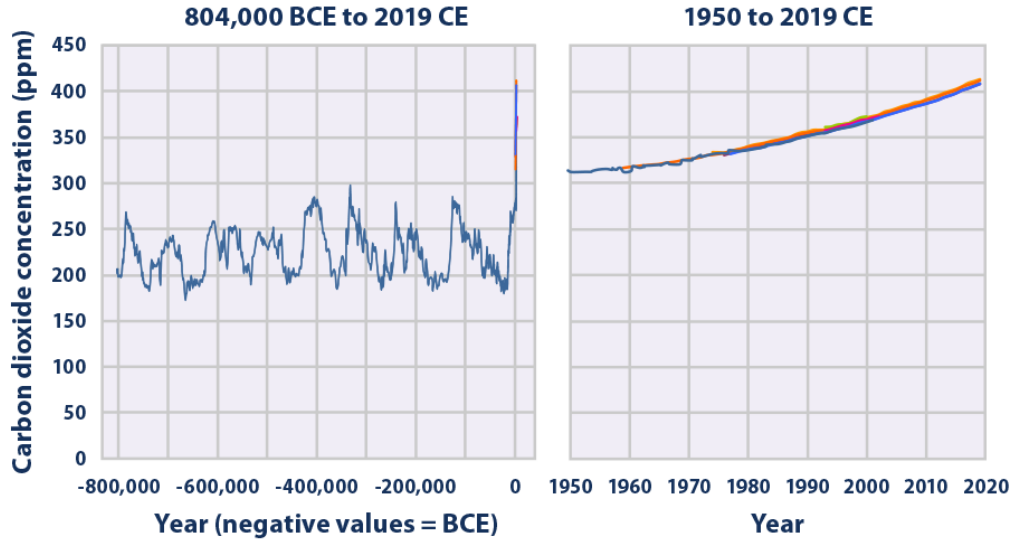


Figure 1.1.1: Historic records of atmospheric CO₂ levels.

Each colour on both figures represents a different data set, with eight different data sets shown. Source by: EPA [34]

radiation from the Sun in the ultraviolet-visible range and reflects infrared radiation back due to the different surface temperatures of the two bodies (Wiens displacement law page 197 of [98]). Greenhouse gases are gases which absorb and radiate infrared radiation in all directions. The infrared radiation that the Earth reflects towards space is therefore radiated in all directions by the greenhouse gases, with some of the radiation remaining within the atmosphere and warming the Earth's surface. Thus, the greenhouse gases cause the greenhouse effect. The most notable greenhouse gases are water vapour and CO₂, so the increasing atmospheric CO₂ levels increases the greenhouse effect the Earth experiences. To mitigate the negative impacts of raising atmospheric CO₂ levels the 2015 Paris Agreement has led to a global agreement to reach a 50% reduction in emissions by 2030 and net-zero by 2050 [84].

Humans contribute to the rise of atmospheric CO₂ levels through burning fossil fuels and deforestation. In the global bid to reduce atmospheric CO₂ levels most attention is given to finding alternative fuel sources, however, progress

may also be made by reducing the amount of energy required to produce goods and provide services. The metal industry is the world's largest industrial source of CO₂ emissions at 25% of total industrial emissions (Serrenho et al. [87]). Allwood et al. [9] estimate that fuel efficiencies alone would not be enough for the UK metal industry to achieve its 2030 emissions target so material efficiency and demand reduction are necessary, this estimate was confirmed by Gutowski et al. [41]. In particular, due to the high costs of energy, the steel industry is highly energy efficient and there are marginal gains to be made on this front. However, significant gains may be made by efficient use of material, as a quarter of steel used in the production process is scrapped, see page 54 of [8].

1.1.1 Metal forming

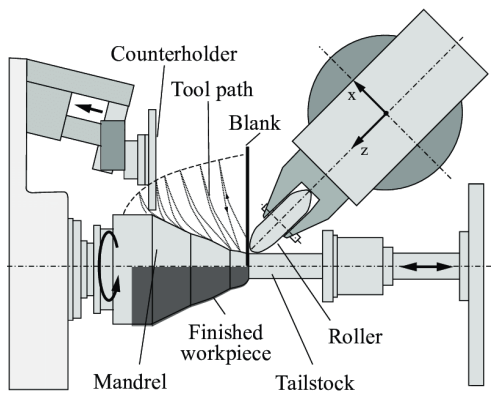
The **Use Less Group** headed by Professor Julian Allwood at the University of Cambridge have developed new technologies with the intention of reducing yield loss in metal production processes. The Use Less Group have developed two new technologies to aid in material efficiency for metal forming, flexible ring rolling [24] and flexible metal sheet spinning [71]. A considerable amount of scrapped metal comes from the manipulation of metal sheets, which are rolled into a uniform way and then cut and trimmed to product specification, and our work focuses on aiding the efficiency of this process.

Traditional metal sheet spinning uses a mandrel and a roller (figure 1.1.2a), the roller applies a force on the metal sheet until it deforms to the shape of the mandrel. This means that a specific mandrel is required for every product and that metal sheets may not be designed flexibly. Music and Allwood [71] found that the mandrel only makes contact with the metal sheet in three locations and this motivated them to design the flexible asymmetric spinning machine [71] which replaced the mandrel with three support rollers, see figure 1.1.2. Industrial use of the flexible asymmetric spinning machine is hindered by failures such as wrinkling and foldback [79] and preventing these failures

may be possible with faster and more accurate predictions of the behaviour of the sheet through new analytical and numerical models. However, at present the models available are limited in their predictive capacity through computational costs and accuracy [72]. This provides the motivation for the mathematical study of the mechanics behind metal sheet spinning.

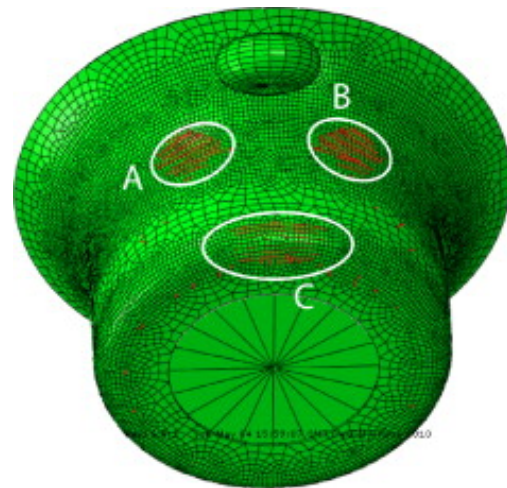
Modelling a metal sheet subject to three rollers is depicted in the schematic 1.1.3, which shows three cylinders deforming a metal sheet. The deformation of the entire system may be considered from the summation of each roller, so to understand the deformation more deeply we pay attention to only one of these rollers. In particular, we consider the setting in schematic 1.1.4 which depicts a single roller along an elastic half-space. We consider a purely elastic media as low forces cause the metal sheet to experience very small amounts of plastic deformation and largely elastic deformation. We note that one may recover the system in 1.1.3 by superimposing a neighbouring roller or by imposing a symmetry boundary condition along the dotted centre line.

The understanding of elastic deformation is a necessary basic step towards the further understanding and modelling of elastoplastic deformations, common in manufacturing processes. As an example, strip rolling is a metal forming processes involving a pair of rollers squeezing and thinning a sheet of metal. Provided the sheet is sufficiently wide, the process can be modelled as two-dimensional (plane strain) and steady state, and purely plastic models exist that agree well with finite element simulations [22, 68]. However, neglecting elasticity precludes the modelling of important effects such as spring-back and curvature; indeed, the direction a metal sheet curves after passing between two asymmetric rollers is currently an unsolved problem, with no agreement between experimental, computational and mathematical studies [67]. This motivates the research undertaken in this thesis, investigating the vastly simplified situation consisting of a single roller rolling along a purely-elastic half-space, from which it is hoped understanding and further modelling can be developed that will contribute to future studies of elastoplastic deformation.



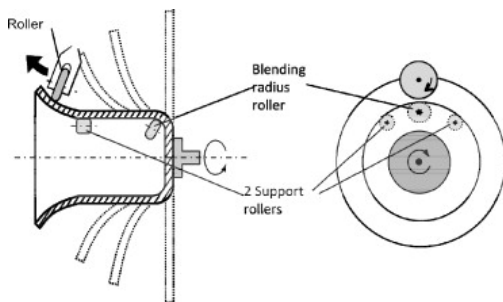
(a) A schematic of traditional metal sheet spinning.

Source by: Rentsch et al. [82]



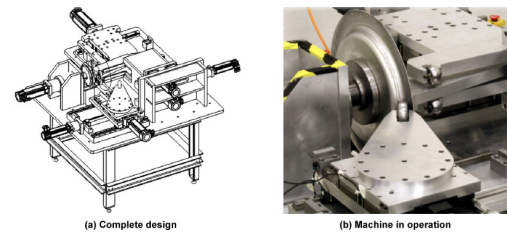
(b) The location of the contact pressure between the metal sheet and mandrel.

Source by: Music and Allwood [71]



(c) A schematic of flexible asymmetric metal sheet spinning.

Source by: Music and Allwood [71]



(d) The flexible asymmetric metal sheet spinning machine.

Source by: Music and Allwood [71]

Figure 1.1.2: The development of the flexible asymmetric metal sheet spinning [71].

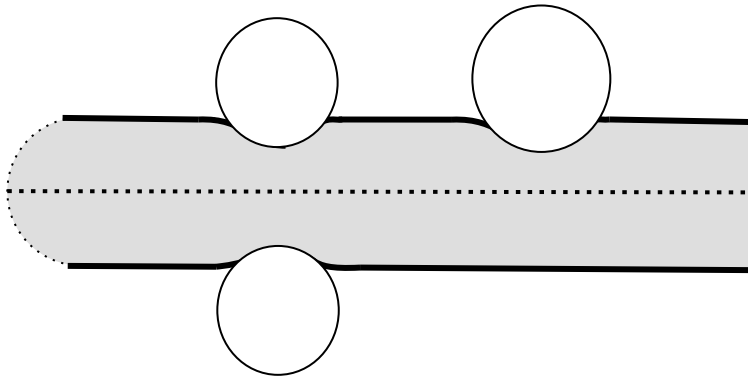


Figure 1.1.3: A schematic of three rollers deforming a metal sheet.

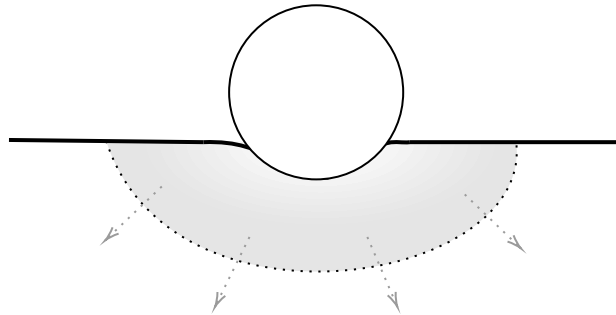


Figure 1.1.4: A schematic of a roller deforming an elastic half-space.

1.2 Contact mechanics

We now discuss some results in static contact problems before the additional consideration of rolling contact. The static model of an elastic half-space deformed by a rigid punch has been of interest for a substantial time. Hertz [44] founded the field of contact mechanics at the end of the 19th century by considering the elastic deformation due to a frictionless rigid punch. Friction was considered in a static setting by Cattaneo [21] and Mindlin [66] who used an inner stick region and outer slip regions. Spence [90] presented an approach for parabolic punches into an elastic half-space with stick-slip friction. More recently, Zhupanska and Ulitko [102], Zhupanska [101] modelled the deformation of an elastic half-space due to a rigid cylindrical indenter. Our work seeks to expand on the ideas applied in Zhupanska and Ulitko [102] by applying the frictional model to an asymmetric rolling problem instead.

Zhupanska and Ulitko [102] developed a static contact problem modelling the deformation of an elastic half-space by a rigid cylindrical punch under friction. The punch was progressively loaded in accordance with Spence's self-similarity, which ensures that the ratio of the stick-slip zones remain constant while loading. However, due to the hysteretic nature of friction, it is likely that the solution found by Zhupanska and Ulitko [102] is not unique, as a cylinder pushed into an elastic half-space would produce a different deformation pattern from a cylinder pushed further into the elastic half-space before being partially retracted. We compensate by considering a rigid cylinder rolling along the surface of the elastic half-space, therefore the entire history of the process is specified into the model and so a unique steady state solution is to be expected. Zhupanska and Ulitko [102] considers a symmetric contact problem which restricts the solution space of their problem to a smaller class of frictional contact problems. Their approach made use of Papkovitch-Neuber potentials (see page 79 of [46]), a planar bipolar conformal map and the scalar Wiener-Hopf technique to find a solution. In particular, their use of the planar bipolar conformal map includes an obscure claim to

remove the singular behaviour at infinity which we could not verify. Thus, we propose an alternative contact problem, the deformation of an elastic half-space by a rigid cylindrical roller under friction. We assume that a sufficient amount of time has passed since the roller was initially pressed into the half-space for any initial behaviour to decay. Additionally, we consider the setting of possibly asymmetric contact and stick-slip zones. In the limit of zero rolling speed, our solution should reduce to a solution to the static problem considered by Zhupanska and Ulitko [102].

The behaviour of rolling contact has been explored much less thoroughly since the frictional resistance is smaller but importantly not negligible. Reynolds [83] produced an early experiment to study rolling contact and found that the contact region separates into stick and slip zones. Carter [20] and Fromm [37] both independently derived analytical models for two-dimensional rolling contact by assuming a pressure profile in the contact region, an approach known as Hertzian theory. Alternatively, a variational theory for rolling contact has been developed and implemented algorithmically by Kalker [52]. Summaries of these rolling problems and other classical results may be found in the two seminal books by Johnson [49] and Popov [80]. In recent years the analytical models for rolling has seen less development, with a focus to use numerical methods such as the boundary element method [5] or the finite element method [60]. To the best of the author's knowledge, an analytical solution of a cylinder rolling along an elastic half-space under a stick-slip model of friction has been unexplored.

There are many possible models of friction between surfaces in contact. Common models in metal forming include Coulomb friction, where the tangential force is proportional to the normal force, relative slip, where the tangential force is proportional to the slipping velocity, and "friction factor", where the tangential force is a specified constant. The Coulomb friction model is the simplest friction model that is also well established outside of metal forming, and it is the friction model used here. Under Coulomb friction, two surfaces in contact can be in one of two states: slipping, where the tangential force

T resists the slipping and is proportional to the normal force N , $T = \mu N$; and non-slipping, where $|T| < \mu N$ and the surfaces do not move with respect to one another. In general, for a rigid cylinder rolling along and indenting an elastic half-space, some of the contact surface may slip in one direction, some may slip in the other direction, and in between will be a region of no slip. This general situation would result in a 4×4 Wiener–Hopf problem owing to the four points where the boundary conditions on the elastic half-space change. Instead, if the cylinder is rotating sufficiently fast then the entire contact region will be slipping in a single direction, this results in a 2×2 Wiener–Hopf problem owing to the two points where the boundary conditions on the elastic half-space change, which is a considerable simplification. The matrix Wiener–Hopf problem considered in the 2×2 regime, while mathematically interesting in its own right, develops the mathematical tools for the more complicated 4×4 model of stick-slip rolling.

A brief overview of the literature is mentioned briefly here but an in-depth review of the literature is discussed in the introductions to chapters 3, 4 and 5.

1.3 Thesis outline

A detailed description of the physical problem to be solved together with its mathematical formulation is given in chapter 2, including the general solution for a convected elastic half-space in section 2.4. Chapter 3 presents a background to the Wiener–Hopf technique and an example of applying it to a scalar contact problem, finally we outline the matrix Wiener–Hopf technique applied to the two contact problems in chapters 4 and 5. Some useful definitions for the Wiener–Hopf technique and its numerical implementation is included in appendix A. Chapter 4 applies the matrix Wiener–Hopf technique to the limit of full-slip, the case where the angular velocity is much greater than the convection speed. Within chapter 4 is the development of a free-boundary method to locate the contact points. Chapter 5 applies the same

matrix Wiener–Hopf technique to the case of stick-slip friction, with some discussion on the complications which arise from the application of the free-boundary method. Finally, chapter 6 discusses some open problems which may follow on from this thesis, with two extensions outlined in appendices B and C.

Chapter 2

The governing equations

2.1 Introduction

We consider the situation shown schematically in figure 2.1.1.

A rigid cylinder of radius R is pushed into an elastic half-space $y < 0$ with a force \mathbf{F} , resulting in a maximum indentation of depth ϵ . The cylinder is rotated clockwise with a torque T , giving an angular velocity Ω , and the cylinder therefore translates in the positive x -direction across the half-space at a linear velocity V . We choose a frame of reference moving with the cylinder, such that the centre of the cylinder is located at $x = 0$ and $y = R - \epsilon$, with \mathbf{e}_x and \mathbf{e}_y unit vectors in the x - and y -directions respectively. We label material particles in the elastic half-space by the location $\hat{\mathbf{X}}$ which is their location at time $t = 0$ in the absence of the cylinder. In the absence of the cylinder and in the convected frame, such a material particle would be located at $\mathbf{X} = \hat{\mathbf{X}} - Vt\mathbf{e}_x$ at time t . With the cylinder present, the material particle has been displaced, and is instead located at $\mathbf{x} = \mathbf{X} + \mathbf{u}$, where $\mathbf{u} = (u, v)$ is the displacement in the elastic half-space.

We derive the nonlinear boundary conditions in the Eulerian configuration.

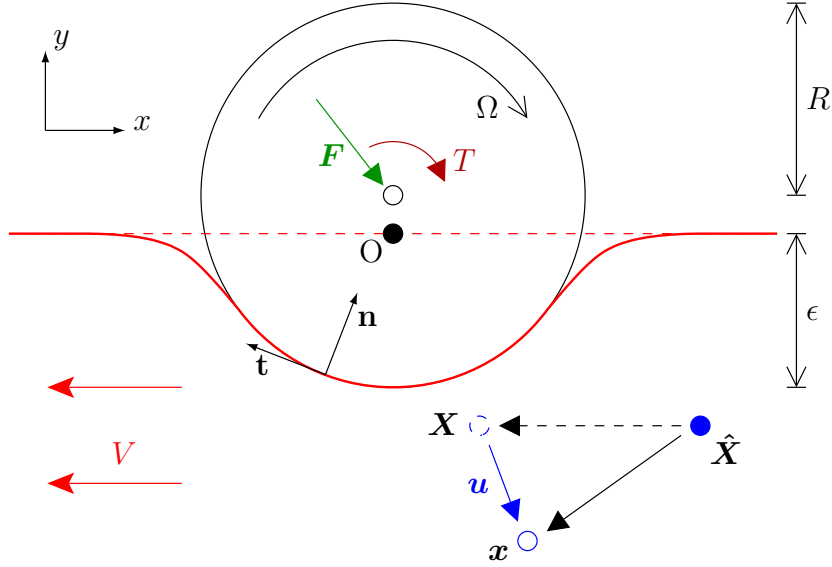


Figure 2.1.1: A schematic of a rigid cylinder rolling along an elastic half-space. The cylinder moves at a linear velocity V in the x -direction along the surface of the elastic half-space. The origin of the coordinate system (labelled O) is taken in a frame of reference moving with the cylinder, directly below the centre of the cylinder at the height of the undeformed elastic surface. The cylinder of radius R rolls about its centre axis with angular velocity Ω , and a force F and torque T are applied to the centre of the cylinder, causing the cylinder to be indented by ϵ into the elastic half-space. A material point at location \hat{X} at time $t = 0$ would have moved to location X at time t without the cylinder being present, but has instead moved to a location x due to the deformation caused by the cylinder, giving an elastic displacement $u = X - x$.

In the Eulerian configuration, a material particle is referred to using the deformed location \mathbf{x} , therefore the displacement $\mathbf{u}(\mathbf{x}, t)$ and the undeformed position $\mathbf{X}(\mathbf{x}, t)$ are both functions of \mathbf{x} and t . Thus the displacement in the Eulerian configuration is defined to be

$$\mathbf{u}(\mathbf{x}, t) = \mathbf{x} - \mathbf{X}(\mathbf{x}, t).$$

To calculate the elastic velocity, let $\hat{\mathbf{x}}(t, \hat{X})$ be the location of a material particle at time t whose undeformed location was \hat{X} at time $t = 0$. Thus,

$$\hat{\mathbf{x}}(t) = \mathbf{X}(\hat{\mathbf{x}}(t), t) + \mathbf{u}(\hat{\mathbf{x}}(t), t) = \hat{X} - Vte_x + \mathbf{u}(\hat{\mathbf{x}}(t), t).$$

Taking the time derivative with $\hat{\mathbf{X}}$ fixed, we find

$$\mathbf{v} = \left. \frac{\partial \hat{\mathbf{x}}}{\partial t} \right|_{\hat{\mathbf{X}}} = -V \mathbf{e}_x + \left. \frac{\partial \mathbf{u}}{\partial t} \right|_x + \mathbf{v} \cdot \left. \frac{\partial \mathbf{u}}{\partial \mathbf{x}} \right|_t. \quad (2.1)$$

which is an implicit equation for the material particle velocity $\mathbf{v}(\mathbf{x}, t)$.

Newton's law of motion, or equivalently conservation of momentum, gives the governing equations in the bulk of the material as

$$\rho \left(\frac{\partial \mathbf{v}}{\partial t} + \mathbf{v} \cdot \frac{\partial \mathbf{v}}{\partial \mathbf{x}} \right) = \nabla \cdot \boldsymbol{\tau}, \quad (2.2)$$

where $\boldsymbol{\tau}$ is the Cauchy stress tensor.

The surface of the elastic half-space is given by $y = \eta(x)$. Where the elastic half-space is in contact with the cylinder, for $-a \leq x \leq d$, the displacement of the elastic half-space is known, and the material either sticks to the cylinder or slips [12] depending on the frictional regime we are considering. Outside of the contact region, the surface is stress-free. We derive each of these boundary conditions separately.

2.2 Derivation of the boundary conditions

The derivation of the boundary conditions is non-standard; the derivation is carried out with respect to the deformed variable, \mathbf{x} , rather than the undeformed variable, \mathbf{X} . The deformed variable is considered as it is useful for deriving the stick boundary condition.

2.2.1 Contact boundary condition

The contact boundary condition comes from the physical condition that the elastic half-space cannot penetrate the rigid cylinder. This means that a

material particle on the surface of the elastic half-space (given by $Y = 0$), when in contact with the cylinder, must be deformed to lie on the surface of the cylinder. By writing $y = Y + v$, and noting that the cylinder centre is located at $(0, R - \epsilon)$, we deduce that

$$x^2 + (y - R + \epsilon)^2 = R^2 \quad \iff \quad -a < x < d \quad \text{and} \quad Y = 0. \quad (2.3)$$

The unknown limits of the contact region are labeled by the location of $-a, d$ and are to be found as part of the solution.

2.2.2 Stick boundary condition

The stick boundary condition comes from property that the elastic media is “stuck” to the cylinder and so the elastic surface and the cylinder have the same velocity here, $\mathbf{v}_c = \mathbf{v}_e$. Other names for this boundary condition may be the adhesion boundary condition or the no-slip boundary condition. Hence, the elastic velocity equation (2.1) becomes

$$\mathbf{v}_c = -V\mathbf{e}_x + \left. \frac{\partial \mathbf{u}}{\partial t} \right|_x + \mathbf{v}_c \cdot \left. \frac{\partial \mathbf{u}}{\partial \mathbf{x}} \right|_t, \quad (2.4)$$

which holds in the regions specified by the frictional regime we are considering.

2.2.3 Slip boundary condition

The “slip” boundary condition comes from the physical condition that the elastic medium is slipping past the rigid cylinder, and is chosen to satisfy the Coulomb law of dry friction, $(\boldsymbol{\tau} \cdot \mathbf{n}) \cdot \mathbf{t} = \pm \mu_0 (\boldsymbol{\tau} \cdot \mathbf{n}) \cdot \mathbf{n}$ [12], where $\boldsymbol{\tau}(\mathbf{x}, t)$ is the Cauchy stress tensor. The (non-unit) outward normal to the cylinder may be taken as $\mathbf{n} = (x, y + \epsilon - R)^T$, and the tangent vector to the cylinder may be taken as $\mathbf{t} = (y - R + \epsilon, -x)^T$. Explicitly, the Coulomb friction law

becomes

$$\begin{aligned} & \begin{pmatrix} x\tau_{xx} + (y + \epsilon - R)\tau_{xy} \\ x\tau_{xy} + (y + \epsilon - R)\tau_{yy} \end{pmatrix} \cdot \begin{pmatrix} y + R - \epsilon \\ -x \end{pmatrix} \\ &= \pm\mu_0 \begin{pmatrix} x\tau_{xx} + (y + \epsilon - R)\tau_{xy} \\ x\tau_{xy} + (y + \epsilon - R)\tau_{yy} \end{pmatrix} \cdot \begin{pmatrix} x \\ y + R - \epsilon \end{pmatrix}, \end{aligned}$$

then by expanding and rearranging we find

$$\begin{aligned} & \frac{x}{(y - R + \epsilon)}(\tau_{xx} - \tau_{yy}) + \left(1 - \left(\frac{x}{y - R + \epsilon}\right)^2\right)\tau_{xy} \\ &= \pm\mu_0 \left[\left(\frac{x}{y - R + \epsilon}\right)^2 \tau_{xx} + \frac{2x}{y - R + \epsilon} \tau_{xy} + \tau_{yy} \right]. \quad (2.5) \end{aligned}$$

The slip boundary conditions hold in regions specified by the frictional regime we are considering. The convention for slip directions are $\pm = +$ if the cylinder is exerting a friction force on the elastic half-space in the negative x -direction, meaning that the angular velocity Ω is sufficiently large and positive (a wheel-spin type condition), whereas $\pm = -$ if Ω is sufficiently negative (a locked-wheel braking type condition).

To determine the direction of slip, the velocity of the surface of the cylinder in the clockwise direction, $v_c = R\Omega$, should be compared to the velocity of the elastic material in the same direction, $v_e = \mathbf{v} \cdot \mathbf{t}/|\mathbf{t}|$. If $v_c > v_e$ then $\pm = +$, while if $v_c < v_e$ then $\pm = -$. Note that v_e is a function of the location x . In chapter 4 we assume that one of these inequalities holds throughout the contact region; in other words, there are no regions of sticking, only slip. Alternatively, in chapter 5 one of these inequalities hold in the contact region, except where sticking occurs and $v_c = v_e$.

2.2.4 Stress-free boundary condition

The final boundary conditions are outside of the contact region, $-\infty < x < -a$ and $d < x < \infty$. In these regions the elastic surface is free of traction, and so $\boldsymbol{\tau} \cdot \mathbf{n} = \mathbf{0}$. Here the outward normal is taken to the deformed half-space surface $y = \eta(x)$, so that $\mathbf{n} = (-d\eta/dx, 1)$. This gives the boundary conditions

$$-\frac{d\eta}{dx}\tau_{xx} + \tau_{xy} = -\frac{d\eta}{dx}\tau_{xy} + \tau_{yy} = 0 \quad \text{at } y = \eta(x). \quad (2.6)$$

2.3 Linearisation of the governing equations

We linearise the boundary conditions by first introducing nondimensional $O(1)$ quantities, denoted by a star. We set

$$\mathbf{u} = \epsilon \mathbf{u}^*, \quad \mathbf{x} = \sqrt{\epsilon R} \mathbf{x}^*, \quad t = \frac{\sqrt{\epsilon R}}{V} t^*, \quad \mathbf{v} = V \mathbf{v}^*.$$

The scaling results from assuming that displacements \mathbf{u} are of the order of the maximum vertical displacement of the elastic medium (ϵ) due to the roller. Similarly, we assume lengthscales for the position vector \mathbf{x} to be dictated by the size of the contact region, bounded by $x^2 + (R - \epsilon)^2 = R^2$; expanding for small ϵ/R , this results in the contact region being bounded approximately by $|x^*| < \sqrt{2}$. The relevant timescale is taken as the time taken for the undeformed material to convect past the contact region, giving $t = t^* \sqrt{\epsilon R}/V$. The velocity of the elastic solid may similarly be written as $\mathbf{v} = V \mathbf{v}^*$ in terms of the convection speed of the cylinder.

We now proceed to linearise the governing equations, under the assumption that the dimensionless parameter $\epsilon/R \ll 1$. Under these assumptions, the

velocity equation (2.1) becomes

$$\mathbf{v}^* = -\mathbf{e}_x + \sqrt{\frac{\epsilon}{R}} \left(\frac{\partial \mathbf{u}^*}{\partial t^*} + \mathbf{v}^* \cdot \frac{\partial \mathbf{u}^*}{\partial \mathbf{x}^*} \right) = -\mathbf{e}_x + \sqrt{\frac{\epsilon}{R}} \left(\frac{\partial \mathbf{u}^*}{\partial t^*} - \frac{\partial \mathbf{u}^*}{\partial x^*} \right) + O\left(\frac{\epsilon}{R}\right). \quad (2.7)$$

Similarly, the strain tensor ε becomes

$$\begin{aligned} \varepsilon &= \frac{1}{2}(\nabla \mathbf{u} + \nabla \mathbf{u}^T) + O(|\mathbf{u}|^2) \\ &= \sqrt{\frac{\epsilon}{R}} \begin{pmatrix} \frac{\partial u^*}{\partial x^*} & \frac{1}{2} \left(\frac{\partial u^*}{\partial y^*} + \frac{\partial v^*}{\partial x^*} \right) \\ \frac{1}{2} \left(\frac{\partial u^*}{\partial y^*} + \frac{\partial v^*}{\partial x^*} \right) & \frac{\partial v^*}{\partial y^*} \end{pmatrix} + O\left(\frac{\epsilon}{R}\right), \end{aligned}$$

and hence strains are small and we may assume linear elasticity. Using the isotropic linear stress–strain relationship, the Cauchy stress tensor becomes

$$\begin{aligned} \tau &= \lambda \sqrt{\frac{\epsilon}{R}} \tau^* = \lambda \sqrt{\frac{\epsilon}{R}} \begin{pmatrix} \tau_{xx}^* & \tau_{xy}^* & 0 \\ \tau_{xy}^* & \tau_{yy}^* & 0 \\ 0 & 0 & \tau_{zz}^* \end{pmatrix} \\ &= \lambda \sqrt{\frac{\epsilon}{R}} \begin{pmatrix} (1 + 2\mu/\lambda) \frac{\partial u^*}{\partial x^*} + \frac{\partial v^*}{\partial y^*} & \frac{\mu}{\lambda} \left(\frac{\partial u^*}{\partial y^*} + \frac{\partial v^*}{\partial x^*} \right) & 0 \\ \frac{\mu}{\lambda} \left(\frac{\partial u^*}{\partial y^*} + \frac{\partial v^*}{\partial x^*} \right) & \frac{\partial u^*}{\partial x^*} + (1 + 2\mu/\lambda) \frac{\partial v^*}{\partial y^*} & 0 \\ 0 & 0 & \left(\frac{\partial u^*}{\partial x^*} + \frac{\partial v^*}{\partial y^*} \right) \end{pmatrix}. \end{aligned} \quad (2.8)$$

Substituting this into the momentum equation (2.2) simplifies to give

$$\frac{V^2 \rho}{\lambda} \left(\frac{\partial}{\partial t^*} - \frac{\partial}{\partial x^*} \right)^2 \mathbf{u}^* = \nabla^* \cdot \tau^* + O\left(\sqrt{\frac{\epsilon}{R}}\right),$$

where λ is Lamé's first parameter, μ is the shear modulus, and ρ is the material density. Hence, to leading order, the governing equations are the usual

equations of linear elasticity, only with an extra advection term included:

$$\begin{aligned} \frac{V^2 \rho}{\lambda} \left(\frac{\partial}{\partial t^*} - \frac{\partial}{\partial x^*} \right)^2 u^* &= \left(1 + \frac{2\mu}{\lambda} \right) \frac{\partial^2 u^*}{\partial x^{*2}} + \left(1 + \frac{\mu}{\lambda} \right) \frac{\partial^2 v^*}{\partial x^* \partial y^*} + \frac{\mu}{\lambda} \frac{\partial^2 u^*}{\partial y^{*2}}, \\ \frac{V^2 \rho}{\lambda} \left(\frac{\partial}{\partial t^*} - \frac{\partial}{\partial x^*} \right)^2 v^* &= \left(1 + \frac{2\mu}{\lambda} \right) \frac{\partial^2 v^*}{\partial y^{*2}} + \left(1 + \frac{\mu}{\lambda} \right) \frac{\partial^2 u^*}{\partial x^* \partial y^*} + \frac{\mu}{\lambda} \frac{\partial^2 v^*}{\partial x^{*2}}. \end{aligned} \quad (2.9)$$

It remains to apply the linearisation to the boundary conditions.

2.3.1 Linearised boundary conditions

Using the scaling above, the contact boundary condition (2.3) with $y = Y + v$ may be linearised directly. Noting that $Y = 0$ on the surface, this leads to

$$(\sqrt{\epsilon R} x^*)^2 + (R - \epsilon(v^* + 1))^2 = R^2 \quad \Rightarrow \quad v^* = \frac{1}{2} x^{*2} - 1 + O\left(\frac{\epsilon}{R}\right),$$

to be applied for $-a^* < x^* < d^*$.

We recall the nonlinear stick boundary condition (2.4) and linearise in line with (2.7) to give

$$\mathbf{v}_c^* = -\mathbf{e}_x + \sqrt{\frac{\epsilon}{R}} \left(\frac{\partial \mathbf{u}^*}{\partial t^*} \Big|_x - \frac{\partial \mathbf{u}^*}{\partial \mathbf{x}^*} \Big|_t \right) + O\left(\frac{\epsilon}{R}\right). \quad (2.10)$$

We further assume that when stick occurs, the speed of the roller is close to its convection speed

$$v_c^* = \frac{\Omega R}{V} = 1 - W \sqrt{\frac{\epsilon}{R}} + O\left(\frac{\epsilon}{R}\right), \quad (2.11)$$

with W parametrising the speed of the roller. Then by taking the dot product of (2.10) with \mathbf{t}^1 and substituting in (2.11) we derive the stick boundary

¹The vertical displacement of the free surface $y = \eta(x)$ is of the order of the elastic displacement, and we therefore rescale so that $\eta(x) = \epsilon \eta^*(x^*)$ with η^* assumed $O(1)$, giving $y^* = \sqrt{\epsilon/R} \eta^*(x^*) \ll 1$. Using this scaling makes the tangential vector in the contact region become $\mathbf{t} = (\frac{\epsilon}{R}(1 + v^*) - 1, -\sqrt{\frac{\epsilon}{R}} x^*)$.

condition

$$\left. \frac{\partial u^*}{\partial t^*} \right|_x - \left. \frac{\partial u^*}{\partial x^*} \right|_t = W + O\left(\sqrt{\frac{\epsilon}{R}}\right) \quad \text{for } y^* = 0.$$

Expanding the slip (2.5) and free (2.6) boundary conditions as a Taylor's series about $y^* = 0$ then gives

$$\begin{aligned} \tau_{xy} \mp \mu_0 \tau_{yy} &= 0 + O\left(\sqrt{\frac{\epsilon}{R}}\right) & \text{for } y^* = 0, & \quad (2.12a) \\ \tau_{xy} = \tau_{yy} &= 0 + O\left(\sqrt{\frac{\epsilon}{R}}\right) & \text{for } y^* = 0. & \end{aligned}$$

Note that the rescaled velocity of the roller is $v_c^* = R\Omega/V$, and that the rescaled velocity of the elastic material in the same direction is $v_e^* = 1 + O(\sqrt{\epsilon/R})$, and so in the friction boundary condition (2.12a) we have $\pm = \text{sgn}(R\Omega/V - 1)$.

2.3.2 Full-slip

The linearised differential equations to solve are therefore

$$\begin{aligned} \frac{V^2 \rho}{\lambda} \left(\frac{\partial}{\partial t} - \frac{\partial}{\partial x} \right)^2 u &= (1 + 2\mu/\lambda) \frac{\partial^2 u}{\partial x^2} + (1 + \mu/\lambda) \frac{\partial^2 v}{\partial x \partial y} + \frac{\mu}{\lambda} \frac{\partial^2 u}{\partial y^2}, \\ \frac{V^2 \rho}{\lambda} \left(\frac{\partial}{\partial t} - \frac{\partial}{\partial x} \right)^2 v &= (1 + 2\mu/\lambda) \frac{\partial^2 v}{\partial y^2} + (1 + \mu/\lambda) \frac{\partial^2 u}{\partial x \partial y} + \frac{\mu}{\lambda} \frac{\partial^2 v}{\partial x^2}, \end{aligned}$$

to be solved for $-\infty < x < \infty$ and $y < 0$, subject to boundary conditions along $y = 0$. These boundary conditions are given by

$$\begin{aligned} \text{Contact:} & \quad v(x, 0) = \frac{x^2}{2} - 1, & \text{for } -a \leq x \leq d, \\ \text{Slip:} & \quad \tau_{xy} \mp \mu_0 \tau_{yy}(x, 0) = 0, & \text{for } -a \leq x \leq d, \\ \text{Stress-free:} & \quad \tau_{xy}(x, 0) = \tau_{yy}(x, 0) = 0, & \text{for } x < -a, d < x. \end{aligned}$$

2.3.3 Full-stick

The linearised differential equations to solve are therefore

$$\begin{aligned}\frac{V^2\rho}{\lambda}\left(\frac{\partial}{\partial t}-\frac{\partial}{\partial x}\right)^2u &= (1+2\mu/\lambda)\frac{\partial^2u}{\partial x^2}+(1+\mu/\lambda)\frac{\partial^2v}{\partial x\partial y}+\frac{\mu}{\lambda}\frac{\partial^2u}{\partial y^2}, \\ \frac{V^2\rho}{\lambda}\left(\frac{\partial}{\partial t}-\frac{\partial}{\partial x}\right)^2v &= (1+2\mu/\lambda)\frac{\partial^2v}{\partial y^2}+(1+\mu/\lambda)\frac{\partial^2u}{\partial x\partial y}+\frac{\mu}{\lambda}\frac{\partial^2v}{\partial x^2},\end{aligned}$$

to be solved for $-\infty < x < \infty$ and $y < 0$, subject to boundary conditions along $y = 0$. These boundary conditions are given by

$$\begin{aligned}\text{Contact:} \quad v(x, 0) &= \frac{x^2}{2} - 1, & \text{for } -a \leq x \leq d, \\ \text{Stick:} \quad \frac{Du}{Dt}(x, 0) &= W, & \text{for } -a \leq x \leq d, \\ \text{Stress-free:} \quad \tau_{xy}(x, 0) = \tau_{yy}(x, 0) &= 0, & \text{for } x < -a \text{ \& } d < x.\end{aligned}$$

2.3.4 Stick-slip

The linearised differential equations to solve are therefore

$$\begin{aligned}\frac{V^2\rho}{\lambda}\left(\frac{\partial}{\partial t}-\frac{\partial}{\partial x}\right)^2u &= (1+2\mu/\lambda)\frac{\partial^2u}{\partial x^2}+(1+\mu/\lambda)\frac{\partial^2v}{\partial x\partial y}+\frac{\mu}{\lambda}\frac{\partial^2u}{\partial y^2}, \\ \frac{V^2\rho}{\lambda}\left(\frac{\partial}{\partial t}-\frac{\partial}{\partial x}\right)^2v &= (1+2\mu/\lambda)\frac{\partial^2v}{\partial y^2}+(1+\mu/\lambda)\frac{\partial^2u}{\partial x\partial y}+\frac{\mu}{\lambda}\frac{\partial^2v}{\partial x^2},\end{aligned}$$

to be solved for $-\infty < x < \infty$ and $y < 0$, subject to boundary conditions along $y = 0$. These boundary conditions are given by

$$\begin{aligned}
 \text{Contact:} \quad & v(x, 0) = \frac{x^2}{2} - 1, & \text{for } -a \leq x \leq d, \\
 \text{Stick:} \quad & \frac{Du}{Dt}(x, 0) = W, & \text{for } -b \leq x \leq c, \\
 \text{Slip:} \quad & \tau_{xy} \mp \mu_0 \tau_{yy}(x, 0) = 0, & \text{for } x < -b \ \& \ c < x, \\
 \text{Stress-free:} \quad & \tau_{yy}(x, 0) = 0, & \text{for } x < -a \ \& \ d < x.
 \end{aligned}$$

The unknown transitions of the stick-slip zones are labeled by the location of $-b, d$ and are to be found as part of the solution also.

For clarity of notation we drop $*$ from the nondimensional quantities.

The full-slip and stick-slip problems may be found in chapters 4 and 5. Whereas the full-stick and a two roller problem may be seen in appendix B and C.

2.4 General solution

As the differential equation is the same throughout we derive the general solution here and find the specific solution by considering the boundary conditions in the frictional regime we consider. For the governing equations, we have the standard linear elasticity equations and an additional advection term by considering a frame of reference moving with the cylinder in the horizontal direction. Then by taking a Fourier transform of the resulting governing equation we may formulate the general solution, where the mixed boundary problem is required for the full solution. Taking Fourier transforms of the boundary conditions over their respective intervals enables the mixed boundary value problem to be formulated into a matrix Wiener–Hopf equation which we may solve.

The elastic half-space is assumed to be linear isotropic where is Lamé's first parameter, is the shear modulus, and is the material density. We consider (2.9), set $\mathbf{u}(x, y, t) = \hat{\mathbf{u}}(x, y)e^{i\omega t}$, and differentiate with respect to time twice to find,

$$\rho V^2 \left(i\omega - \frac{\partial}{\partial x} \right)^2 \hat{\mathbf{u}} = (\lambda + \mu) \nabla \nabla \cdot \hat{\mathbf{u}} + \mu \nabla^2 \hat{\mathbf{u}}. \quad (2.13)$$

The $e^{i\omega t}$ is added to generate a strip of analyticity in the complex k -plane, with $|\omega| \ll 1$ and $\text{Im}(\omega) < 0$ to ensure a causal solution. The temporal frequency, ω , will be considered in the steady state limit, $|\omega| \rightarrow 0$, and so has no effect on the boundary conditions after linearisation.

Fourier transforming the x -dependency gives a general solution to the governing equation (2.13). Defining the Fourier transform and inversion considered throughout on a variable $\phi(x, y)$,

$$\tilde{\phi}(k, y) = \int_{-\infty}^{\infty} \phi(x, y) e^{ikx} dx, \quad \phi(x, y) = \frac{1}{2\pi} \int_{-\infty}^{\infty} \tilde{\phi}(k, y) e^{-ikx} dk.$$

The notation $\tilde{\phi}(k, y)$ represents a transformed variable. Then by applying the transforms to the governing equation, the following is derived

$$\begin{aligned} \mu \frac{\partial^2 \tilde{u}}{\partial y^2} - ik(\lambda + \mu) \frac{\partial \tilde{v}}{\partial y} + (\rho V^2(\omega + k)^2 - (\lambda + 2\mu)k^2) \tilde{u} &= 0, \\ (\lambda + 2\mu) \frac{\partial^2 \tilde{v}}{\partial y^2} - ik(\lambda + \mu) \frac{\partial \tilde{u}}{\partial y} + (\rho V^2(\omega + k)^2 - \mu k^2) \tilde{v} &= 0. \end{aligned}$$

To enable a physically attainable solution deformations must decay far from the roller so an ansatz which decays in the negative y -direction is apt. A solution may be found by taking the following ansatz

$$\tilde{u}(k, y) = A(k)e^{\gamma(k)y}, \quad \tilde{v}(k, y) = A(k)B(k)e^{\gamma(k)y},$$

where $A(k), B(k)$ and $\gamma(k)$ are as yet unknown functions. Applying the ansatz to the transformed governing equation gives the following equations

to solve

$$\begin{aligned}\mu\gamma^2 + ik(\lambda + \mu)B\gamma + (\rho(\omega + kV)^2 - (\lambda + 2\mu)k^2) &= 0, \\ (\lambda + 2\mu)B\gamma^2 + ik(\lambda + \mu)\gamma + (\rho(\omega + kV)^2 - \mu k^2)B &= 0,\end{aligned}$$

which we may rearrange to form a single fourth order polynomial by eliminating B . Solving the fourth order polynomial gives the solutions

$$\begin{aligned}\gamma(k) &= \pm \sqrt{\left(1 - \frac{\rho V^2}{\lambda + 2\mu}\right) \left(k - \frac{\rho V \omega}{\lambda + 2\mu - \rho V^2}\right)^2 - \frac{\rho \omega^2}{\lambda + 2\mu - \rho V^2}}, \\ &= \pm \sqrt{\left(1 - \frac{\rho V^2}{\mu}\right) \left(k - \frac{\rho V \omega}{\mu - \rho V^2}\right)^2 - \frac{\rho \omega^2}{\mu - \rho V^2}}.\end{aligned}$$

Therefore, due to the decay in the elastic media, only two terms of the solutions to the fourth order polynomial remain, $\gamma_1(k)$ and $\gamma_2(k)$,

$$\gamma_1(k) = \sqrt{k^2 - \frac{\rho V^2}{\lambda + 2\mu}(\omega + k)^2}, \quad \gamma_2(k) = \sqrt{k^2 - \frac{\rho V^2}{\mu}(\omega + k)^2}.$$

To ensure the asymptotic behaviour of the solution as $k \rightarrow 0$ is correct, we define $u(x, y)$ and $v(x, y)$ in the following way. If we do not define $u(x, y)$ and $v(x, y)$ in this way, the general solution fails due to the asymptotic behaviour of $B_1(k)$, which would tend to infinity as k approaches zero. To prevent this problem we define in the following way,

$$\begin{aligned}u(x, y) &= \frac{1}{2\pi} \int_{-\infty}^{\infty} \left[\hat{A}_1(k) \hat{B}_1(k) e^{y\gamma_1(k)} + A_2(k) e^{y\gamma_2(k)} \right] e^{-ikx} dk, \\ v(x, y) &= \frac{1}{2\pi} \int_{-\infty}^{\infty} \left[\hat{A}_1(k) e^{y\gamma_1(k)} + A_2(k) B_2(k) e^{y\gamma_2(k)} \right] e^{-ikx} dk.\end{aligned}\tag{2.14}$$

Explicitly, this defines the functions $\gamma_1(k)$, $\gamma_2(k)$, $B_1(k)$ and $B_2(k)$, as

$$\gamma_1(k) = \sqrt{k^2 - \frac{\rho V^2}{\lambda + 2\mu} (\omega + k)^2}, \quad \gamma_2(k) = \sqrt{k^2 - \frac{\rho V^2}{\mu} (\omega + k)^2}$$

$$B_1(k) = \frac{k}{i\gamma_1(k)} = \frac{1}{\sqrt{\frac{\rho V^2 (1 + \frac{\omega}{k})^2}{\lambda + 2\mu} - 1}}, \quad B_2(k) = \frac{ik}{\gamma_2(k)} = \frac{-1}{\sqrt{\frac{\rho V^2 (1 + \frac{\omega}{k})^2}{\mu} - 1}}.$$

This leaves only two unknowns remaining, $\hat{A}_1(k)$ and $A_2(k)$, which are to be found by considering the boundary conditions. Note that we want the branch cuts of $B_1(k)$ and $B_2(k)$ to be chosen appropriately according to the branch cuts of $\gamma_1(k)$ and $\gamma_2(k)$, which themselves should be chosen such that $\text{real}(\gamma) > 0$. Observe that $\hat{B}_1(k) \rightarrow 0$ as $k \rightarrow 0$, which simplifies the general solution into a form which agrees with the $k \rightarrow 0$ limit of the fourth order polynomial.

The functions $\hat{A}_1(k)$ and $A_2(k)$ are unknown and so solving the problem is reduced to finding $\hat{A}_1(k)$ and $A_2(k)$. To find the particular solution for each of the regimes we take Fourier transforms of boundary conditions over their respective regions. Due to the boundary conditions differing in their respective regions we seek a technique to enables us to solve such problems.

Chapter 3

The Wiener–Hopf technique

3.1 Introduction

The disjoint physics of contact mechanics and friction leads to mathematical models of them to be naturally formulated into mixed boundary value problems. A famous technique for solving these types of problems is the Wiener–Hopf technique, which uses integral transforms of the disjoint boundary conditions to construct complex functions which are analytic in overlapping domains. In the overlapping domain the analytic functions may be assembled into a Wiener–Hopf equation; the solution is derived by applying Wiener–Hopf splittings, analytic continuation, and Liouville’s theorem¹.

The methodology outlined in the previous paragraph is known as the Wiener–Hopf technique and was first formulated by Norbert Wiener and Eberhard Hopf in their landmark paper in 1931 [99]. The technique was invented whilst considering the solution with respect to $f(x)$ to the following integral

¹See appendix A for the definition and some further basic results in complex analysis.

equation

$$\int_0^{\infty} K(x-y)f(y)dy = g(x), \quad x > 0, \quad (3.1)$$

where $g(x)$ is known and the kernel is

$$K(x) = \frac{1}{2\pi} \int_{|x|}^{\infty} \frac{e^{-y}}{y} dy.$$

Their method begins by introducing an additional unknown function $h(x)$ for x negative

$$\int_0^{\infty} K(x-y)f(y)dy = \begin{cases} g(x), & x > 0, \\ h(x), & x \leq 0. \end{cases} \quad (3.2)$$

Taking a Fourier transform of (3.2) leads to the Wiener–Hopf equation

$$G^+(k) + H^-(k) = K(k)F^+(k),$$

where we may proceed by taking what is known as a Wiener–Hopf factorisation of the kernel $K(k)$. The superscripts \pm indicate the domain of analyticity of the functions, which shall be discussed in more depth throughout this chapter. This brings us to what is thought to be the first Wiener–Hopf equation, to see how this may be solved refer to the texts by Wiener [99] or Lawrie and Abrahams [61] as we shall focus on extensions and applications to the technique from here on.

The technique Wiener and Hopf originally developed was for solving the integral equation (3.1) in question, and the direct relation of it to mixed boundary value problems was yet to come. Copson [27] provided an example of how the Wiener–Hopf technique may be applied to the classic Sommerfeld half-plane problem [89]. However, the most significant development in relating the Wiener–Hopf technique to mixed boundary value problems came from Jones [50] who constructed the Wiener–Hopf equation directly from a mixed boundary value problem. Shortly after, the book colloquially known

as the “Wiener–Hopf Bible” was published by Noble [74], which contains the most comprehensive account of the scalar Wiener–Hopf technique. Noble’s classic text contains a brief discussion on simultaneous scalar Wiener–Hopf equations, which may be arranged into a matrix Wiener–Hopf equation. The matrix Wiener–Hopf technique is in itself an active area of study with the recent review texts [57, 85] and is the format which we shall focus on, nonetheless, we shall illustrate the scalar Wiener–Hopf equation first.

Since its inception, the Wiener–Hopf technique has found itself in a variety of applications, from acoustics and elasticity to probability and even mathematical finance [e.g. 53, 2, 32, 38]. The scalar Wiener–Hopf technique is well understood, with current efforts in the advancement of the technique focussed on developing a constructive matrix Wiener–Hopf technique [57, 85]. The Wiener–Hopf technique has a rich history in contact mechanics [e.g. 90, 102, 65] with Spence [90] using the technique to solve adhesive contact problems with a power-law punch profile. Zhupanska and Ulitko [102] applied the Wiener–Hopf technique to a cylindrical punch but avoids the need for the matrix Wiener–Hopf technique because their symmetric setting allows the use of the planar-bipolar conformal mapping which reduces their problem to a scalar Wiener–Hopf equation. We note that the Riemann–Hilbert problem, the Wiener–Hopf technique’s close relation [55], has been used to solve the contact problems in Galin and Gladwell [39] and Antipov and Arutyunyan [10] also.

In section 3.2 a contact mechanics problem is presented and constructed into a scalar Wiener–Hopf equation, which is then solved in line with the scalar Wiener–Hopf technique. To assist with illustrating the Wiener–Hopf technique the sections 3.2.1 and 3.2.2 discuss the construction of half-range functions and Wiener–Hopf splittings respectively. The matrix Wiener–Hopf technique is introduced in section 3.3. Finally, the iterative method which we apply in chapters 4 and 5 is outlined in section 3.3.1.

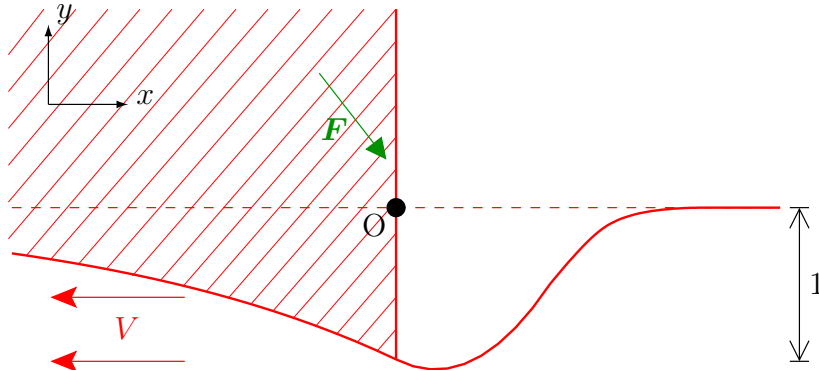


Figure 3.2.1: A schematic of a semi-infinite punch (shaded) sliding along an elastic half-space.

3.2 Scalar Wiener–Hopf technique

To illustrate the scalar Wiener–Hopf technique and its use in contact mechanics we introduce the “toy problem” of a semi-infinite punch sliding along an elastic half-space. This setting is shown schematically in figure 3.2.1.

We consider an elastic half-space $y < 0$ being deformed by a sliding semi-infinite punch with the profile

$$v(x) = -e^x, \quad \text{for } x \leq 0,$$

which is pushed in with a force \mathbf{F} , resulting in the leading edge causing an indentation depth of 1 into the elastic half-space. The punch slides in the positive x -direction across the half-space at a linear velocity V . We choose a frame of reference fixed with the punch, such that the leading edge of the punch is located at $x = 0$, with the origin of the coordinate system (labelled O) taken in a frame of reference moving with the leading edge of the punch at the height of the undeformed elastic surface. The unit vectors are \mathbf{e}_x and \mathbf{e}_y in the x - and y -directions respectively. The elastic half-space has a displacement $\mathbf{u}(\mathbf{x}, t)$ and stress tensor $\tau(\mathbf{x}, t)$, this gives us a similar setting to the rolling cylinder derived in section 2.2, except we have semi-infinite

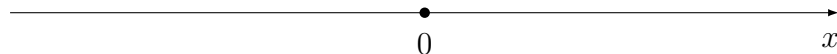
$$\begin{array}{ccc}
\tau_{xy}|_{y=0} - \mu_0\tau_{yy}|_{y=0} = 0 & & \tau_{xy}|_{y=0} = 0 \\
v|_{y=0} = -e^x & & \tau_{yy}|_{y=0} = 0
\end{array}$$


Figure 3.2.2: A diagram of the boundary conditions and their domains for a semi-infinite punch sliding along an elastic half-space.

boundary conditions on the surface of the elastic media.

We model the punch as slipping past the half-space so take a Coulomb law of dry friction as the frictional boundary condition. Thus giving the following boundary conditions,

$$\begin{array}{ll}
\text{Contact:} & v(x, 0) = -e^x, \quad \text{for } x \leq 0, \\
\text{Slip:} & \tau_{xy}(x, 0) - \mu_0\tau_{yy}(x, 0) = 0, \quad \text{for } -\infty < x < \infty, \\
\text{Stress-free:} & \tau_{yy}(x, 0) = 0, \quad \text{for } 0 < x.
\end{array}$$

The punch is assumed to be in forward slip due to the relative difference of the velocities of the two surfaces and we rearrange the stress-free boundary conditions to extend the slip boundary condition across the entire surface of the elastic half-space. The boundary conditions are shown diagrammatically in figure 3.2.2.

In line with Jones [50], we construct the Wiener–Hopf equation by taking Fourier transforms of the boundary conditions. In our case, we take a full-range transform of our boundary conditions and express the unknown components of the boundary conditions as unknown half-range functions, with more details on half-range functions found in section 3.2.1. Firstly, we define the following sets in the complex k -plane,

- upper half-plane: $\mathcal{D}^+ = \{k \in \mathbb{C} : \text{Im}(k) > \alpha; \alpha < 0\}$,
- lower half-plane: $\mathcal{D}^- = \{k \in \mathbb{C} : \text{Im}(k) < \beta; \beta > 0\}$,

- the strip: $\mathcal{D} = \mathcal{D}^+ \cap \mathcal{D}^- = \{k \in \mathbb{C} : \alpha < \text{Im}(k) < \beta\}$.

This defines an upper half-plane \mathcal{D}^+ and lower-half plane \mathcal{D}^- such that there is an overlapping region between them, which is the strip \mathcal{D} . A diagram of these sets in the complex plane is shown in figure 3.2.3. Now we take the full-range Fourier transformations of the boundary conditions

$$\tilde{\Psi}(k) = \int_{-\infty}^{\infty} \tau_{xy}(x, 0) - \mu_0 \tau_{yy}(x, 0) e^{ikx} dx = 0, \quad (3.3)$$

$$\begin{aligned} \widetilde{\tau_{yy}}(k) &= \int_{-\infty}^{\infty} \tau_{yy}(x, 0) e^{ikx} dx = \int_{-\infty}^0 \tau_{yy}(x, 0) e^{ikx} dx, \\ &= \widetilde{\tau_{yy}}^-(k), \end{aligned} \quad (3.4)$$

$$\begin{aligned} \tilde{v}(k) &= \int_{-\infty}^{\infty} v(x, 0) e^{ikx} dx \\ &= \int_0^{\infty} v(x, 0) e^{ikx} dx - \int_{-\infty}^0 e^{(ik+1)x} dx, \\ &= \tilde{v}^+(k) - \frac{1}{ik+1}. \end{aligned} \quad (3.5)$$

The newly defined half-range functions $\widetilde{\tau_{yy}}^-(k)$ and $\tilde{v}^+(k)$ are analytic in \mathcal{D}^- and \mathcal{D}^+ respectively. We note that the term $\frac{1}{ik+1}$ is analytic in \mathcal{D}^- and decays linearly as k tends to infinity.

We consider the general solution (2.14), derived in section 2.4 and is valid here as we similarly consider a convected elastic half-space. Therefore, we may express the Fourier transformed boundary conditions (3.3), (3.4) and (3.5) in terms of the unknowns $\hat{A}_1(k)$ and $A_2(k)$ by recalling the relationships,

$$\begin{aligned} \tilde{u}(k, y) &= \hat{A}_1(k) \hat{B}_1(k) e^{y\gamma_1(k)} + A_2(k) e^{y\gamma_2(k)}, \\ \tilde{v}(k, y) &= \hat{A}_1(k) e^{y\gamma_1(k)} + A_2(k) B_2(k) e^{y\gamma_2(k)}. \end{aligned}$$

Relating the transformed boundary conditions to $\hat{A}_1(k)$ and $A_2(k)$ allows us to relate them to one another, and therefore to construct the Wiener–Hopf equation. This approach is the same for both the full-slip and stick-slip cases which is discussed further in sections 4.2 and 5.2 respectively.

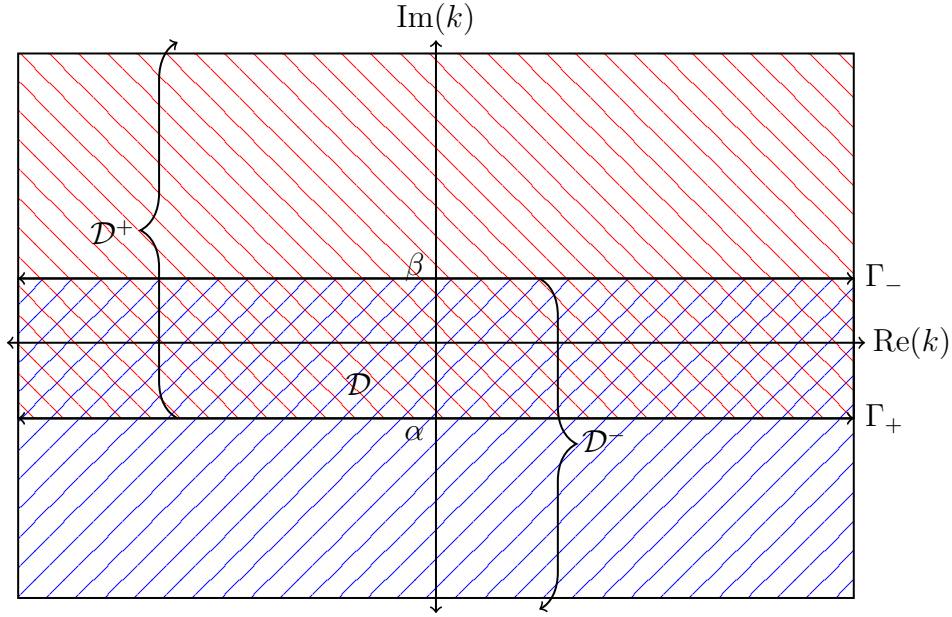


Figure 3.2.3: A diagram of the complex k -plane with the upper half-plane, lower half-plane and strip shown.

By using the plane strain relationship (2.8), $\tilde{\Psi}(k)$ may be expressed in terms of the unknown functions $\hat{A}_1(k)$ and $A_2(k)$. Then (3.3) can be used to eliminate the unknown function $\hat{A}_1(k)$,

$$\begin{aligned}
 \tilde{\Psi}(k) &= \left[\mu(\hat{B}_1(k)\gamma_1(k) - ik) - \mu_0 \left((\lambda + 2\mu)\gamma_1(k) - ik\lambda\hat{B}_1(k) \right) \right] \hat{A}_1(k) \\
 &\quad + \left[\mu(\gamma_2(k) - ikB_2(k)) - \mu_0 \left((\lambda + 2\mu)B_2(k)\gamma_2(k) - ik\lambda \right) \right] A_2(k) \\
 &= m_1^-(k)\hat{A}_1(k) + m_2^-(k)A_2(k) = 0 \iff \hat{A}_1(k) = -\frac{m_2^-(k)}{m_1^-(k)}A_2(k),
 \end{aligned} \tag{3.6}$$

where the known functions $m_1^-(k)$ and $m_2^-(k)$ are defined from equations (3.6). Then expressing the remaining boundary conditions, (3.4) and (3.5),

in terms of $A_2(k)$ gives

$$\begin{aligned}\widetilde{\tau}_{yy}(k) &= \left[(\lambda + 2\mu)\gamma_1(k) - ik\lambda\widehat{B}_1(k) \right] \widehat{A}_1(k) \\ &\quad + \left[(\lambda + 2\mu)B_2(k)\gamma_2(k) - ik\lambda \right] A_2(k) \\ &= n_1(k)\widehat{A}_1(k) + n_2(k)A_2(k) = \left(n_2(k) - n_1(k)\frac{m_2^-(k)}{m_1^-(k)} \right) A_2(k)\end{aligned}\quad (3.7)$$

$$\widetilde{v}(k) = \widehat{A}_1(k) + B_2(k)A_2(k) = \left(B_2(k) - \frac{m_2^-(k)}{m_1^-(k)} \right) A_2(k), \quad (3.8)$$

with the known functions $n_1(k)$ and $n_2(k)$ defined from (3.7). Then we may eliminate $A_2(k)$ from equations (3.7) and (3.8) to find

$$\frac{\widetilde{\tau}_{yy}(k)}{n_2(k)m_1^-(k) - n_1(k)m_2^-(k)} = \frac{\widetilde{v}(k)}{B_2(k)m_1^-(k) - m_2^-(k)}.$$

Substituting in the relations given in equations (3.4) and (3.5) and rearranging gives a scalar Wiener–Hopf equation

$$K(k)\widetilde{\tau}_{yy}^-(k) = \widetilde{v}^+(k) - \frac{1}{ik+1} \in \mathcal{D}, \quad (3.9)$$

with the Wiener–Hopf kernel, $K(k)$, defined as

$$K(k) = \frac{B_2(k)m_1^-(k) - m_2^-(k)}{n_2(k)m_1^-(k) - n_1(k)m_2^-(k)}, \quad \text{with } K(k) = O\left(\frac{1}{|k|}\right) \text{ as } |k| \rightarrow \infty. \quad (3.10)$$

We note that this kernel is the same function we seek to multiplicatively split in the full-slip regime and appears in the stick-slip regime too.

To progress further we seek to employ the Wiener–Hopf technique, which relies on finding a Wiener–Hopf factorisation or multiplicative splitting of the Wiener–Hopf kernel $K(k)$. A more detailed discussion of Wiener–Hopf factorisation may be found in section 3.2.2.2, for now, we define the factorisation

of the kernel $K(k)$ as

$$K(k) = K_+(k)K_-(k).$$

The functions $K_-(k)$ and $K_+(k)$ are analytic non-zero in \mathcal{D}^+ and \mathcal{D}^- respectively and the subscripts \pm are used to denote multiplicative factorisations. Both $K_-(k)$ and $K_+(k)$ behave like $|k|^{-\frac{1}{2}}$ as $|k| \rightarrow \infty$ in their respective domains. Note the kernel $K(k)$ appears in chapters 4 and 5, with the details on its factorisation given in section 4.4.1.1. If we can find a factorisation of (3.10), then we may divide the equation (3.9) by $K_+(k)$ to find

$$K_-(k)\widetilde{\tau}_{yy}^-(k) = \frac{\widetilde{v}^+(k)}{K_+(k)} - \frac{1}{K_+(k)(ik+1)}. \quad (3.11)$$

The next key step is to apply a Wiener–Hopf decomposition or an additive splitting of the forcing term to the equation

$$\frac{1}{K_+(k)(ik+1)} = F^+(k) + F^-(k).$$

The functions $F^+(k)$ and $F^-(k)$ are analytic in \mathcal{D}^+ and \mathcal{D}^- respectively, and the superscripts \pm are used to denote additive decompositions. To see a more detailed discussion of Wiener–Hopf decompositions see section 3.2.2.1. Applying the decomposition to our Wiener–Hopf equation (3.11) and rearranging,

$$\underbrace{\frac{\widetilde{v}^+(k)}{K_+(k)} - F^+(k)}_{\text{upper}} = \underbrace{K_-(k)\widetilde{\tau}_{yy}^-(k) + F^-(k)}_{\text{lower}} \equiv J(k), \quad (3.12)$$

where we may find a function, $J(k)$ say, which is defined in the strip \mathcal{D} . As the **upper** side of equation (3.12) is analytic in \mathcal{D}^+ and the **lower** side of the equation is analytic in \mathcal{D}^- , then by analytic continuation $J(k)$ must be entire. In general, the behaviour of $J(k)$ is found by examining the asymptotic behaviour of the **upper** and **lower** sides of (3.12). For example, if both sides

grew at most like $|k|^n$ as $|k| \rightarrow \infty$, then by an application of the extended Liouville's Theorem (see appendix A) we find that $J(k)$ is a polynomial of degree at most n .

We derive the asymptotic behaviour of the half-range functions by examining the edge conditions. The edge conditions are the behaviour of the boundary conditions as they approach the limits of their domain, throughout this thesis we pay close attention to them as their locations are unknown and we seek to find them as part of the solution, however, for this toy problem the location of the boundary junction is known. The edge conditions at the junction for this problem they are

$$\lim_{x \rightarrow 0^+} v(x, 0) = -1, \quad \lim_{x \rightarrow 0^-} \tau_{yy}(x, 0) = |k|^{-\frac{1}{2}}.$$

To impose the edge conditions on the half-range functions we consider the definition of the half-range function and apply integration by parts repeatedly,

$$\begin{aligned} \tilde{v}^+(k) &= \int_0^\infty v(x, 0) e^{ikx} dx, \\ &= \sum_{n=0}^\infty \frac{\partial^n v}{\partial x^n}(0, 0) \left(\frac{-1}{ik} \right)^{n+1}. \end{aligned}$$

This determines the asymptotic behaviour of $\tilde{v}^+(k)$ to be

$$\tilde{v}^+(k) = \frac{1}{ik} + O(|k|^{-2}) \text{ as } |k| \rightarrow \infty.$$

Applying the edge conditions to both half-range functions gives the asymptotic behaviour

$$\begin{aligned} \tilde{v}^+(k) &\sim |k|^{-1} \text{ as } |k| \rightarrow \infty \in \mathcal{D}^+, \\ \widetilde{\tau_{yy}}^-(k) &\sim |k|^{-\frac{1}{2}} \text{ as } |k| \rightarrow \infty \in \mathcal{D}^-. \end{aligned}$$

Hence, the function $J(k)$ has the asymptotic behaviours

$$J(k) \leq \begin{cases} |k|^{-\frac{1}{2}} & \text{as } |k| \rightarrow \infty \in \mathcal{D}^+, \\ |k|^{-1} & \text{as } |k| \rightarrow \infty \in \mathcal{D}^-. \end{cases} \quad (3.13)$$

Equation (3.13) shows that $J(k)$ tends to zero in both half-planes and so by Liouville's Theorem (see appendix A) it is identically zero. Therefore, the solution to the Wiener–Hopf equation is

$$\tilde{v}^+(k) = K_+(k)F^+(k), \quad \widetilde{\tau_{yy}^-}(k) = -\frac{F^-(k)}{K_-(k)}.$$

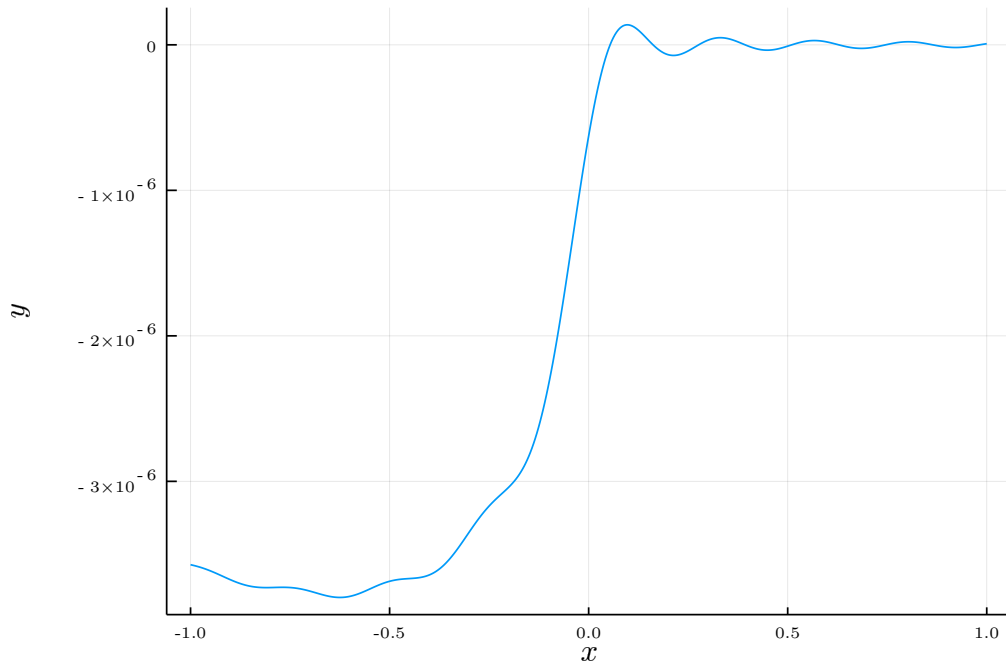
A demonstration of the Wiener–Hopf technique in the context of a contact problem has been explained, which will aid us in the more intricate settings we wish to explore in chapters 4 and 5.

Thus, we have applied the Wiener–Hopf technique to a scalar equation to find the two unknown terms, $\tilde{v}^+(k)$ and $\widetilde{\tau_{yy}^-}(k)$, from which one can evaluate the unknown functions $\hat{A}_1(k)$, $A_2(k)$. To illustrate the solution for the toy problem we plot the stresses in the half-space in figure 3.2.4. The solution is found by numerically inverting

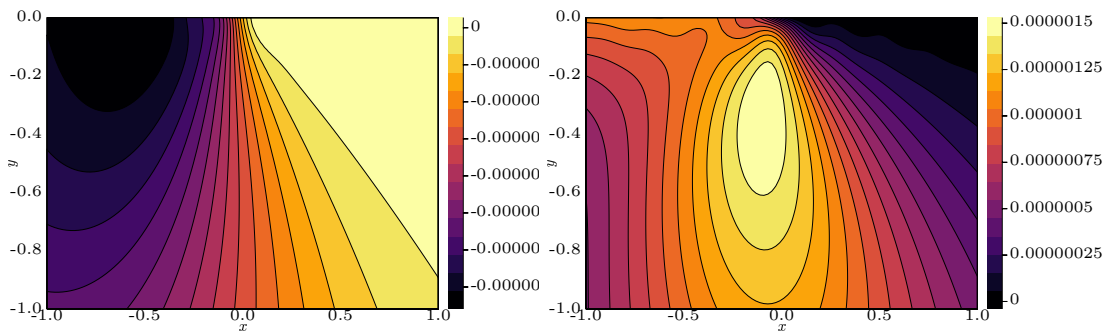
$$\begin{aligned} \tau_{yy}(x, 0) &= \frac{1}{2\pi} \int_{-\infty}^{\infty} \widetilde{\tau_{yy}}(k, 0) e^{-ikx} dk, \\ &= \frac{1}{2\pi} \int_{-\infty}^{\infty} \widetilde{\tau_{yy}^-}(k) e^{-ikx} dk, \end{aligned}$$

by applying a quadrature rule. We note that by finding $\hat{A}_1(k)$ and $A_2(k)$ from equations (3.6) and (3.7) we may find the stresses inside the half-space which are shown in the contour plots 3.2.4b and 3.2.4c. The figure 3.2.4a shows the normal stress on the surface of the elastic half-space which returns to zero away from the punch, as we have imposed in the boundary conditions. Figure 3.2.4a shows some oscillatory behaviour near the transition point which is from the Gibbs Phenomena caused by the numerical method and is discussed in more depth in sections 4.5 and 5.6.3. The remaining figures in 3.2.4 show

that the magnitudes of stress in the half-space are localised around the punch, as one would intuitively expect.



(a) The profile plot of $\tau_{yy}(x, 0)$.



(b) The stress distribution for $\tau_{yy}(x, y)$.

(c) The stress distribution for $\tau_{xy}(x, y)$.

Figure 3.2.4: Plots of the solution to the toy problem for Metal parameter values from table 4.1.

3.2.1 Half-range transforms

To apply the Wiener–Hopf technique we must take Fourier transforms of our boundary conditions over semi-infinite and finite regions. For this purpose, we shall define half-range Fourier transforms and show that finite-range transforms may be written as the difference of half-range transforms. Once all our boundary conditions are transformed over their respective regions they are then assembled into a Wiener–Hopf problem.

We define a half-range Fourier transforms with respect to the point $x = L$ by considering the full-range Fourier transform and splitting as follows,

$$\begin{aligned}\tilde{\phi}^L(k, y) &= \int_{-\infty}^{\infty} \phi(x, y) e^{ik(x-L)} dx \\ &= \int_L^{\infty} \phi(x, y) e^{ik(x-L)} dx + \int_{-\infty}^L \phi(x, y) e^{ik(x-L)} dx \\ &= \tilde{\phi}_+^L(k, y) + \tilde{\phi}_-^L(k, y).\end{aligned}$$

The half-range functions $\tilde{\phi}_+^L(k, y)$ and $\tilde{\phi}_-^L(k, y)$ analytic in \mathcal{D}^+ and \mathcal{D}^- respectively (see page 12 of [74]). The shifted full-range transforms may be related to one centred at $x = 0$ by

$$\tilde{\phi}^L(k, y) e^{ikL} = \tilde{\phi}(k, y).$$

Finally, the transformation of a finite interval may be related to half-range transforms in the following way

$$\begin{aligned}\tilde{\phi}^{[L_1, L_2]}(k, y) &= \int_{L_2}^{L_1} \phi(x, y) e^{ikx} dx, \\ &= \tilde{\phi}_-^{L_1}(k, y) e^{ikL_1} - \tilde{\phi}_-^{L_2}(k, y) e^{ikL_2} \\ &= \tilde{\phi}_+^{L_2}(k, y) e^{ikL_2} - \tilde{\phi}_+^{L_1}(k, y) e^{ikL_1}.\end{aligned}$$

This gives the tools to transform the boundary conditions over their respective regions.

3.2.2 Wiener–Hopf splittings

A Wiener–Hopf splitting is the separation of a function into its upper and lower parts. In the following we explain how scalar functions may be additively and multiplicatively split, as well as an illustrative examples.

3.2.2.1 Wiener–Hopf decomposition

The Cauchy transform may be used to calculate the additive decomposition [29, 74], for $k \in \mathbb{C}$ and $F(k)$ entire

$$\begin{aligned} F(k) &= \frac{1}{2\pi i} \int_{\Gamma_+} \frac{F(x)}{x-k} dx & - & \quad \frac{1}{2\pi i} \int_{\Gamma_-} \frac{F(x)}{x-k} dx \\ &= \mathcal{C}_{\Gamma_+}[F](k) & - & \quad \mathcal{C}_{\Gamma_-}[F](k) \\ &= F^+(k) & + & \quad F^-(k). \end{aligned}$$

The contours Γ_+ or Γ_- pass below or above k , respectively, as shown in figure 3.2.3. It is further required that $F(k) \rightarrow 0$ as $|k| \rightarrow \infty$ for the Cauchy transform to hold. The purpose of this decomposition is to separate $F(k)$ into components which are analytic in \mathcal{D}^+ or \mathcal{D}^- .

We outline a simple example of additive decomposition without the need to apply the Cauchy transform. Consider the function $F(k) = \frac{1}{(k-i)(k+i)}$, which has singularities at $k = \pm i$. The singularities in $F(k)$ may be separated additively,

$$\begin{aligned} F(k) &= \frac{1}{(k-i)(k+i)}, \\ &= \frac{i}{2(k+i)} & - & \quad \frac{i}{2(k-i)} \\ &= F^+(k) & + & \quad F^-(k). \end{aligned}$$

The function $F^+(k)$ has its singularity in \mathcal{D}^- and the function $F^-(k)$ has its singularity in \mathcal{D}^+ , so are both analytic in the correct regions.

3.2.2.2 Wiener–Hopf factorisation

The multiplicative factorisation of a function may be derived through the additive splitting and the use of the logarithm. For an entire complex function, $K(k)$,

$$\begin{aligned} K(k) &= e^{[\log(K)]^+ + [\log(K)]^-} \\ &= K_+(k)K_-(k), \end{aligned}$$

where we denote multiplicative splittings by subscripts \pm and additive splittings by superscripts \pm . The additive decomposition of $\log(K)$ may be found via the Cauchy transform, as outlined previously. The requirement of the asymptotic behaviour of $K(k)$ in the multiplicative factorisation is $K(k) \rightarrow 1$ as $|k| \rightarrow \infty$. Hence $\log(K) \rightarrow 0$ as $|k| \rightarrow \infty$, this asymptotic behaviour may be generated by normalising $K(k)$ by a known entire function $\gamma(k)$, which can be multiplicatively factorised [74].

We outline a simple example of multiplicative factorisation without the need to apply the Cauchy transform. Consider the function $K(k) = \sqrt{(k+i)(k-i)}$, which has branch-cut singularities at $k = \pm i$, so again we express $K(k)$ such that these singularities are separated,

$$\begin{aligned} K(k) &= \sqrt{(k+i)(k-i)}, \\ &= \sqrt{(k+i)}\sqrt{(k-i)} \\ &= K^+(k) K^-(k). \end{aligned}$$

The function $K^+(k)$ has its branch-cut in \mathcal{D}^- and the function $K^-(k)$ has its branch-cut in \mathcal{D}^+ , hence both are analytic in the correct regions.

Next the scalar Wiener–Hopf equation is generalised to the matrix Wiener–Hopf equation, which has a matrix kernel $\mathbf{K}(k)$ with vector half-range and forcing functions $\widetilde{\boldsymbol{\phi}}^+(k)$, $\widetilde{\boldsymbol{\phi}}^-(k)$ and $\mathbf{F}(k)$.

3.3 Matrix Wiener–Hopf technique

The Wiener–Hopf problem which arises in chapters 4 and 5 are a series of coupled Wiener–Hopf equations and these equations are then assembled into a linear system before applying the matrix analogue of the scalar Wiener–Hopf technique. A matrix Wiener–Hopf equation is composed of the vector unknown functions, $\widetilde{\phi}^+(k)$ and $\widetilde{\phi}^-(k)$, the forcing vector, $\mathbf{F}(k)$, and the matrix kernel, $\mathbf{K}(k)$. An example of an n -dimensional matrix Wiener–Hopf equation is

$$\begin{pmatrix} \widetilde{\phi}_1^+(k) \\ \widetilde{\phi}_2^+(k) \\ \vdots \\ \widetilde{\phi}_n^+(k) \end{pmatrix} = \begin{pmatrix} K_{11}(k) & K_{21}(k) & \dots & K_{n1}(k) \\ K_{12}(k) & K_{22}(k) & \dots & K_{n2}(k) \\ \vdots & \vdots & \ddots & \vdots \\ K_{1n}(k) & K_{2n}(k) & \dots & K_{nn}(k) \end{pmatrix} \begin{pmatrix} \widetilde{\phi}_1^-(k) \\ \widetilde{\phi}_2^-(k) \\ \vdots \\ \widetilde{\phi}_n^-(k) \end{pmatrix} + \begin{pmatrix} F_1(k) \\ F_2(k) \\ \vdots \\ F_n(k) \end{pmatrix},$$

where there are $2n$ unknowns $\widetilde{\phi}_n^\pm(k)$. To solve this system we may use a technique analogous to the scalar case but complications arise in the factorisation of the kernel $\mathbf{K}(k)$. The factorisation of a matrix kernel is an ongoing open problem within the Wiener–Hopf community.

In the scalar Wiener–Hopf technique, the Wiener–Hopf factorisation of the scalar kernel function may be found by taking the additive decomposition of the logarithm of the kernel and then raising to the exponential to recover the kernel. The generalisation of the scalar technique to the matrix setting fails due to matrix multiplication being non-commutative, which we will now demonstrate. As in the scalar case, we write our matrix kernel as

$$\mathbf{K}(k) = e^{\log(\mathbf{K})}.$$

Then we may compute the additive decomposition of $\log(\mathbf{K})(k)$ by computing the additive decomposition of the scalar elements of $\log(\mathbf{K})(k)$,

$$\log(\mathbf{K})(k) = [\log(\mathbf{K})(k)]^+ + [\log(\mathbf{K})(k)]^-.$$

This approach breaks down as the relationship

$$e^{[\log(\mathbf{K})(k)]^+ + [\log(\mathbf{K})(k)]^-} = e^{[\log(\mathbf{K})(k)]^+} e^{[\log(\mathbf{K})(k)]^-}$$

only exists if the matrices $[\log(\mathbf{K})(k)]^+$ and $[\log(\mathbf{K})(k)]^-$ are commutative, which is only true in special cases. Additionally, we note that the logarithm of a matrix is not well-defined for all matrices, see Hall [42] for more details. At present there are no general constructive methods for solving matrix Wiener–Hopf problems, with many methods developed on a case by case basis.

In the text Noble [74], there is a brief discussion on the topic of simultaneous Wiener–Hopf equations which are then formulated into a general matrix Wiener–Hopf equation. A solution is proposed for the general matrix Wiener–Hopf equation by using the idea in Heins [43] to consider commutative factorisation, however, no illustrative examples were given in the text. Noble mentions the results by Muskhelishvili [73], who examines the related vectorial Riemann–Hilbert problem permits a factorisation but Noble notes that at the time of writing no constructive method exists either.

There has been extensive developments in the factorisation of matrix functions which has recently culminated in the review text Kisil et al. [57], with some constructive methods beginning to appear. In particular, there is no general constructive approach to factorise any matrix kernel into its upper and lower components. Moreover, exact solutions only exist in a select few cases, some of these exact solutions include triangular matrices, rational matrices, and commutative matrices such as those of Khropkov-Daniele form. To widen the class of exact solutions to matrix Wiener–Hopf problems, constructive approaches to factorise matrices have been found, some of these approaches may be found in Rogosin and Mishuris [85]. approximate methods have been introduced to extend the solution space even further, these include Padè approximants by Abrahams [3] or the Fredholm factorisation by Daniele [29]. Alternatively, one could do away with an analytical solution and proceed numerically as suggested by Llewellyn Smith and Luca [63] or Colbrook et al. [26].

The matrix Wiener–Hopf equations we consider are derived from their mixed boundary value problems in chapters 4 and 5. The boundary conditions switch at unknown labeled junctions and so taking Fourier transforms of the boundary conditions leads to a series of coupled scalar Wiener–Hopf equations. The coupled Wiener–Hopf equations may be assembled into a matrix Wiener–Hopf equation or vice versa and it is to our fortune that the iterative method [56, 81] exists to approximate the solution to such systems. We shall outline the iterative method in the following section.

3.3.1 Iterative method

We outline the iterative method which we shall apply to the matrix Wiener–Hopf equations in chapters 4 and 5. The iterative method is a technique for solving triangular matrix Wiener–Hopf equations with exponential factors Kisil [56] and Priddin et al. [81]. It was first developed in Kisil [56] for 2×2 matrices and then extended to $n \times n$ matrices in Priddin et al. [81], and is one of few constructive n -dimensional matrix Wiener–Hopf techniques [51, 96, 85]. The method has been applied to problems in acoustics by Kisil and Ayton [53] and crack propagation by Livasov and Mishuris [62].

The method considers a matrix Wiener–Hopf such as (3.14) and approximates the exponential terms to zero. Once an initial approximation has been made the matrix Wiener–Hopf may be considered as a series of decoupled scalar Wiener–Hopf equations, in these scalar equations one may use additive and multiplicative decompositions to arrive at a form in which Liouville’s Theorem may be applied. The approximation is corrected by reintroducing the exponential terms and iterating through the coupled scalar equations, additively decomposing the corrected forcing into a form where Liouville’s may be applied once again.

To illustrate the iterative method, we introduce the notation $\tilde{\phi}_{\pm}^{(L)j}(k)$ to indicate the j th iteration of an unknown upper or lower function from the point L . Consider the following triangular matrix Wiener–Hopf equation

with exponential factors,

$$\begin{pmatrix} A_{11}(k) & & & & \\ A_{21}(k)e^{ikL_{21}} & A_{22}(k) & & & \\ \vdots & \ddots & \ddots & & \\ A_{n1}(k)e^{ikL_{n1}} & A_{n2}(k)e^{ikL_{n2}} & \dots & A_{nn}(k) & \end{pmatrix} \begin{pmatrix} \tilde{\phi}_+^{(1)}(k) \\ \tilde{\phi}_+^{(2)}(k) \\ \vdots \\ \tilde{\phi}_+^{(n)}(k) \end{pmatrix} = \quad (3.14)$$

$$\begin{pmatrix} B_{11}(k) & B_{12}(k)e^{-ikL_{12}} & \dots & B_{1n}(k)e^{-ikL_{1n}} \\ & B_{22}(k) & \ddots & B_{2n}(k)e^{-ikL_{2n}} \\ & & \ddots & \vdots \\ & & & B_{nn}(k) \end{pmatrix} \begin{pmatrix} \tilde{\phi}_-^{(1)}(k) \\ \tilde{\phi}_-^{(2)}(k) \\ \vdots \\ \tilde{\phi}_-^{(n)}(k) \end{pmatrix} + \begin{pmatrix} F_1(k) \\ F_2(k) \\ \vdots \\ F_n(k) \end{pmatrix}.$$

The elements within both matrices are assumed to be known and defined in the strip \mathcal{D} with the elements in the forcing vector defined similarly.

Then as instructed in Priddin et al. [81], we make an initial approximation by setting the non-diagonal entries in the matrix to zero which neglects the coupling between equations. This is justified by considering the behaviour of the exponential terms in the extremities of the strip, which approximates either e^{-ikL} or e^{ikL} terms to zero. Thus as a first approximation we may set all exponential entries in the matrices to zero,

$$\begin{pmatrix} A_{11}(k) & & & & \\ & A_{22}(k) & & & \\ & & \ddots & & \\ & & & A_{nn}(k) & \end{pmatrix} \begin{pmatrix} \tilde{\phi}_+^{(1)0}(k) \\ \tilde{\phi}_+^{(2)0}(k) \\ \vdots \\ \tilde{\phi}_+^{(n)0}(k) \end{pmatrix} =$$

$$\begin{pmatrix} B_{11}(k) & & & & \\ & B_{22}(k) & & & \\ & & \ddots & & \\ & & & B_{nn}(k) & \end{pmatrix} \begin{pmatrix} \tilde{\phi}_-^{(1)0}(k) \\ \tilde{\phi}_-^{(2)0}(k) \\ \vdots \\ \tilde{\phi}_-^{(n)0}(k) \end{pmatrix} + \begin{pmatrix} F_1(k) \\ F_2(k) \\ \vdots \\ F_n(k) \end{pmatrix}.$$

As we have decoupled each row for the initial approximation, we may now solve each row of the matrix Wiener–Hopf problem by considering them as scalar equations. To minimise the number of multiplicative factorisations

required we divide the i th row by $A_{ii}(k)$ for $i < \frac{n}{2}$ and $B_{ii}(k)$ otherwise, hence the scalar Wiener–Hopf equations are

$$\begin{aligned}
\tilde{\phi}_+^{(1)0}(k) &= B_{11}(k)\tilde{\phi}_-^{(1)0}(k) + F_1(k), \\
&\vdots \\
\tilde{\phi}_+^{(\frac{n}{2}-1)0}(k) &= B_{\frac{n}{2}-1, \frac{n}{2}-1}(k)\tilde{\phi}_-^{(\frac{n}{2}-1)0}(k) + F_{\frac{n}{2}-1}(k), \\
A_{\frac{n}{2}, \frac{n}{2}}(k)\tilde{\phi}_+^{(\frac{n}{2})0}(k) &= \tilde{\phi}_-^{(\frac{n}{2})0}(k) + F_{\frac{n}{2}}(k), \\
&\vdots \\
A_{nn}(k)\tilde{\phi}_+^{(n)0}(k) &= \tilde{\phi}_-^{(n)0}(k) + F_n(k).
\end{aligned}$$

Then we apply the scalar Wiener–Hopf technique to each of the equations, where we shall assume that our functions decay sufficiently in \mathcal{D}^+ and \mathcal{D}^- to give the following initial solutions,

$$\begin{aligned}
\tilde{\phi}_+^{(1)0}(k) &= B_{11+}(k) \left[\frac{F_1(k)}{B_{11+}(k)} \right]^+, & \tilde{\phi}_-^{(1)0}(k) &= -\frac{1}{B_{11-}(k)} \left[\frac{F_1(k)}{B_{11+}(k)} \right]^-, \\
\tilde{\phi}_+^{(2)0}(k) &= B_{22+}(k) \left[\frac{F_2(k)}{B_{22+}(k)} \right]^+, & \tilde{\phi}_-^{(2)0}(k) &= -\frac{1}{B_{22-}(k)} \left[\frac{F_2(k)}{B_{22+}(k)} \right]^-, \\
&\vdots & & \vdots \\
\tilde{\phi}_+^{(n)0}(k) &= \frac{1}{A_{nn+}(k)} \left[\frac{F_n(k)}{A_{nn-}(k)} \right]^+, & \tilde{\phi}_-^{(n)0}(k) &= -A_{nn+}(k) \left[\frac{F_n(k)}{A_{nn-}(k)} \right]^-.
\end{aligned}$$

For subsequent iterations we reintroduce the coupling (exponential terms), consider the scalar Wiener–Hopf equations within the matrix, and rearrange to minimise factorisations as before. We continue to consider each row as scalar Wiener–Hopf equations by treating the reintroduced terms as a forcing

by using their current approximation,

$$\begin{aligned}
\tilde{\phi}_+^{(1)j}(k) &= B_{11}(k)\tilde{\phi}_-^{(1)j}(k) + F_1(k) \\
&\quad + \sum_{m=2}^n B_{1m}(k)e^{-ikL_{1m}}\tilde{\phi}_-^{(m)j-1}(k) \\
&\quad \vdots \\
\tilde{\phi}_+^{(\frac{n}{2}-1)j}(k) &= B_{\frac{n}{2}-1, \frac{n}{2}-1}(k)\tilde{\phi}_-^{(\frac{n}{2}-1)j}(k) + F_{\frac{n}{2}-1}(k) \\
&\quad + \sum_{m=1}^{\frac{n}{2}-2} A_{mn}(k)e^{ikL_{mn}}\tilde{\phi}_+^{(m)j}(k) \quad + \sum_{m=\frac{n}{2}}^n B_{m1}(k)e^{-ikL_{m1}}\tilde{\phi}_-^{(m)j-1}(k) \\
A_{\frac{n}{2}, \frac{n}{2}}(k)\tilde{\phi}_+^{(\frac{n}{2})j}(k) &= \tilde{\phi}_-^{(\frac{n}{2})j}(k) + F_{\frac{n}{2}}(k) \\
&\quad + \sum_{m=1}^{\frac{n}{2}-1} A_{mn}(k)e^{ikL_{mn}}\tilde{\phi}_+^{(m)j}(k) \quad + \sum_{m=\frac{n}{2}+1}^n B_{m1}(k)e^{-ikL_{m1}}\tilde{\phi}_-^{(m)j-1}(k) \\
&\quad \vdots \\
A_{nn}(k)\tilde{\phi}_+^{(n)j}(k) &= \tilde{\phi}_-^{(n)j}(k) + F_n(k) \\
&\quad + \sum_{m=1}^{n-1} A_{mn}(k)e^{ikL_{mn}}\tilde{\phi}_+^{(m)j}(k) \quad .
\end{aligned}$$

The summations are comprised entirely of known terms and so we define a new forcing to include them,

$$\begin{aligned}
\tilde{\phi}_+^{(1)j}(k) &= B_{11}(k)\tilde{\phi}_-^{(1)j}(k) + \widehat{F}_1(k) \\
&\quad \vdots \\
\tilde{\phi}_+^{(\frac{n}{2}-1)j}(k) &= B_{\frac{n}{2}-1, \frac{n}{2}-1}(k)\tilde{\phi}_-^{(\frac{n}{2}-1)j}(k) + \widehat{F}_{\frac{n}{2}-1}(k) \\
A_{\frac{n}{2}, \frac{n}{2}}(k)\tilde{\phi}_+^{(\frac{n}{2})j}(k) &= \tilde{\phi}_-^{(\frac{n}{2})j}(k) + \widehat{F}_{\frac{n}{2}}(k) \\
&\quad \vdots \\
A_{nn}(k)\tilde{\phi}_+^{(n)j}(k) &= \tilde{\phi}_-^{(n)j}(k) + \widehat{F}_n(k)
\end{aligned}$$

Finally, we apply the scalar Wiener–Hopf technique to each of the scalar equations to approximate the solution at the j th iteration. Hence, the j th

solution is

$$\begin{aligned}
\tilde{\phi}_+^{(1)j}(k) &= B_{11+}(k) \left[\frac{\widehat{F}_1(k)}{B_{11+}(k)} \right]^+, & \tilde{\phi}_-^{(1)j}(k) &= -\frac{1}{B_{11-}(k)} \left[\frac{\widehat{F}_1(k)}{B_{11+}(k)} \right]^- \\
\tilde{\phi}_+^{(2)j}(k) &= B_{22+}(k) \left[\frac{\widehat{F}_2(k)}{B_{22+}(k)} \right]^+, & \tilde{\phi}_-^{(2)j}(k) &= -\frac{1}{B_{22-}(k)} \left[\frac{\widehat{F}_2(k)}{B_{22+}(k)} \right]^- \\
&\vdots & & \vdots \\
\tilde{\phi}_+^{(n)j}(k) &= \frac{1}{A_{nn+}(k)} \left[\frac{\widehat{F}_n(k)}{A_{nn-}(k)} \right]^+, & \tilde{\phi}_-^{(n)j}(k) &= -A_{nn+}(k) \left[\frac{\widehat{F}_n(k)}{A_{nn-}(k)} \right]^- .
\end{aligned}$$

We may iterate through the j th iteration equations until a convergence criteria has been met, such as

$$\|\tilde{\phi}_+^{(n)j}(k) - \tilde{\phi}_+^{(n)j-1}(k)\| < \text{tolerance},$$

where the tolerance is some specified amount. To see more analysis on the convergence of the iterative method see Priddin et al. [81]. Thus, we have outlined the iterative method which we have used throughout. To see the implementation of this method refer to sections 4.4 and 5.4, where more discussion may be found.

Chapter 4

Rolling contact in the full-slip regime

4.1 Introduction

In this chapter we consider the setting where the magnitude of the angular velocity for the cylinder is either sufficiently larger or sufficiently smaller than the magnitude of the convection velocity, causing the contact region to be fully slipping. In this setting we have imposed a full-slip friction law, which simplifies the stick-slip friction boundary conditions by removing the central sticking region. A solely slipping friction law means that the half-space experiences uniform behaviour in the contact region. The uniform behaviour within the contact region means that there are only two junctions between boundary conditions and therefore a 2×2 matrix Wiener–Hopf equation is to be expected. The junctions between the boundary conditions are the unknown boundaries of the contact region and are referred to as the contact points.

As outlined in chapter 1, the model of an elastic half-space deformed by a rigid punch has been of interest for a considerable time, but we shall re-

view the literature in greater depth here. Hertz [44] founded the field of contact mechanics at the end of the 19th century by considering the elastic deformation due to a frictionless rigid punch. Half a century later, the understanding of contact mechanics was extended when Cattaneo [21] and Mindlin [66] both considered elastic deformation of two cylinders under friction, setting the boundary conditions as an inner stick region and outer slip regions. Ciavarella [23] generalised Cattaneo’s contact problem at the end of the 20th century, by formulating the problem in the slip regions as integral equations rather than conditions on displacement. The development of adhesive contact problems were led by Mossakovskii [70], who used an incremental approach which was later used in both used in Goodman [40] and Borodich and Keer [16]. Alternatively, Spence [90] showed that a self-similar approach for contact problems may be used instead of the incremental one, with Spence’s approach making use of the scalar Wiener–Hopf technique also. Spence formulated this approach by considering parabolic indenters and imposed the self-similar property that the ratio of the stick-slip zones remain constant. The use of self-similarity has been implemented further in Borodich and Galanov [15], which investigated the effects of varying the punch profile and frictional behaviour. As discussed in chapter 1, Zhupanska and Ulitko [102], Zhupanska [101] modelled the deformation of an elastic half-space due to a rigid cylindrical indenter, however, the model presented by Zhupanska and Ulitko [102] appears to be non-unique and so we consider a steady rolling cylindrical indenter to compensate.

In general, for a rigid cylinder rolling along and indenting an elastic half-space, some of the contact region will be sticking and the rest will be slipping. A stick-slip regime would lead to a 4×4 Wiener–Hopf problem, which is considered in chapter 5. However in this chapter, we consider the regime where the contact region is entirely slipping and this leads to a 2×2 Wiener–Hopf problem instead. The full-slip regime occurs from a sufficiently large or sufficiently small angular velocity, Ω , and is derived in chapter 2. This regime, which by analogy to a car may be thought of as a “wheel spin” or “locked braking wheel” regime, is largely ignored in the literature, although

it is discussed by O’Sullivan and King [76] and Wang et al. [97]. It is worth noting that Zhupanska and Ulitko [102] considers a full-stick simplification instead of full-slip and used a conformal mapping method to derive a scalar (1×1) Wiener–Hopf problem, but it is difficult to generalise to the rolling cylinder case as it cannot be assumed that the contact region is symmetric.

The problem posed here will turn out to result in a 2×2 matrix Wiener–Hopf problem, amenable to solutions using various methods based on the Wiener–Hopf technique [e.g. 74]. Such solution methods are well understood in the 1×1 scalar case [e.g. 54], but are more difficult in the matrix case, and no universal method of solution is known; a review of approaches to solving matrix Wiener–Hopf problems is given by Rogosin and Mishuris [85]. In particular, there is only a small class of matrix Wiener–Hopf problems which may be solved exactly [29]. Otherwise approximate methods are required, with for example Padé approximants [3] having been successfully applied to problems in elastodynamics [4]. Another popular approximate method in electromagnetism is the use of Fredholm factorisation [30]. Instead, here we adopt an iterative method first developed by Kisil [56], intended to approximate the solution to 2×2 matrix Wiener–Hopf problems with exponential factors, which has successfully been applied to problems in acoustics [53], and has subsequently been extended to $n \times n$ matrices by Priddin et al. [81], including discussions on how to implement such a procedure numerically. The implementation requires numerical evaluations of Cauchy integrals (as in the scalar case), for which spectrally accurate numerical methods have been developed by Slevinsky and Olver [88], Olver [75], Trogdon and Olver [95]. We note in passing that Wiener–Hopf problems bear a close relationship to Riemann–Hilbert problems [55] and so one may alternatively frame the problem as a Riemann–Hilbert problem and solve that problem numerically [95, 63], although this is not pursued further here.

One final complication of our contact problem is that the location of the contact region itself is unknown, and is required to be solved as part of the problem [46]. Such free-boundary problems are inherently more complicated

than comparable problems where the location of the boundary is fixed or is known a priori, and there is no generally applicable methodology for solving free-boundary problems [47]. One typical approach in contact mechanics is to frame the problem as a variational inequality [33, 35]. An analytical method involving the use of Mellin transforms [28] has also been used in certain cases. Here, we adopt an iterative procedure to re-estimate the contact region based on the solution of the previous estimate, to ensure continuity of the solution on the surface. This technique is specific to the Wiener–Hopf-based solution method used, which in general results in discontinuities at the transitions between boundary conditions.

A description of the physical problem to be solved, together with its mathematical formulation, is given in section 4.2, explicitly stating the boundary conditions and their domains in the full-slip regime. Consideration of boundary conditions and taking the Fourier transform of them leads to the construction of the matrix Wiener–Hopf problem in section 4.3. This Wiener–Hopf problem is then solved using an iterative method in section 4.4, including details of the numerical implementation of the solution method in section 4.4.1. Details of the approach to the free-boundary problem is then presented in section 4.5, illustrated with some numerical results. The results of this analysis and numerics is presented in section 4.6 for a variety of parameters. Finally, in section 4.7, conclusions are discussed along with avenues for potential future research. An extension to a two roller model is discussed in appendix C, with an alternative full-stick model considered in appendix B.

4.2 Mathematical formulation

Consider the system as in the schematic, figure 4.2.1. A cylinder of radius R is pushed into an elastic half-space $y < 0$ with a force \mathbf{F} , resulting in an indentation of depth ϵ and is in contact with the half-space between points $-a$ and d . The entire contact region is in a state of slip, with the direction of slip determined by the roller. The rest of this system is outlined in section

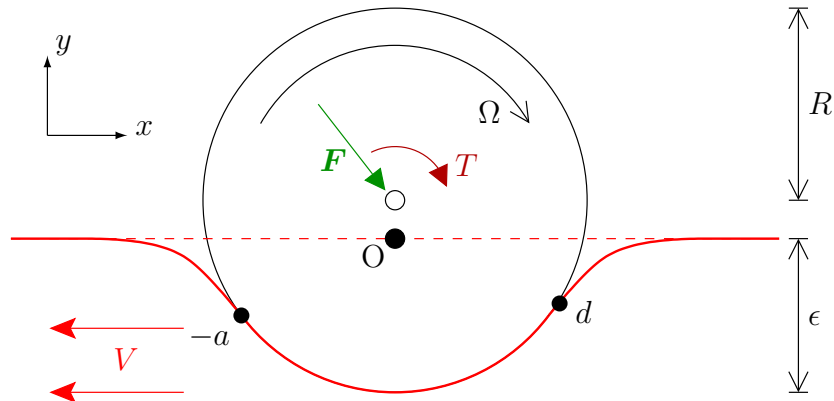


Figure 4.2.1: A schematic of a cylinder rolling along an elastic half-space.

The cylinder moves at a linear velocity V in the x -direction along the elastic half-space. The origin of the coordinate system (labelled O) is taken in a frame of reference moving with the cylinder, directly below the centre of the cylinder at the height of the undeformed elastic surface. The cylinder is in contact with the elastic surface between the points $-a$ and d . The cylinder of radius R rolls about its centre axis with angular velocity Ω , and a force \mathbf{F} and torque T are applied to the centre of the cylinder, causing the cylinder to be indented by ϵ into the elastic half-space.

2.1, so please refer there for the definition of terms.

4.2.1 Boundary conditions

As in the system above, a cylinder rotates on the surface of an elastic half-space, with the cylinder in contact with the surface in the region $-a \leq x \leq d$. The points $-a$ and d are unknown and are to be found as part of the solution. The surface of the half-space is displaced by the rigid cylinder and may not penetrate the cylinder due to a lack of permeability. The half-space slips beneath the cylinder and experiences a frictional effect due to the slipping, where the frictional effect is that of Coulomb friction. Outside of the contact region, the surface of the half-space is free from any stress and so a traction-free boundary condition is imposed, as shown in figure 4.2.2. The resultant mathematical problem is a mixed-free-boundary problem, with two boundary conditions in each region.

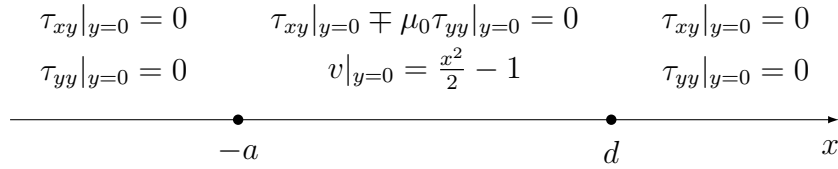


Figure 4.2.2: A diagram of the full-slip boundary conditions on the half-space.

The nonlinear derivation of the boundary conditions from the physical system can be found in section 2.4, with the linearisation of the nonlinear boundary conditions found in section 2.3. The mathematical equivalent to the physical properties are applied to the system shown in the schematic. In this chapter the frictional behaviour is that of full-slip, which gives the following boundary conditions and domains,

$$\text{Contact:} \quad v(x, 0) = \frac{x^2}{2} - 1, \quad \text{for } -a \leq x \leq d, \quad (4.1)$$

$$\text{Slip:} \quad \tau_{xy} \mp \mu_0 \tau_{yy}(x, 0) = 0, \quad \text{for } -a \leq x \leq d, \quad (4.2)$$

$$\text{Stress-free:} \quad \tau_{xy}(x, 0) = \tau_{yy}(x, 0) = 0, \quad \text{for } x < -a, d < x. \quad (4.3)$$

The direction of slip may be in either the forwards (−) or backwards (+) direction and it is determined by the angular velocity of the cylinder.

In summary, there are two boundary conditions in each region with the junctions between these regions being the unknown free-boundary points $-a$ and d . The boundary conditions may be formulated into a matrix Wiener–Hopf problem which is then solved numerically. To locate the free-boundary points an inverse method is sought which iteratively estimates the points by ensuring continuity of the solution.

4.2.2 General solution

We consider the same governing equations as in section 2.4 so use the same general solution derived there, please refer to section 2.4 for the details. We

quote the resultant general solution below

$$\begin{aligned} u(x, y) &= \frac{1}{2\pi} \int_{-\infty}^{\infty} \left[\hat{A}_1(k) \hat{B}_1(k) e^{y\gamma_1(k)} + A_2(k) e^{y\gamma_2(k)} \right] e^{-ikx} dk, \\ v(x, y) &= \frac{1}{2\pi} \int_{-\infty}^{\infty} \left[\hat{A}_1(k) e^{y\gamma_1(k)} + A_2(k) B_2(k) e^{y\gamma_2(k)} \right] e^{-ikx} dk, \end{aligned} \quad (4.4)$$

where

$$\begin{aligned} \gamma_1(k) &= \sqrt{k^2 - \frac{\rho V^2}{\lambda + 2\mu} (\omega + k)^2}, & \gamma_2(k) &= \sqrt{k^2 - \frac{\rho V^2}{\mu} (\omega + k)^2} \\ \hat{B}_1(k) &= \frac{-ik}{\gamma_1(k)} = \frac{1}{\sqrt{\frac{\rho V^2 (1 + \frac{\omega}{k})^2}{\lambda + 2\mu} - 1}}, & B_2(k) &= \frac{ik}{\gamma_2(k)} = -\frac{1}{\sqrt{\frac{\rho V^2 (1 + \frac{\omega}{k})^2}{\mu} - 1}}. \end{aligned}$$

with $\hat{A}_1(k)$ and $A_2(k)$ unknown and are to be found as part of our solution.

4.3 Constructing the matrix Wiener–Hopf equation

The general solution was found by Fourier transforming the governing equations and solving a fourth order polynomial in the Fourier domain. To make further progress, information from the mixed boundary values is required. The transformation of the mixed boundary value problem is troublesome due to the intervals of the spatial domain that the boundary conditions exist over, hence, half-range transforms are used and defined in section 3.2.1 to represent finite range transforms.

The transformed boundary conditions may be assembled into a format where a Wiener–Hopf technique may be applied. In this case a matrix Wiener–Hopf equation is formed, where only very few exact solutions exist. Careful construction of the matrix Wiener–Hopf equation ensures that a format is

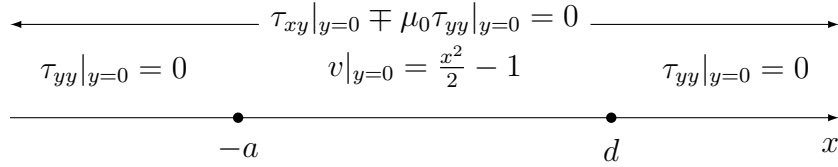


Figure 4.3.1: A diagram of the rearranged full-slip boundary conditions on the half-space.

assembled where the iterative method by Priddin et al. [81] may be applied.

4.3.1 Transformation of the boundary conditions

To construct the simplest matrix Wiener–Hopf equation, it is necessary to consider the boundary conditions carefully. By rearranging the boundary conditions, the size of the matrix Wiener–Hopf equation may be halved. We shall transform each boundary condition over their respective regions and assemble them to form a matrix Wiener–Hopf equation, with a structure suitable for the iterative method to be applied. To enable the application of the iterative method by Priddin et al. [81], the matrices are required to be triangular and have the correct analyticity of the exponential terms.

The first strategy is to minimise the number of junctions between boundary conditions. The key reduction is to rewrite the stress-free boundary conditions (4.3) to include the slip boundary condition (4.2), as shown in figure 4.3.1. Recall the stress-free boundary conditions (4.3) and manipulate to find

$$\tau_{xy}(x, 0) = \tau_{yy}(x, 0) = 0 \iff \tau_{xy} \mp \mu_0 \tau_{yy}(x, 0) = \tau_{yy}(x, 0) = 0.$$

Therefore, the slip boundary condition holds across the entire surface of the half-space and only normal stress is considered outside of the contact region

$$\text{Slip:} \quad \tau_{xy} \mp \mu_0 \tau_{yy}(x, 0) = 0, \quad \text{for } -\infty < x < \infty, \quad (4.5)$$

$$\text{Stress-free:} \quad \tau_{yy}(x, 0) = 0, \quad \text{for } x < -a \ \& \ d < x. \quad (4.6)$$

4.3. CONSTRUCTING THE MATRIX WIENER–HOPF EQUATION 4.3

This rearrangement reduces the number of junctions from four to two which gives a 2×2 matrix Wiener–Hopf equation.

Then by taking a full-range transform of the slip boundary condition (4.5) the following is derived

$$\tau_{xy} \widetilde{\mp} \mu_0 \tau_{yy}(k) = 0 \Rightarrow \hat{A}_1(k) = -\frac{m_2^{\mp}(k)}{m_1^{\mp}(k)} A_2(k) = n(k) A_2(k), \quad (4.7)$$

where the functions $m_i^{\mp}(k)$ are defined from the full-range transforms in (4.12). The rearrangement of the boundary conditions leads to a relationship between $\hat{A}_1(k)$ and $A_2(k)$, which halves the number of unknowns in the system. In this instance reducing the number of junctions reduces the number of unknowns which leads to the reduction in the size of the matrix Wiener–Hopf equation.

To derive the Wiener–Hopf problem the unknown variables will be defined from the half-range transforms of $v(x, 0)$ and $\tau_{yy}(x, 0)$. Recall the boundary conditions (4.1) and (4.6), then taking a full-range transform,

$$\widetilde{\tau}_{yy}(k) = e^{ikd} \widetilde{\tau}_{yy-}^{(d)}(k) = e^{-ika} \widetilde{\tau}_{yy+}^{(-a)}(k), \quad (4.8)$$

$$\widetilde{v}(k) = e^{ikd} \widetilde{v}_+^{(d)}(k) + e^{-ika} \widetilde{v}_-^{(-a)}(k) + f(k), \quad (4.9)$$

where the function $f(k)$ has been defined by the finite transformation

$$\begin{aligned} f(k) &= \int_{-a}^d \left(\frac{x^2}{2} - 1 \right) e^{ikx} dx \\ &= \frac{e^{-ika}}{ik} \left(1 - \frac{a^2}{2} - \frac{a}{ik} + \frac{1}{k^2} \right) - \frac{e^{ikd}}{ik} \left(1 - \frac{d^2}{2} + \frac{d}{ik} + \frac{1}{k^2} \right). \end{aligned}$$

These two scalar Wiener–Hopf equations shall then be manipulated to form the matrix Wiener–Hopf equation by eliminating the full-range transform variables, $\widetilde{\tau}_{yy}(k)$ and $\widetilde{v}(k)$.

4.3.2 Assembling the matrix Wiener–Hopf equation

As in section 3.2, we assemble the matrix Wiener–Hopf equation by relating the two full-range transformed variables $\widetilde{\tau}_{yy}(k)$ and $\widetilde{v}(k)$. We may find this relationship by considering all of the full-range transformations in terms of $\hat{A}_1(k)$ and $A_2(k)$,

$$\begin{aligned}\widetilde{\tau}_{yy}(k) &= \left[(\lambda + 2\mu)\gamma_1 - ik\lambda\hat{B}_1 \right] \hat{A}_1 \\ &\quad + \left[(\lambda + 2\mu)B_2\gamma_2 - ik\lambda \right] A_2 \\ &= n_1(k)\hat{A}_1 + n_2(k)A_2,\end{aligned}\tag{4.10}$$

$$\widetilde{v}(k) = \hat{A}_1 + B_2(k)A_2,\tag{4.11}$$

$$\begin{aligned}\tau_{xy} \mp \mu_0 \widetilde{\tau}_{yy}(k) &= \left[\mu(\gamma_1\hat{B}_1 - ik) \mp \mu_0 \left((\lambda + 2\mu)\gamma_1 - \hat{B}_1 ik\lambda \right) \right] \hat{A}_1 \\ &\quad + \left[\mu(\gamma_2 - ikB_2) \mp \mu_0 \left((\lambda + 2\mu)B_2\gamma_2 - ik\lambda \right) \right] A_2 \\ &= m_1^\mp(k)\hat{A}_1 + m_2^\mp(k)A_2,\end{aligned}\tag{4.12}$$

where the functions $n_1(k)$, $n_2(k)$, $m_1^\mp(k)$ and $m_2^\mp(k)$ are defined by the above. We note that these are the exact same functions found in section 3.2.

To construct the matrix Wiener–Hopf equation we eliminate $\hat{A}_1(k)$ and $A_2(k)$ from the equations (4.7), (4.10) and (4.11). As these equations are the same as those found in section 3.2, we arrive at a similar relationship for $\widetilde{\tau}_{yy}(k)$ and $\widetilde{v}(k)$,

$$\frac{\widetilde{\tau}_{yy}(k)}{n_2(k)m_1^\pm(k) - n_1(k)m_2^\pm(k)} = \frac{\widetilde{v}(k)}{B_2(k)m_1^\pm(k) - m_2^\pm(k)}.$$

The full-range transformed variables may now be replaced with their half-range counterparts from (4.8) and (4.9) to find the two coupled scalar Wiener–

Hopf equations

$$\begin{aligned} K(k)e^{ikd}\widetilde{\tau_{yy}}_{-}^{(d)}(k) &= e^{ikd}\widetilde{v}_{+}^{(d)}(k) + e^{-ika}\widetilde{v}_{-}^{(-a)}(k) + f(k), \\ K(k)e^{-ika}\widetilde{\tau_{yy}}_{+}^{(-a)}(k) &= e^{ikd}\widetilde{v}_{+}^{(d)}(k) + e^{-ika}\widetilde{v}_{-}^{(-a)}(k) + f(k). \end{aligned}$$

These two equations are assembled into a matrix Wiener–Hopf equation and rearranged to impose the necessary structure for the iterative method to be applied. Hence, we arrive at the following (2×2) matrix Wiener–Hopf equation,

$$\begin{pmatrix} 1 & 0 \\ -e^{ik(a+d)} & K(k) \end{pmatrix} \begin{pmatrix} \widetilde{v}_{+}^{(d)}(k) \\ \widetilde{\tau_{yy}}_{+}^{(-a)}(k) \end{pmatrix} = \begin{pmatrix} K(k) & -e^{-ik(a+d)} \\ 0 & 1 \end{pmatrix} \begin{pmatrix} \widetilde{\tau_{yy}}_{-}^{(d)}(k) \\ \widetilde{v}_{-}^{(-a)}(k) \end{pmatrix} + \begin{pmatrix} -e^{-ikd}f(k) \\ e^{ika}f(k) \end{pmatrix}. \quad (4.13)$$

The function $K(k)$ is found by rearranging the transformed boundary conditions and is

$$K(k) = \frac{n(k) + B_2(k)}{n_1(k)n(k) + n_2(k)}, \quad \text{with } K(k) = O\left(\frac{1}{|k|}\right) \text{ as } |k| \rightarrow \infty.$$

It is now possible to apply the iterative method to the matrix Wiener–Hopf problem as the exponential terms are of the required analyticity and the matrices have the required structure. The unknowns in the problem are $\widetilde{v}_{+}^{(d)}(k)$ and $\widetilde{\tau_{yy}}_{+}^{(-a)}(k)$ analytic in \mathcal{D}^+ , with $\widetilde{\tau_{yy}}_{-}^{(d)}(k)$ and $\widetilde{v}_{-}^{(-a)}(k)$ analytic in \mathcal{D}^- .

To ensure that the least singular solutions are found, it is required that $\widetilde{v}_{+}^{(d)}(k)$, $\widetilde{\tau_{yy}}_{+}^{(-a)}(k)$ and $\widetilde{\tau_{yy}}_{-}^{(d)}(k)$, $\widetilde{v}_{-}^{(-a)}(k)$ decay to 0 as $|k| \rightarrow \infty$ in their respective half-planes. This behaviour may be ensured by imposing the edge conditions. For normal stress we find

$$\tau_{yy}(x, 0) \rightarrow 0, \text{ as } x \rightarrow -a^+, \quad \tau_{yy}(x, 0) \rightarrow 0, \text{ as } x \rightarrow d^-.$$

These two edge conditions ensure that the variables $\widetilde{\tau_{yy}}_{+}^{(-a)}(k)$ and $\widetilde{\tau_{yy}}_{-}^{(d)}(k)$

decay quadratically. Whereas the edge conditions for the vertical displacement

$$v(x, 0) \rightarrow \frac{a^2}{2} - 1, \text{ as } x \rightarrow -a^-, \quad v(x, 0) \rightarrow \frac{d^2}{2} - 1, \text{ as } x \rightarrow d^+,$$

ensures linear decay for $\tilde{v}_-^{(-a)}(k)$ and $\tilde{v}_+^{(d)}(k)$.

These edge conditions are imposed to ensure continuity at the transition point and hence to ensure continuity of the solution. The normal stress, $\tau_{yy}(x, 0)$, is known in the stress-free region and the vertical displacement, $v(x, y)$, is known in the contact region. For the solution to be continuous, we require that these boundary conditions are valid at the point of transition. The imposition of the continuity conditions on the boundary conditions in their unknown regions leads us to derive the asymptotic behaviour of the unknown half-range functions.

4.4 Application of the iterative method

The mathematical formulation of the physical problem has been derived and formulated into a matrix Wiener–Hopf problem. The presence of the exponential factors in the matrix Wiener–Hopf (4.13) suggests applying the approximate factorisation method developed by [56, 81] is suitable. The arrangement of the Wiener–Hopf problem into triangular matrices gives further structure to enable the factorisation more easily. The method considers a matrix Wiener–Hopf such as (4.13) and approximates the exponential terms to zero. Once an initial approximation has been made the matrix Wiener–Hopf equation may be considered as a series of scalar Wiener–Hopf equations. In these scalar equations one may use additive and multiplicative decompositions to arrive at a form in which Liouville’s Theorem may be applied. The approximation is corrected for by iterating through the scalar equations with the exponential terms reintroduced, and additively decomposing the correction term into a form where Liouville’s may be applied again.

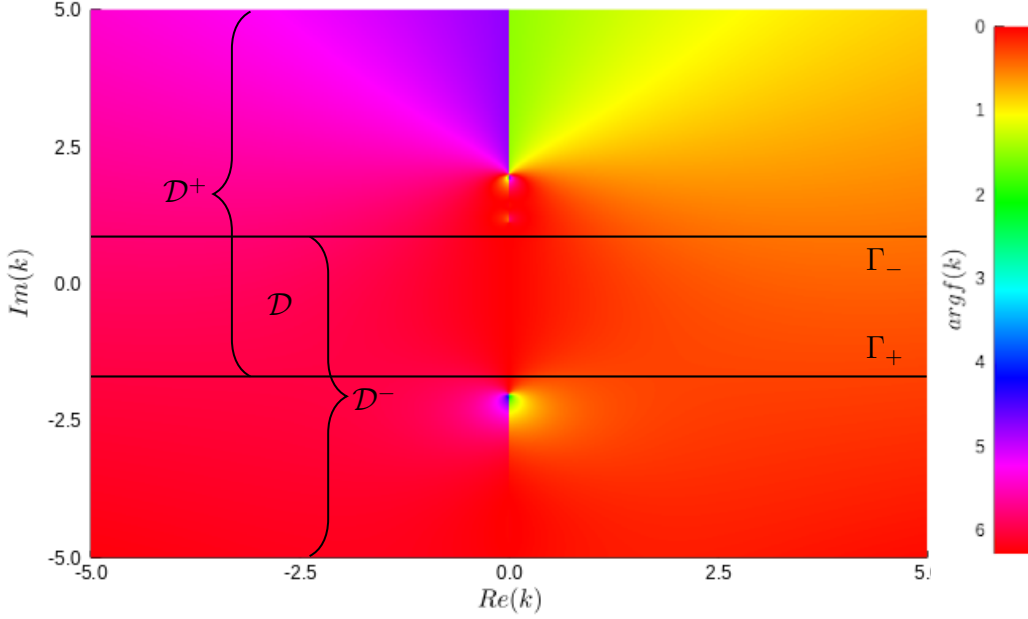


Figure 4.4.1: A figure of the phase-portrait for $K(k)$ with Metal parameters 4.1 and $\omega = -5i$.

To signify that the process is iterative, we introduce the notation $\tilde{\phi}_{\pm}^{(L)n}(k)$ as the n -th iteration of $\tilde{\phi}_{\pm}^{(L)}(k)$. Recalling (4.13) and taking the initial estimate,

$$\begin{pmatrix} 1 & 0 \\ 0 & K(k) \end{pmatrix} \begin{pmatrix} \tilde{v}_{+}^{(d)0} \\ \tilde{\tau}_{yy+}^{(-a)0} \end{pmatrix} = \begin{pmatrix} K(k) & 0 \\ 0 & 1 \end{pmatrix} \begin{pmatrix} \tilde{\tau}_{yy-}^{(d)0} \\ \tilde{v}_{-}^{(-a)0} \end{pmatrix} + \begin{pmatrix} -e^{-ikd}f(k) \\ e^{ika}f(k) \end{pmatrix}.$$

The justification for making such an approximation stems from the choice of inverse contours one may take in the overlapping strip of analyticity \mathcal{D} , with the strip demonstrated in figure 4.4.1. As one may take an inversion contour anywhere within the strip in figure 4.4.1, choosing a contour near the bottom of the strip would set $e^{-ik(a+d)}$ to be close to zero, likewise an inversion contour near the top of the strip would set $e^{ik(a+d)}$ to be close to zero, hence justifying the initial approximation to set both exponential terms to zero.

One may see that both rows of the approximated matrix Wiener–Hopf problem may now be solved, subject to decompositions. Considering each of the

scalar Wiener–Hopf equations from the matrix separately gives,

$$\tilde{v}_+^{(d)0}(k) = K(k)\widetilde{\tau}_{yy-}^{(d)0}(k) - e^{-ikd}f(k), \quad (4.14)$$

$$K(k)\widetilde{\tau}_{yy+}^{(-a)0}(k) = \tilde{v}_-^{(-a)0}(k) + e^{ika}f(k). \quad (4.15)$$

Referring to (4.14), one may take a multiplicative factorisation of $K(k)$ and divide through by $K_+(k)$ and then apply an additive decomposition to the resulting forcing term to give

$$\frac{\tilde{v}_+^{(d)0}(k)}{K_+(k)} = K_-(k)\widetilde{\tau}_{yy-}^{(d)0}(k) - \left[\frac{e^{-ikd}f(k)}{K_+(k)} \right]^+ - \left[\frac{e^{-ikd}f(k)}{K_+(k)} \right]^-.$$

The regions of analyticity may be extended to the entire complex plane via analytic continuation [74], so we may introduce an entire function $J(k)$ such that,

$$\frac{\tilde{v}_+^{(d)0}(k)}{K_+(k)} + \left[\frac{e^{-ikd}f(k)}{K_+(k)} \right]^+ = K_-(k)\widetilde{\tau}_{yy-}^{(d)0}(k) - \left[\frac{e^{-ikd}f(k)}{K_+(k)} \right]^- \equiv J(k).$$

Liouville’s theorem may be applied to the above since we ensured $\widetilde{\tau}_{yy-}^{(d)0}(k) \sim k^{-2}$ as $k \rightarrow \infty$ and the exponential decay of the forcing gives $J(k) = 0$. Applying Liouville’s theorem leads to the initial approximate solutions,

$$\tilde{v}_+^{(d)0}(k) = -K_+(k) \left[\frac{e^{-ikd}f(k)}{K_+(k)} \right]^+, \quad \widetilde{\tau}_{yy-}^{(d)0}(k) = \frac{1}{K_-(k)} \left[\frac{e^{-ikd}f(k)}{K_+(k)} \right]^-.$$

Applying the same argument for equation (4.15) leads to the following initial solutions,

$$\tilde{v}_-^{(-a)0}(k) = -K_-(k) \left[\frac{e^{ika}f(k)}{K_-(k)} \right]^-, \quad \widetilde{\tau}_{yy+}^{(-a)0}(k) = \frac{1}{K_+(k)} \left[\frac{e^{ika}f(k)}{K_-(k)} \right]^+.$$

For subsequent iterations we refer back to the scalar equations in (4.13). The exponential terms are reintroduced and we may continue to use the Wiener–Hopf technique iteratively, so we define the n -th iteration of the equations in (4.16) and (4.17). As in the initial approximation, consider each row of the

matrix Wiener–Hopf problem as scalar equations once again,

$$\tilde{v}_+^{(d)n}(k) = K(k)\tilde{\tau}_{yy-}^{(d)n}(k) - e^{-ik(a+d)}\tilde{v}_-^{(-a)n-1}(k) - e^{-ikd}f(k), \quad (4.16)$$

$$K(k)\tilde{\tau}_{yy+}^{(-a)n}(k) = \tilde{v}_-^{(-a)n}(k) + e^{ik(a+d)}\tilde{v}_+^{(d)n}(k) + e^{ika}f(k). \quad (4.17)$$

We solve each row by treating the reintroduced coupled terms as an additional forcing term by using its most recent approximation.

Then one may simply iterate through these equations, updating the n -th iteration with the solutions from the $n-1$ -th iteration. Explicitly, the solution to the n -th iteration equations will be

$$\begin{aligned} \tilde{v}_+^{(d)n}(k) &= -K_+(k) \left(\left[\frac{e^{-ikd}f(k)}{K_+(k)} \right]^+ + \left[\frac{e^{-ik(a+d)}\tilde{v}_-^{(-a)n-1}}{K_+(k)} \right]^+ \right), \\ \tilde{\tau}_{yy-}^{(d)n}(k) &= \frac{1}{K_-(k)} \left(\left[\frac{e^{-ikd}f(k)}{K_+(k)} \right]^- + \left[\frac{e^{-ik(a+d)}\tilde{v}_-^{(-a)n-1}}{K_+(k)} \right]^- \right), \\ \tilde{v}_-^{(-a)n}(k) &= -K_-(k) \left(\left[\frac{e^{ika}f(k)}{K_-(k)} \right]^- + \left[\frac{e^{ik(a+d)}\tilde{v}_+^{(d)n}}{K_-(k)} \right]^- \right), \\ \tilde{\tau}_{yy+}^{(-a)n}(k) &= \frac{1}{K_+(k)} \left(\left[\frac{e^{ika}f(k)}{K_-(k)} \right]^+ + \left[\frac{e^{ik(a+d)}\tilde{v}_+^{(d)n}}{K_-(k)} \right]^+ \right). \end{aligned}$$

The overview of the iterative method has omitted details on the computation of the Wiener–Hopf splittings, which shall be examined in the next section. Our implementation of the iterative method typically converges to a precision of 10^{-8} within three or four iterations, where we define convergence to be the difference between consecutive iterations at an arbitrary point on the real line. There is no general discussion of convergence for the iterative method however there are some comprehensive studies in [81] and [56] which examine scattering by n -plates and a 2×2 case respectively. To find the solution all that one needs to compute is the Wiener–Hopf splittings, however, to implement this in a practical sense it is best to proceed numerically.

4.4.1 Wiener–Hopf splittings

To implement the iterative method it is necessary to develop a numerical approach to accurately compute the decompositions at each iteration. For this purpose we use a spectral method developed by Olver [75] which more generally is a numerical technique to compute singular integrals both accurately and fast.

To illustrate the spectral method in greater detail, consider a function $f(k)$, which one wishes to additively decompose numerically. To perform such a decomposition, a Cauchy transform may be used and calculated via the spectral method [88]. Thus, the first step is to expand f in a weighted orthogonal polynomial basis,

$$f(k) \approx w(k) \sum_{j=0}^{n-1} f_j p_j(k),$$

where the sequence of polynomials $p_j(x)$ is orthogonal with respect to the weight $w(x)$. Throughout we use Chebychev polynomials of the first kind as the orthogonal basis. Then taking the Cauchy transform gives

$$\mathcal{C}f(k) \approx \sum_{j=0}^{n-1} f_j \mathcal{C}[w p_j](k),$$

which is quick to compute as the Cauchy transform of the weighted polynomials satisfies a three-term recurrence relation [95]. The Cauchy transforms of these functions are typically calculated for the unit interval $\mathbb{I} = [-1, 1]$, and mapped to the contour that one desires through certain mappings.

We recall the classical result that orthogonal polynomials satisfies the three-term recurrence relationship found in appendix A. Then taking the Cauchy transform of the polynomial basis satisfies the same recurrence relation-

which decays at infinity and has branch cut singularities along $(-\infty i, c_1 i)$ and $(c_2 i, \infty i)$ ¹ as shown in figure 4.4.1. Therefore, we consider these contours for the factorisation

$$\begin{aligned}\Gamma_+ &= \{k \in \mathbb{C} : \text{Im}(k) = c_1 \forall k\}, \\ \Gamma_- &= \{k \in \mathbb{C} : \text{Im}(k) = c_2 \forall k\},\end{aligned}$$

which is illustrated in figure 4.4.1 additionally.

Trogon and Olver [95] and Llewellyn Smith and Luca [63] show that various mappings on the interval, \mathbb{I} , may be used with Plemelj's lemma to prove that a Cauchy transform of a contour may be expressed as mapped Cauchy transforms. The implementation here makes use of two mappings in particular, a linear map $l_i(k) = k + c_i$ for $i = 1, 2$, and the real line map developed by Llewellyn Smith and Luca [63], $r(k) = \frac{k+k^3}{(1-k^2)^2}$. Observe that by using both mappings together, one can map the contours Γ_{\pm} to the interval \mathbb{I} , this can be done in the following way $\Gamma_{\pm} = l_i(r([-1, 1])) = \{l_i(r(x)) : -1 \leq x \leq 1\}$ thus

$$\begin{aligned}\mathcal{C}_{\Gamma_{\pm}}[f](k) &= \mathcal{C}_{\mathbb{R}}[f \circ l_i](l_i^{-1}(k)) \\ &= \sum_{j=1}^4 \mathcal{C}_{[-1,1]}[f \circ l_i \circ r](r_j^{-1}(l_i^{-1}(k))) \\ &\quad - 2\mathcal{C}_{[-1,1]}[f \circ l_i \circ r](l_i^{-1}(1)) - 2\mathcal{C}_{[-1,1]}[f \circ l_i \circ r](l_i^{-1}(-1)),\end{aligned}$$

where the functions l_i^{-1} and r_j^{-1} are inverses to l and r respectively, and the subtracted terms are to remove the behaviour at infinity. The Cauchy transform of the Γ_{\pm} contours can be expressed as the composition of multiple mappings as each mapped Cauchy transform satisfies Plemelj's lemma.

¹We define

$$c_1 = \frac{\rho V^2 \omega - V \omega \sqrt{2\rho(\lambda + \mu)}}{2(\lambda + \mu) - \rho V^2}, \quad c_2 = \frac{\rho V^2 \omega + V \omega \sqrt{2\rho(\lambda + \mu)}}{2(\lambda + \mu) - \rho V^2}.$$

and choose V to ensure $c_1 > 0$ and $c_2 < 0$.

Finally, we find $K_+(k)$ and $K_-(k)$ in the following way

$$\begin{aligned}
 K(k) &= \frac{e^{\log(\gamma(k)K(k))}}{\gamma(k)}, \\
 &= \frac{e^{[\log(\gamma(k)K(k))]^+ + [\log(\gamma(k)K(k))]^-}}{\gamma(k)}, \\
 &= \frac{e^{[\log(\gamma(k)K(k))]^+}}{\gamma_+(k)} \frac{e^{[\log(\gamma(k)K(k))]^-}}{\gamma_-(k)}, \\
 &= K_+(k) K_-(k).
 \end{aligned}$$

4.4.1.2 Wiener–Hopf decomposition

We seek to compute the additive decomposition of the forcing terms $F_1(k)$, $F_2(k)$, $\widehat{F}_1(k)$ and $\widehat{F}_2(k)$ where each function contains branch cut singularities and exponentially grows in one of the half-planes. To compute the decompositions efficiently, the exponential term must be carefully considered, as it leads to numerical instabilities and exponential growth. To combat the instabilities, one may deform the integration contour onto the steepest descent contour for the integrand, which turns oscillatory behaviour into exponential decay. To calculate the Cauchy transforms on the steepest descent contours, quadratic maps have been used to map the contour back to the real line. There is a developing alternative method by Trogdon [94], which uses a special polynomial basis for evaluating the Cauchy transform of oscillatory functions however this work is ongoing.

To avoid the exponential growth when computing the Cauchy transforms, we only compute the decompositions where the integrand decays exponentially along the steepest descent contour, and use the relationship $F(k) = F^+(k) + F^-(k)$ to find the value of the remaining term. For example, to find the additive decomposition of the forcing term, $F_1(k) = \frac{e^{ika} f(k)}{K_-(k)}$, we may efficiently compute $F_1^-(k)$ by considering its Cauchy transform and applying steepest descents as the integrand decays in \mathcal{D}^+ . Then the upper component, $F_1^+(k)$, may be found by using $F_1^+(k) = F_1(k) - F_1^-(k)$, thus avoiding

computations involving the exponential growth in \mathcal{D}^- . Therefore, by applying steepest descents to the integrand in the Cauchy transforms we may efficiently compute them and avoid the exponential growth of the remaining term by using the additive relationship.

To compute the Cauchy transforms we require mappings to the unit interval, \mathbb{I} . Similar to section 4.4.1.1, we make use of the real line map developed by Llewellyn Smith and Luca [63] but use a quadratic mapping instead. Trogdon and Olver [95] shows that polynomial maps satisfy Plemelj's lemma provided they if a one-to-one mapping. Hence, we use the quadratic maps $p(k) = c_{1,2} + k \mp ik^2$, and the real line map, $r(k)$ to map the deformed contours Γ_{\pm} to the interval \mathbb{I} , i.e. $\Gamma_{\pm} = p(r([-1, 1])) = \{p(r(x)) : -1 \leq x \leq 1\}$ thus

$$\begin{aligned} \mathcal{C}_{\Gamma_{\pm}}[f](k) &= \sum_{i=1}^2 \mathcal{C}_{\mathbb{R}}[f \circ p](p_i^{-1}(k)) \\ &= \sum_{i=1}^2 \sum_{j=1}^4 \mathcal{C}_{[-1,1]}[f \circ p \circ r](r_j^{-1}(p_i^{-1}(k))) \\ &\quad - 2\mathcal{C}_{[-1,1]}[f \circ p \circ r](p_i^{-1}(1)) - 2\mathcal{C}_{[-1,1]}[f \circ p \circ r](p_i^{-1}(-1)), \end{aligned}$$

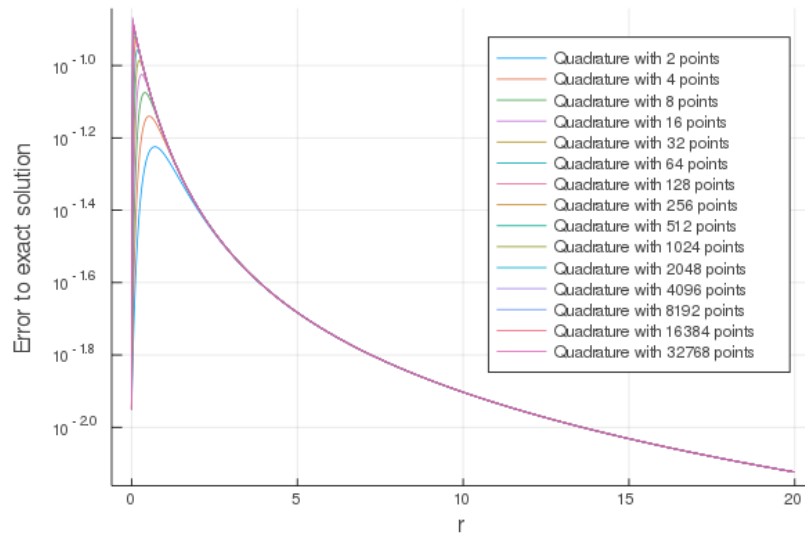
where the functions $p_i^{-1}(k)$ and $r_j^{-1}(k)$ are inverses to $p(k)$ and $r(k)$ respectively, and the behaviour at infinity is subtracted.

4.4.1.3 Convergence

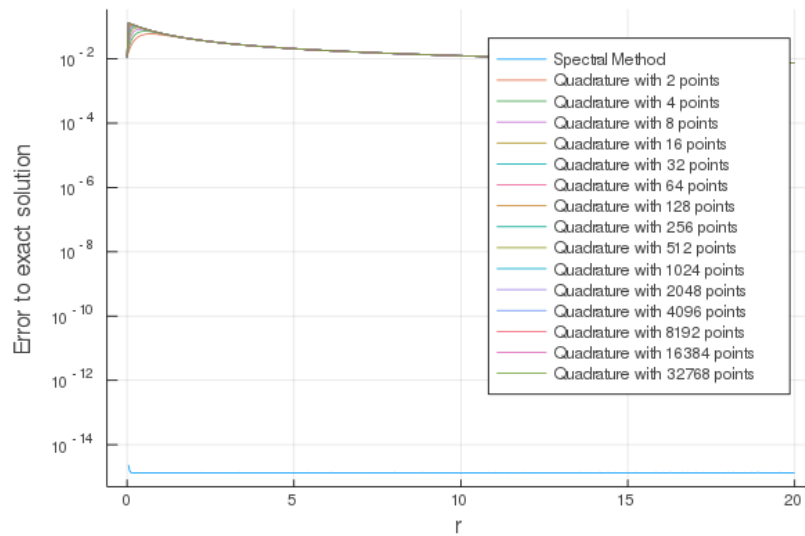
The accuracy of the numerical method used to compute the Cauchy transforms will be discussed here briefly. The standard method used to compute Cauchy transforms numerically is via a quadrature rule, which approximates the branch cut due to the contour Γ_{\pm} by a series of poles. This means a quadrature rule gives higher errors near to the contour, so one may deform the contour in line with Cauchy's integral theorem [1] away from the region of interest. More recently, there has been a move to compute Cauchy transforms (and more generally singular integrals) via a spectral method, as out-

lined by Slevinsky and Olver [88], Olver [75], and implemented numerically in the Julia software packages `SingularIntegralEquations`, `ApproxFun` and `WienerHopf`. An outline of this method is to expand a function in terms of weighted orthogonal polynomials and then compute the Cauchy transform on those polynomials to give a highly accurate numerical method but see section 4.4.1 for more details.

To illustrate the benefit of the spectral method over quadrature, figures have been included to show the error to the exact solution for a Gauss-Hermite quadrature rule (f_Q) and the spectral method (f_S). Figure 4.4.2a shows the exact error for the quadrature rule used to compute the upper decomposition of a test function $f(z) = \frac{1}{(z-8.5-8.5i)\sqrt{z+10i}}$, which has the upper decomposition $f_+(z) = \frac{1}{z-8.5-8.5i} \left[\frac{1}{\sqrt{z+10i}} - \frac{1}{\sqrt{8.5+18.5i}} \right]$. Figure 4.4.2a shows the error of the quadrature rule to the exact solution as $z = ri$ approaches the integration contour ($r \rightarrow 0$), where we see the error increases despite increasing the resolution of the quadrature rule. The figure, 4.4.2b, includes the exact error for the spectral method and the quadrature rule, where we see the error for the spectral method is close to machine precision up to the contour. A benefit of the spectral method is that it is highly accurate up to and on the contour.



(a) A plot of the errors from applying the Gauss-Hermite quadrature rule with increasing resolution.



(b) A plot comparing the errors from applying a Gauss-Hermite quadrature rule and the spectral method.

Figure 4.4.2: Plots of the exact error ($\|f(z) - f_+(z)\|_2$) of numerical methods to compute the upper decomposition of the function $f(z) = \frac{1}{(z-8.5-8.5i)\sqrt{z+10i}}$. The figures show the exact error with $z = ri$ in the interval $[0, 20]$ for 500 equidistant points.

A comparison is made between the two numerical methods as the methods are evaluated near the contour.

4.5 Free-boundary problem

Throughout it has been assumed that the contact points, $-a$ and d , are known. Taking this assumption allows a solution to be found where the junction points may be located as an inverse problem. The assumption enables the application of the matrix Wiener–Hopf technique to find a solution and then we implement an minimisation method which locates the junction points. The validation of the junction points is found by ensuring continuity of the solution as it approaches $-a$ and d . The minimisation method implemented here is the secant method [77], which re-estimates the junction points by locating the roots. There are two minimisation problems for each contact point and it is unclear which minimisation problem to impose, so we consider the example in section 4.5.1, which explains which minimisation problem we should solve.

We recall the edge conditions

$$\begin{aligned} \tau_{yy}(x, 0) &\rightarrow 0 \text{ as } x \rightarrow -a^+, & \tau_{yy}(x, 0) &\rightarrow 0 \text{ as } x \rightarrow d^-, \\ v(x, 0) &\rightarrow \frac{a^2}{2} - 1 \text{ as } x \rightarrow -a^-, & v(x, 0) &\rightarrow \frac{d^2}{2} - 1 \text{ as } x \rightarrow d^+. \end{aligned}$$

Imposing these edge conditions numerically gives a route for imposing a method to locate the contact points however it is only necessary to impose one of these conditions, which discussed in section 4.5.1. To formulate the minimisation problem more formally, the free-boundary problem is cast as the following minimisation problems,

$$\mathbf{min}_{\chi^j} \|\tau_{yy}^j(\chi^j, 0)\|, \quad \mathbf{min}_{\chi^j} \left\| v^j(\chi^j, 0) - \frac{\chi^{j2}}{2} + 1 \right\|.$$

We define the initial and j -th iteration junction points and solution which

corresponds as

$$\begin{aligned}\chi^0 &= (a^0, d^0), & \tau^0(x) &= \tau_{yy}^0(x, 0), & v^0(x) &= v^0(x, 0), \\ \chi^j &= (a^j, d^j), & \tau^j(x) &= \tau_{yy}^j(x, 0), & v^j(x) &= v^j(x, 0).\end{aligned}$$

To find an initial solution, we take two initial guesses of the junction points, χ^0, χ^1 and find the corresponding solutions $\tau_{yy}^0(x, 0), \tau_{yy}^1(x, 0)$ and $v^0(x, 0), v^1(x, 0)$. Then we find the subsequent iterations of junction point by implementing a secant method. We may find the $j + 1$ -th iteration of junction points, χ^{j+1} , by solving the following equations

$$\begin{aligned}\chi^{j+1} &= \left(a^j - \tau^j(-a^j) \left(\frac{a^j - a^{j-1}}{\tau^j(-a^j) - \tau^{j-1}(-a^{j-1})} \right), d^j - \tau^j(d^j) \left(\frac{d^j - d^{j-1}}{\tau^j(d^j) - \tau^{j-1}(d^{j-1})} \right) \right), \quad (4.18) \\ &= \left(a^j - v^j(-a^j) \left(\frac{a^j - a^{j-1}}{v^j(-a^j) - v^{j-1}(-a^{j-1})} \right), d^j - v^j(d^j) \left(\frac{d^j - d^{j-1}}{v^j(d^j) - v^{j-1}(d^{j-1})} \right) \right).\end{aligned}$$

This procedure is iterated until successive iterations are below a tolerance,

$$\|\chi^j - \chi^{j-1}\| \leq \text{tol}.$$

Once converged the final χ^j will give a solution where the junction points are accurately estimated and ensure continuity of the solution. In equation (4.18) it is clear that only one of the edge conditions need to be imposed and we find which one in the following.

The figures in 4.5.1 shows an implementation to find the free-boundary points $-a$ and d based on ensuring the continuity of $\tau_{yy}(x, 0)$, whereas the figures in 4.5.2 shows the results for ensuring the continuity of $v(x, 0)$. It is clear that we cannot simultaneously impose the continuity of both of these functions and so we must examine the asymptotic behaviour of the half-range variables to understand more. The large k asymptotic behaviour derived for continuous behaviour across the boundary for the half-range variables is

$$\tilde{v}_+^{(d)}(k) \sim \frac{2 - d^2}{2ik}, \quad \tilde{v}_-^{(-a)}(k) \sim \frac{a^2 - 2}{2ik}, \quad \tilde{\tau}_-^{(d)}(k) \sim \frac{C_2}{k^2}, \quad \tilde{\tau}_+^{(-a)}(k) \sim \frac{C_3}{k^2}.$$

However, when computing the behaviour for the solution we find the asymp-

otic behaviours

$$\tilde{v}_+^{(d)}(k) \sim \frac{C_d}{k^{\frac{3}{2}}}, \quad \tilde{v}_-^{(-a)}(k) \sim \frac{C_a}{k^{\frac{3}{2}}}, \quad \tilde{\tau}_-^{(d)}(k) \sim C_2, \quad \tilde{\tau}_+^{(-a)}(k) \sim C_3,$$

which may explain why the continuity of both functions may not be enforced. However in the special case where $a = d = \sqrt{2}$, the asymptotic behaviour

$$\tilde{v}_+^{(d)}(k) \sim \frac{C_d}{k^{\frac{3}{2}}}, \quad \tilde{v}_-^{(-a)}(k) \sim \frac{C_a}{k^{\frac{3}{2}}}, \quad \tilde{\tau}_-^{(d)}(k) \sim \frac{C_2}{k}, \quad \tilde{\tau}_+^{(-a)}(k) \sim \frac{C_3}{k}.$$

We discuss a short example in section 4.5.1 which clarifies which minimisation problem we should impose.

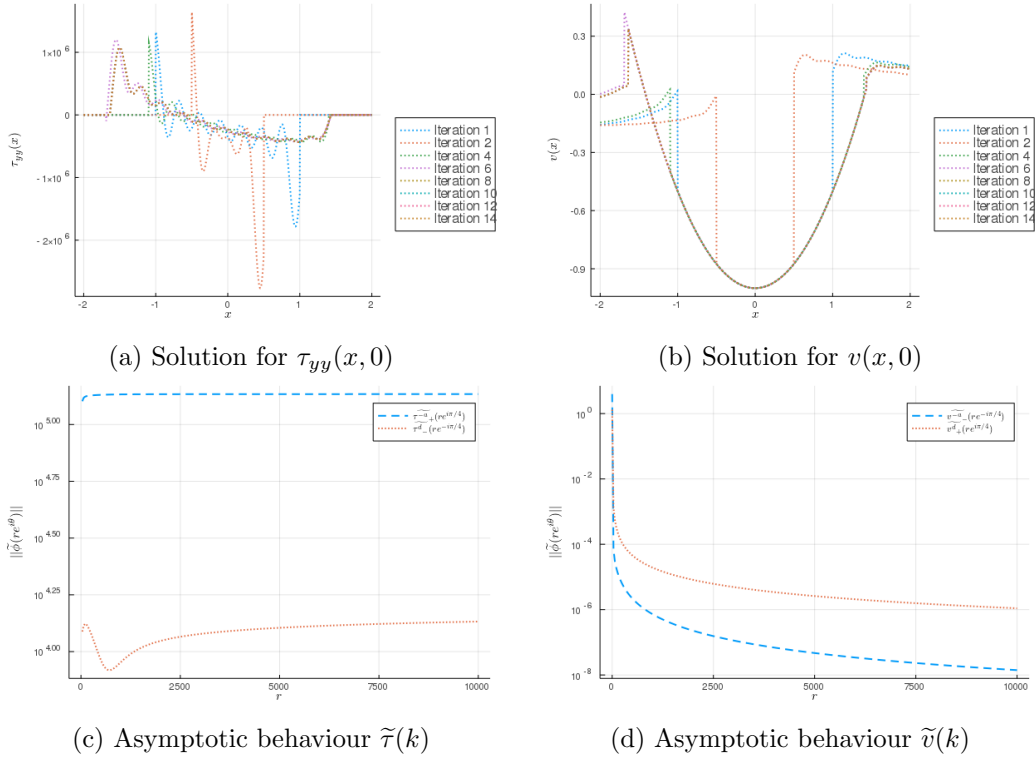


Figure 4.5.1: Plots of the solution and asymptotic behaviour for the Metal parameter values from table 4.1 and backwards slip. The contact points are determined by the continuity of $\tau(x, 0)$, and are found to be $-1.636, 1.4462$.

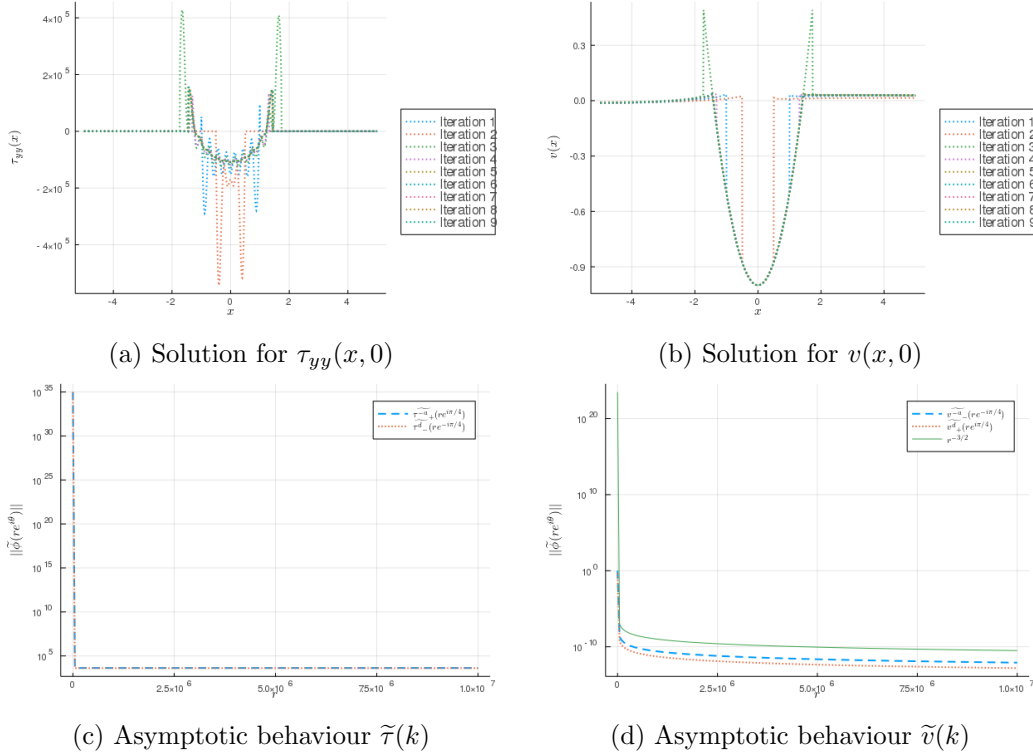


Figure 4.5.2: Plots of the solution and asymptotic behaviour for Metal parameter values from table 4.1 and backwards slip. The contact points are determined by the continuity of $v(x, 0)$, and are found to be $-1.4395, 1.4386$.

4.5.1 Example

This example shows how we should consider the Fourier inversion of $\tilde{v}(k)$ therefore indicating which edge condition the free-boundary method should be applied to. We explore the Fourier inversion of $\tilde{v}(k)$ and conclude that the edge conditions are satisfied if equation (4.19) is inverted rather the considering the inversion of the half-range functions as in equation (4.20). Consider the example

$$v(x) = \begin{cases} e^{-\lambda(x-d)} \left(\frac{d^2}{2} - 1 + \left(d + \lambda \left(\frac{d^2}{2} - 1 \right) \right) (x-d) \right), & d < x, \\ \frac{x^2}{2} - 1, & -a \leq x \leq d, \\ e^{\lambda(x+a)} \left(\frac{a^2}{2} - 1 + \left(-a - \lambda \left(\frac{a^2}{2} - 1 \right) \right) (x+a) \right), & x < -a. \end{cases}$$

By taking a full-range Fourier transform we may find the relationship

$$\tilde{v}(k) = e^{ikd}\tilde{v}_+^{(d)}(k) + e^{-ika}\tilde{v}_-^{(-a)}(k) + f(k)$$

This leads to the half range functions

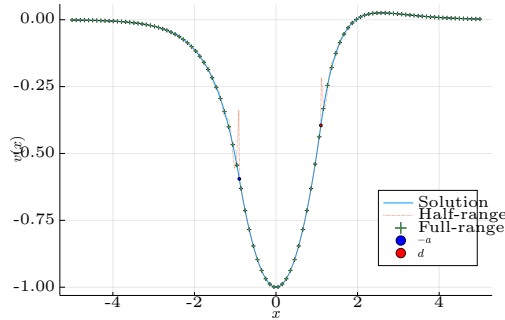
$$\begin{aligned}\tilde{v}_+^{(d)}(k) &= \frac{2-d^2}{2(ik-\lambda)} + \frac{2d+\lambda(d^2-2)}{2(ik-\lambda)^2}, \\ \tilde{v}_-^{(-a)}(k) &= \frac{a^2-2}{2(ik+\lambda)} + \frac{2a+\lambda(a^2-2)}{2(ik+\lambda)^2}.\end{aligned}$$

These functions have the large $|k|$ behaviour we would expect from the edge conditions and are known.

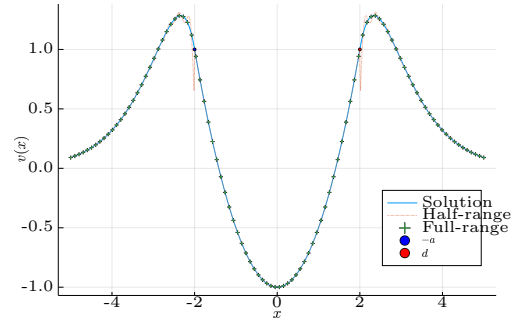
In figures 4.5.3 plots are shown of the solution for this example, with the Fourier inversion of $\tilde{v}(k)$ based on (4.19) or (4.20),

$$\begin{aligned}v(x,0) &= \frac{1}{2\pi} \int_{-\infty}^{\infty} \tilde{v}_+^{(d)}(k)e^{ik(d-x)} + \tilde{v}_-^{(-a)}(k)e^{-ik(a+x)} + f(k)e^{-ikx} dk \quad (4.19) \\ &= \begin{cases} \frac{1}{2\pi} \int_{-\infty}^{\infty} \tilde{v}_+^{(d)}(k)e^{ik(d-x)} dk, & d < x, \\ \frac{1}{2\pi} \int_{-\infty}^{\infty} f(k)e^{-ikx} dk, & -a \leq x \leq d, \\ \frac{1}{2\pi} \int_{-\infty}^{\infty} \tilde{v}_-^{(-a)}(k)e^{-ik(a+x)} dk, & x < -a. \end{cases} \quad (4.20)\end{aligned}$$

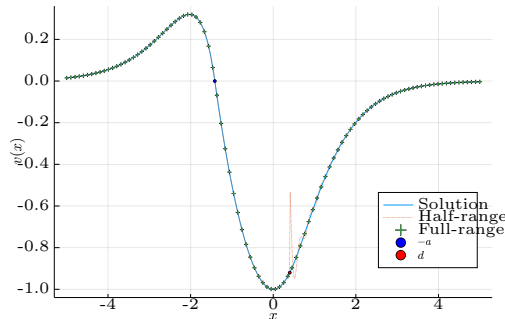
It is clear to see that by inverting in line with (4.19) the solution is continuous. An explanation for this may be found by considering the inversion in (4.20), if one solely inverted $\frac{1}{2\pi} \int_{-\infty}^{\infty} \tilde{v}_+^{(d)}(k)e^{ik(d-x)} dk$ then the solution would be zero for $x < d$ and $v(x,0)$ for $x > d$, and this discontinuity causes Gibbs Phenomena [93] in the numerical method. Therefore, by considering the method in (4.20), the inability to satisfy the edge conditions is due to Gibbs Phenomena caused by discontinuities at the contact points.



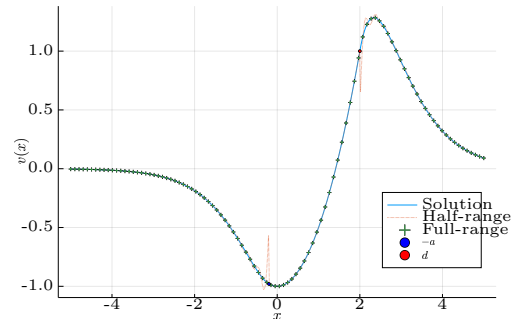
(a) This figure shows the plot $v(x, 0)$ profile with $-a, d = -0.9, 1.1$.



(b) This figure shows the plot $v(x, 0)$ profile with $-a, d = -2, 2$.



(c) This figure shows the plot $v(x, 0)$ profile with $-a, d = -\sqrt{2}, 0.4$.



(d) This figure shows the plot $v(x, 0)$ profile with $-a, d = -0.2, 2$.

Figure 4.5.3: Plots of the example contact problem with the inversion methods of equations 4.19 and 4.20.

4.5.2 Convergence

The result of the example 4.5.1 shows that we should only consider the inversion of $\tilde{v}(k)$ by numerically calculating the integral in (4.19), and doing so ensures continuity of $v(x, 0)$. Therefore, the minimisation problem we consider is

$$\min_{\chi^j} \|\tau_{yy}^j(\chi^j, 0)\|$$

Algorithm 1: Pseudocode for the implementation of the free-boundary method for locating the junction points $-a$ and d .

```

1 Function FreeBoundary  $(-a, d)$ ;
   Input : Initial estimates:  $\chi^0 = (-a^0, d^0)$ 
2 Let  $i = 0$ 
3 while Successive terms are below a tolerance  $\|\chi^j - \chi^{j-1}\| \leq tol$  do
4   | Solve the mixed boundary value problem to find a solution  $\mathbf{u}^j(x, y)$ .
5   | Calculate  $\tau_{yy}^j(x, 0)$  and estimate two roots  $(-a^{j+1}, d^{j+1})$  as in
   | equation (4.21).
6   | Set the roots as  $\chi^{i+1} = (-a^{j+1}, d^{j+1})$ .
7   | Set  $i = i + 1$ .
8 end
Output: Converged junction points  $\chi = (-a, d)$  and corresponding
           solution.

```

to locate the contact points. Therefore, we calculate χ^{j+1} by considering

$$\begin{aligned}
 a^{j+1} &= a^j - \tau^j(-a^j) \left(\frac{a^j - a^{j-1}}{\tau^j(-a^j) - \tau^{j-1}(-a^{j-1})} \right), \\
 d^{j+1} &= d^j - \tau^j(d^j) \left(\frac{d^j - d^{j-1}}{\tau^j(d^j) - \tau^{j-1}(d^{j-1})} \right).
 \end{aligned} \tag{4.21}$$

The figure 4.5.4 shows the evaluation of $\tau_{yy}(x, 0)$ at the contact points for the first 17 iterations of the free-boundary method. The method terminates once the evaluation of τ_{yy} is below the preset tolerance of 10^{-8} , which requires 17 iterations but the solution is approximately close to the solution after the third iteration. After 10 iterations the error is approximately 10^{-6} and begins to oscillate for further iterations. The oscillatory behaviour is due to the free-boundary method oscillating around the converged solution, suggesting that a tolerance bound of 10^{-6} being more apt. To see plots of the profile of $\tau_{yy}(x, 0)$ please see the figures in section 4.6.

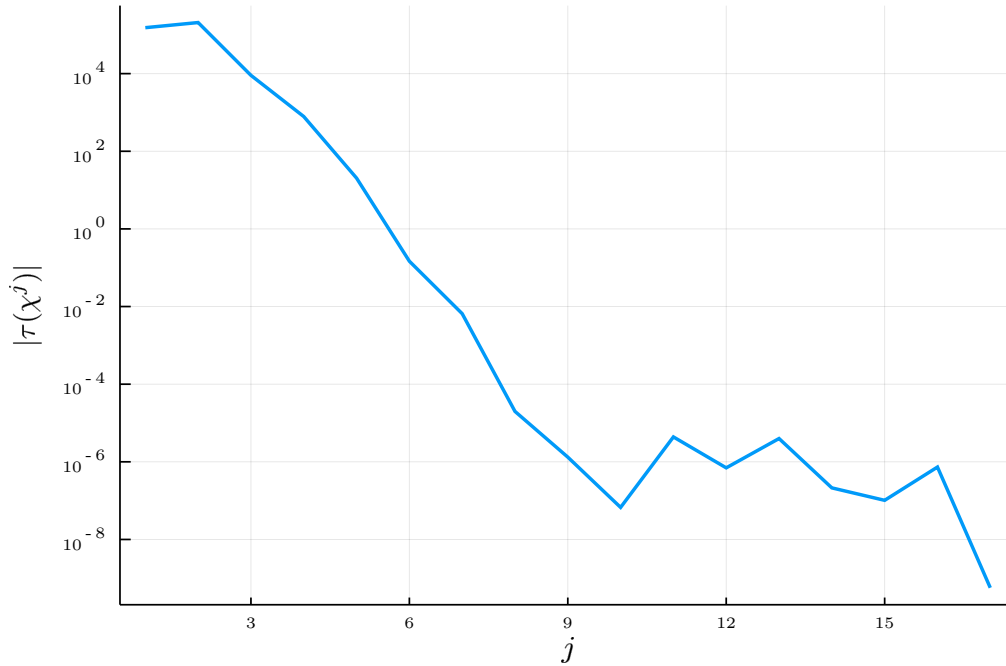


Figure 4.5.4: A plot of the the error at each iteration for applying the minimisation algorithm to locate the contact points based on the continuity of $\tau_{yy}(\chi^j, 0)$, with Metal parameters taken from table 4.1.

4.6 Results

The application of the iterative procedure gives an approximation to the terms $\tilde{v}_+^{(d)}(k)$, $\tilde{v}_-^{(-a)}(k)$, $\tilde{\tau}_-^{(d)}(k)$ and $\tilde{\tau}_+^{(-a)}(k)$, from which one can numerically evaluate the unknown functions $\hat{A}_1(k)$, $A_2(k)$, and therefore the solution $\mathbf{u}(x, y)$. To find the displacement and stresses the Fourier transforms are inverted, which is computed via a Gaussian quadrature rule. To illustrate,

the normal stress may be evaluated as follows,

$$\begin{aligned}\tau_{yy}(x, 0) &= \frac{1}{2\pi} \int_{-\infty}^{\infty} \widetilde{\tau}_{yy}(k, 0) e^{-ikx} dk \\ &= \frac{1}{2\pi} \int_{-\infty}^{\infty} \widetilde{\tau}_{yy-}^{(d)}(k) e^{ik(d-x)} dk \\ &\approx \sum_{i=0}^n w_i \widetilde{\tau}_{yy-}^{(d)}(k_i) e^{ik_i(d-x)},\end{aligned}$$

where k_i are the nodes and w_i are the weight for the quadrature rule. Then the approximation for $\tau_{yy}(x, 0)$ may be found by closing the contour in either the upper or lower half-plane for $\widetilde{\tau}_{yy+}^{(-a)}(k)$ or $\widetilde{\tau}_{yy-}^{(d)}(k)$ respectively, giving

$$\tau_{yy}(x, 0) = \begin{cases} 0, & d < x, \\ \frac{1}{2\pi} \int_{-\infty}^{\infty} \widetilde{\tau}_{yy}(k, 0) e^{-ikx} dk, & -a \leq x \leq d, \\ 0, & x < -a. \end{cases}$$

A plot of the solution of the normal stress, $\tau_{yy}(x, 0)$, for given parameter values is shown in figure 4.6.1a. The plot validates the method used as it shows the behaviour one would expect from the boundary conditions, namely that the normal stress on the free-boundary is equal to zero.

Again by contour integration one can deduce that

$$v(x, 0) = \begin{cases} \frac{1}{2\pi} \int_{-\infty}^{\infty} \widetilde{v}_+^{(d)}(k) e^{ik(d-x)} dk, & d < x, \\ \frac{1}{2\pi} \int_{-\infty}^{\infty} f_{-a}^d(k) e^{-ikx} dk, & -a \leq x \leq d, \\ \frac{1}{2\pi} \int_{-\infty}^{\infty} \widetilde{v}_-^{(-a)}(k) e^{-ik(a+x)} dk, & x < -a. \end{cases}$$

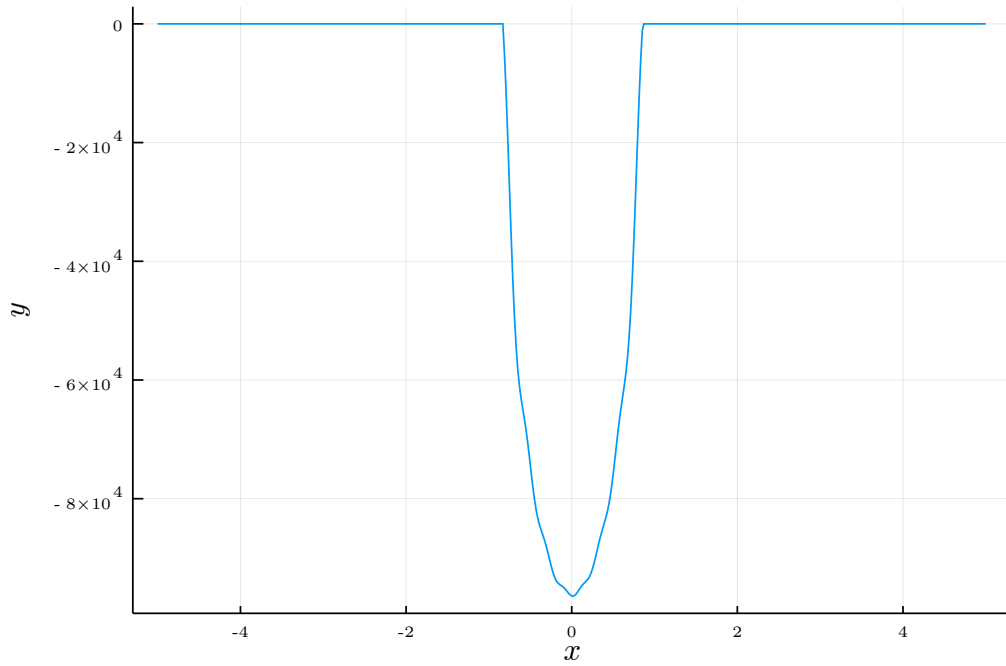
However, as we saw in section 4.5.1, it is better to invert

$$v(x, 0) = \frac{1}{2\pi} \int_{-\infty}^{\infty} \widetilde{v}_+^{(d)}(k) e^{ik(d-x)} + \widetilde{v}_-^{(-a)}(k) e^{-ik(a+x)} + f(k) e^{-ikx} dk$$

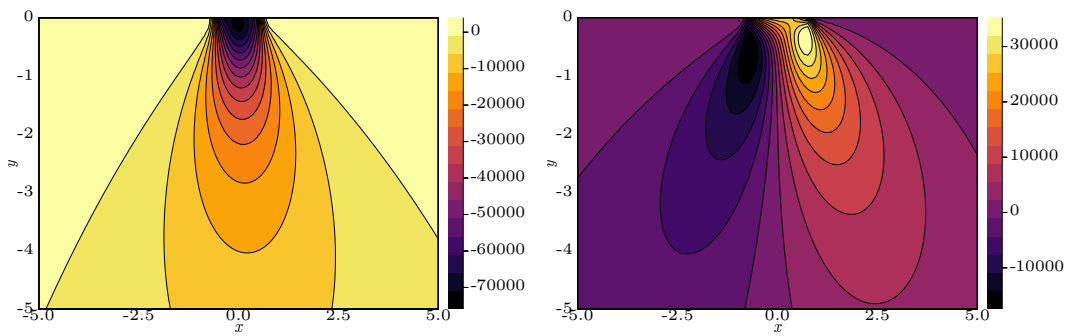
instead to avoid Gibbs Phenomena. An approximation to the terms $\tau_{yy}(x, 0)$ and $v(x, 0)$ has been made, so by using the equations (4.10) and (4.11) an

approximation to the displacement terms may be made.

The figures in 4.6.1 illustrate the solution with the parameters based on that of structural steel [11]. The continuity at the junction points for $\tau_{yy}(x, 0)$ is ensured by applying the optimisation method detailed in the proceeding section. A contour plot of the distribution of the stresses within the elastic material is included, which shows the concentration of the stresses to be around the cylinder and away from the surface. The stresses are calculated by evaluating (4.4) through a Gaussian quadrature rule and relating it to $\tau_{xy}(x, y)$ and $\tau_{yy}(x, y)$. The traction on the surface of the elastic media may be found to be $\mathbf{T} = (-\tau_{xy}(x, 0), -\tau_{yy}(x, 0))$, which in this case faces in the positive- x and positive- y direction.



(a) This figure shows the plot $\tau_{yy}(x, 0)$ profile.



(b) This figure shows a contour plot of $\tau_{yy}(x, y)$.

(c) This figure shows a contour plot of $\tau_{xy}(x, y)$.

Figure 4.6.1: Plots of the solution for Metal values from table 4.1 with backwards slip and the contact points found to be $-0.82514, 0.85749$.

4.6.1 Parameter study

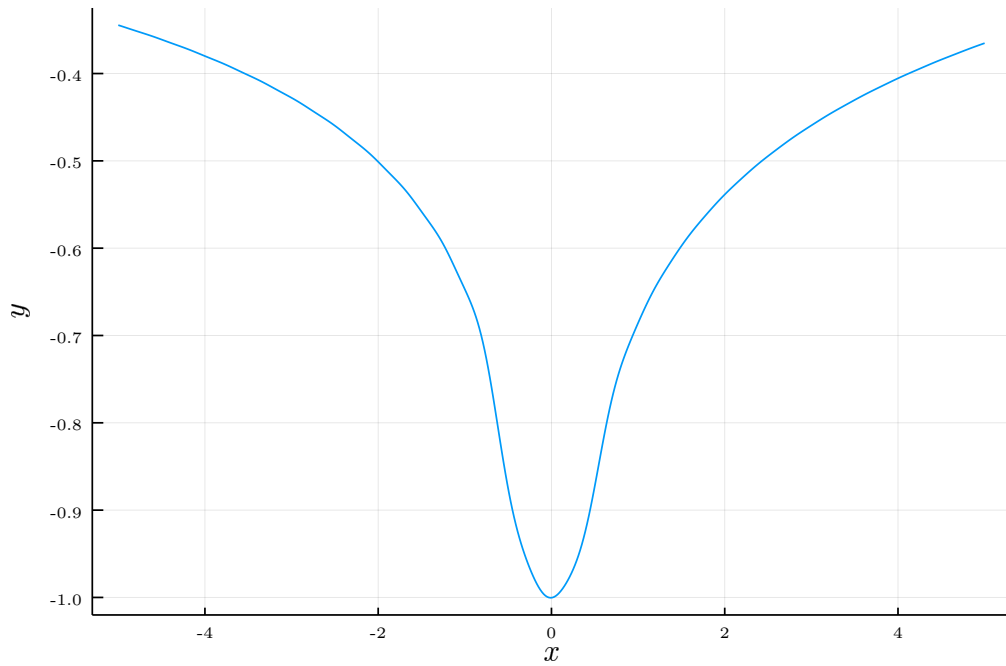
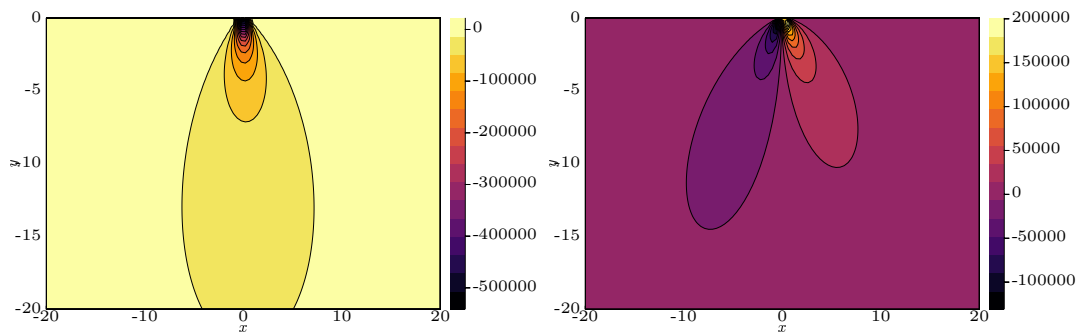
The technique implemented here is valid for any choice for the parameters λ, μ, μ_0 and ρ provided the convection speed of the cylinder, V , is adjusted to ensure that a strip of analyticity remains. Thus, the requirement on V is then

$$V^2 < \frac{\mu}{\rho},$$

which will lead to the singular points and branch cuts of $K(k)$ being away from the real line. However, the closer V is to zero leads to solutions which are simpler to decompose as the singular points or branch cuts are more equidistant from the real line. In table 4.1, there is a set of parameter values for Metal (structural steel [11]) and an Alternative set of parameter values to illustrate the general validity of the results. The Alternative parameters solution is shown in figures 4.6.2 and shows plots of the profile of $\tau_{yy}(x, 0)$ and contour plots of the stresses. The figure 4.6.2a shows that there exists a unique solution to the free-boundary problem for the Alternative parameters. As there is little dependency on the material parameters we shall mainly include plots for the Metal parameter set in table 4.1.

Parameter	Metal values	Alternative values	Dimensions
λ	210000	10000	MPa
μ	81000	1000000	MPa
μ_0	0.3	0.3	-
ρ	7850	1250	kg m ⁻³
V	1	10	-
ω	-0.03125i	-0.03125i	-

Table 4.1: The parameter values used in the full-slip regime.

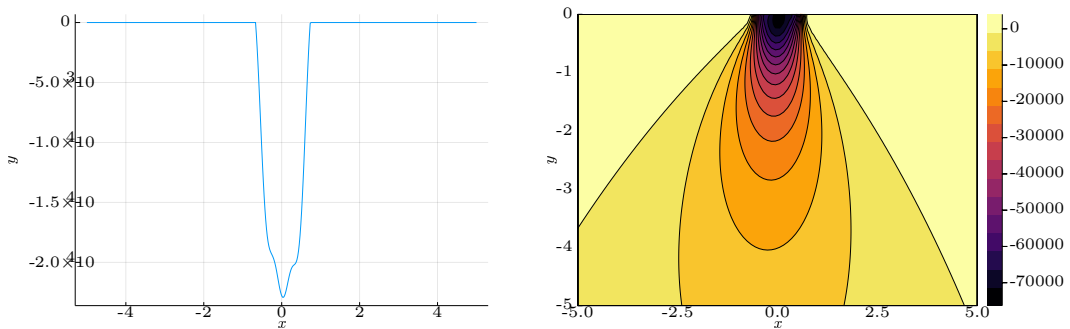
(a) This figure shows the plot $v(x, 0)$ profile.(b) This figure shows a contour plot of $\tau_{yy}(x, y)$.(c) This figure shows a contour plot of $\tau_{xy}(x, y)$.Figure 4.6.2: Plots of the solution for Alternative values from table 4.1 with forwards slip and the contact points found to be $-0.88374, 0.87925$.

4.6.1.1 Forward and backwards slip

In the nonlinear derivation of the boundary conditions it was found that either forwards or backwards slip were valid boundary conditions with each representing a different physical system, either wheel spinning or locking respectively. To illustrate that these two physical systems are indeed realisable, the figures 4.6.3 and 4.6.4 have been included, showing the existence of a solution for both slipping configurations under the Metal parameter set 4.1.

The figures 4.6.3 and 4.6.4 show a comparison of the solution found for both forward slip and backwards slip boundary conditions. The junction points $-a$ and d for both slipping configurations are found to be different, suggesting the direction of slip being an important factor in determining the location of the contact points. A notable difference between the two slipping configurations may be seen in the figures 4.6.3b and 4.6.4b, which shows the distribution of $\tau_{yy}(x, y)$ for both configurations and in particular that the direction where the elastic media experiences the most stress differs. The difference of forward and backward slip is verified in the plots 4.6.3a and 4.6.4a, which shows opposing signs for $\tau_{xy}(x, 0)$. The physical difference of these two slip directions may be seen in the traction too, as traction for forward slip faces in the positive- x and positive- y direction whereas traction for backward slip faces in the negative- x and positive- y direction.

Forward slip

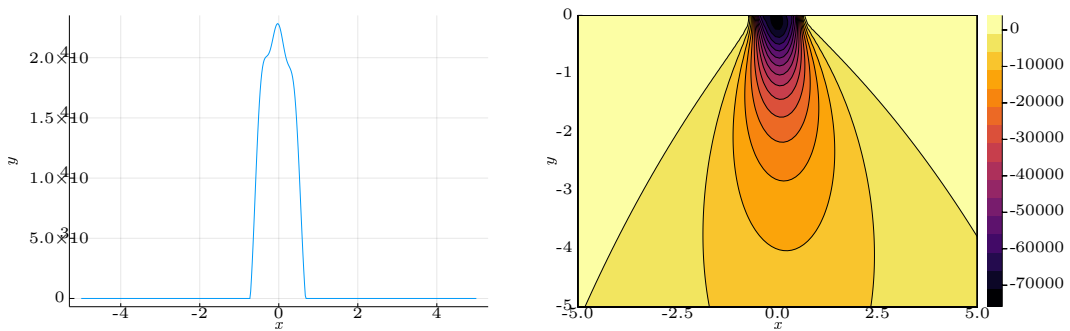


(a) This figure shows the plot $\tau_{xy}(x, 0)$ profile.

(b) This figure shows a contour plot for $\tau_{yy}(x, y)$.

Figure 4.6.3: Plots of the solution for Metal values from table 4.1 with forwards slip and the contact points found to be $-0.77637, 0.92200$.

Backward slip



(a) This figure shows the plot $\tau_{xy}(x, 0)$ profile.

(b) This figure shows a contour plot for $\tau_{yy}(x, y)$.

Figure 4.6.4: Plots of the solution for Metal values from table 4.1 with backwards slip and the contact points found to be $-0.82514, 0.85749$.

4.6.1.2 Small frequency limit

In our approach the temporal frequency, ω , was introduced into the governing equations to generate a strip of analyticity in the complex k -plane. However, physically we are interested in the steady state case which corresponds to the limit as $\omega \rightarrow 0$. Here we shall discuss the effects of taking the limit of $\omega \rightarrow 0$ and seek to address the following questions

1. Does the limit $\omega \rightarrow 0$ converge?
2. What is a good approximation to $\omega = 0$?

The introduction of ω allows a strip of analyticity for the Wiener–Hopf technique to be applied. The quantity which is impacted the most is the function $K(k)$, which is multiplicatively decomposed. Without the introduction of ω , $K(k)$ would have two branch cuts extending from the origin to infinity, but by introducing a purely imaginary ω , the branch points are separated to above and below the origin. In some sense the temporal frequency parametrises the branch points and hence the strip. Taking the limit of $\omega \rightarrow 0$ coalesces these branch points and the solution converges as seen in figure 4.6.7.

The singularity in the multiplicative decomposition increases the computational cost of taking the Cauchy transform, as it is required that the function be Lipschitz continuous to be approximated by a orthogonal polynomial basis. We may still find an expansion but as we decrease ω we increase the number of terms needed for the expansion, see fig 4.6.5. The computational cost of finding the expansion increases with the number of terms linearly, but then calculating the Cauchy transform becomes very computationally costly. To mitigate the computational costs associated with small ω values we may pre-compute the $K(k)$ values required in the additive decompositions but we do note that an increased computational cost is unavoidable.

To observe how the solution behaves as ω varies, the figures 4.6.6 and 4.6.7 have been included. Due to the presence of $\gamma_1(k)$ and $\gamma_2(k)$ in the solution,

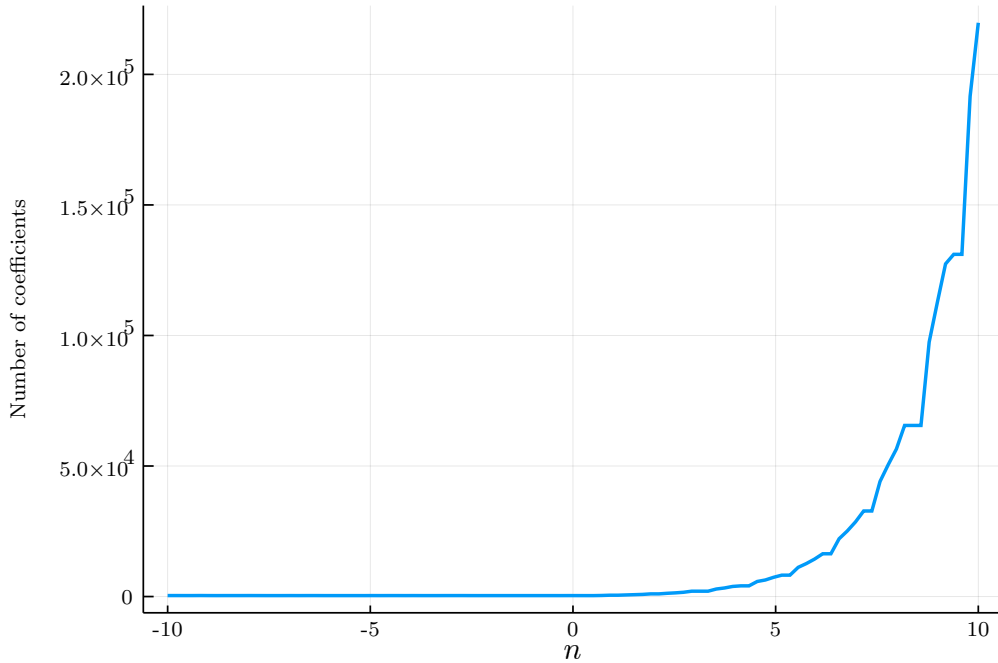


Figure 4.6.5: The number of spectral coefficients required to approximate $K(k)$ to machine precision for $\omega = -2^{-n}i$ with Metal parameters in table 4.1.

one would expect the solution to decay faster for larger ω , which is seen from the two sets of figures. For small ω , there appears to be very little difference between the plots of the vertical profile and the stress distribution, showing that $\omega = -0.03125i$ is a sufficiently small approximation.

In summary, we see that the solution converges in the limit $\omega \rightarrow 0$ from figures 4.6.6 and 4.6.7. In the small ω case we are faced with increased computational costs in computing the Wiener–Hopf splittings but approximating $\omega = -0.03125i$ gives a converged solution without being too computationally costly.

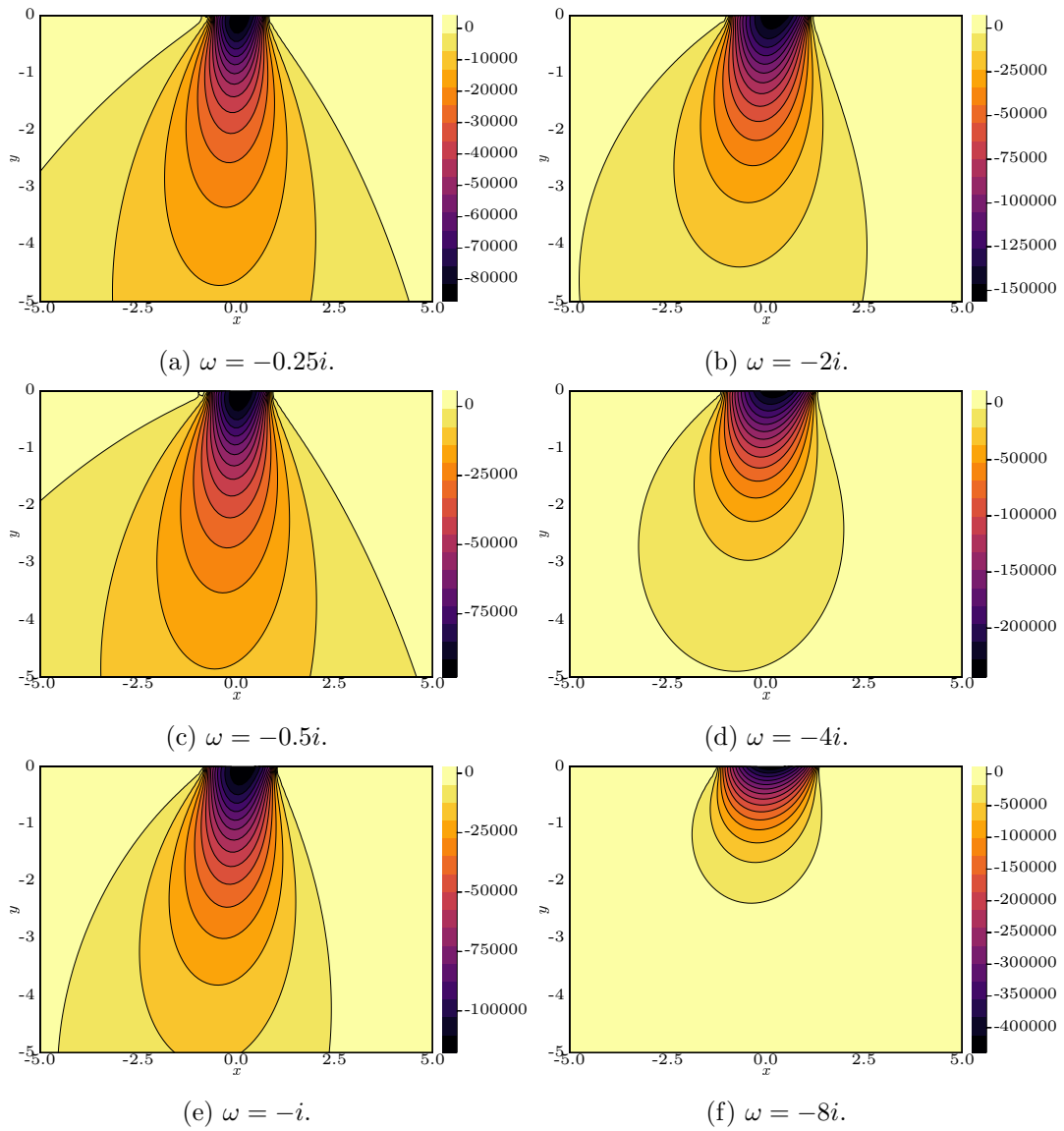


Figure 4.6.6: Contour plots of $\tau_{yy}(x, y)$ under the Metal parameter values from table 4.1 and forward slip with increasing ω .

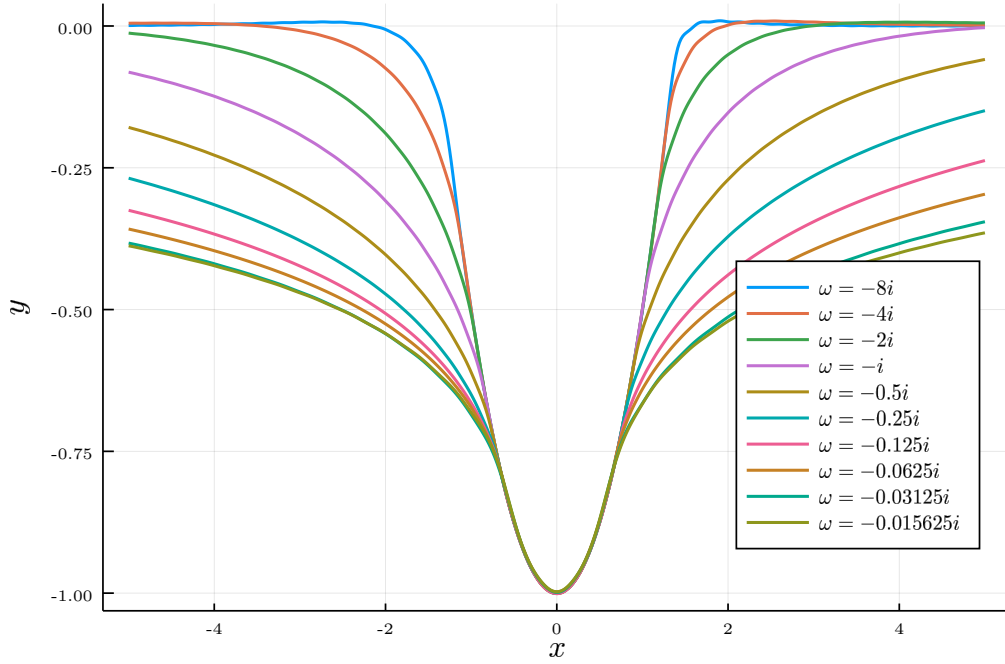


Figure 4.6.7: Contour plots of $v(x, 0)$ under the Metal parameter values from table 4.1 and forward slip with decreasing ω .

4.6.2 Von Mises yield criterion

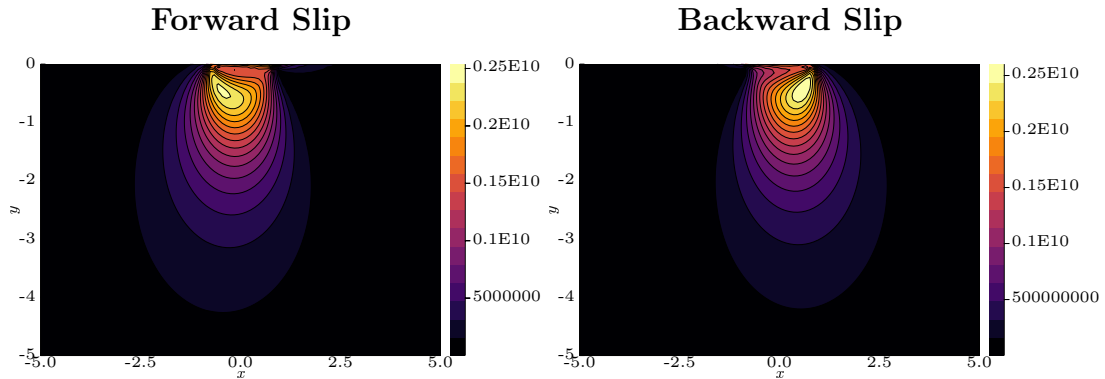
To introduce elastic-plastic modelling into the problem, we may consider the locations where the half-space begins to transition to elastic-plastic behaviour. The location where the half-space yields may be found by the following equation,

$$(\tau_{xx} - T)^2 + 2\tau_{xy}^2 + (\tau_{yy} - T)^2 \leq \tau_Y^2,$$

where $T = (\tau_{xx} + \tau_{yy} + \tau_{zz})/3$ which may be interpreted as the location where the elastic energy reaches a critical value.

The figures 4.6.8b and 4.6.8a show the magnitude of Von Mises yield in the elastic half-space for both forwards and backwards slip. In the regions directly beneath the cylinder, the magnitude of elastic energy is greatest for

both, suggesting that these are the regions where the plastic behaviour is most likely to occur.



(a) This figure shows a contour plot of the magnitude of the Von Mises criterion for forward slip.

(b) This figure shows a contour plot of the magnitude of the Von Mises criterion for backward slip.

Figure 4.6.8: Contour plots of the magnitude of the Von Mises yield criterion in both directions of slip for the Metal parameter values 4.1.

4.7 Conclusion

We have developed a model of an elastic half-space deformed by a cylindrical roller. The friction law assumed here is that of full-slip, which leads to a 2×2 matrix Wiener–Hopf problem. Due to the positions of the exponential terms within the matrices an iterative method which initially decouples the scalar Wiener–Hopf equations is suitable. Finally, the free-boundary problem is solved using an inverse method which makes an initial estimate and iteratively finds better estimates.

The method employed here requires the introduction of a small wavenumber to introduce a strip of analyticity, which enables a matrix Wiener–Hopf problem to be constructed. Alternative approaches may be suitable for the free-boundary problem too, with it bearing great similarities to floating body problems Lannes [59].

The limit of full-slip is interesting due to the simplification that it provides to the matrix Wiener–Hopf over the frictional case. The method employed here applies to a stick-slip friction law but the matrix Wiener–Hopf will be considerably more challenging to solve but is considered in the proceeding chapter 5. The full-stick limit provides a scenario where a special case adaptation of the iterative method [56] may be required, as the scalar Wiener–Hopf equations cannot be decoupled easily, see appendix B for more details.

Chapter 5

Rolling contact in the stick-slip regime

5.1 Introduction

In this chapter we consider the setting where the magnitude of the angular velocity for the cylinder is close to the magnitude of the convection velocity for the half-space. In this setting we have imposed a stick-slip friction law, which gives an additional sticking region to the full-slip friction law explored in chapter 4. The introduction of the central sticking region consequently expands the 2×2 matrix Wiener–Hopf equation into a 4×4 matrix Wiener–Hopf equation, and introduces two additional free-boundary points which are the stick-slip transition points.

We define the stick-slip friction law to be the division of the contact region into a central sticking region between two independent slipping regions. Friction is a complex phenomena and the stick-slip friction law is one of many models used to approximate it, with variations to stick-slip existing such as those driven by rough surfaces, distances, or velocities [e.g. 13, 100]. Experimental evidence of stick-slip friction was first discovered by Reynolds

[83] in 1876 and continues to appear in somewhat recent experiments Heslot et al. [45]. One may observe stick-slip phenomena more readily in the erratic behaviour seen as two seemingly smooth objects slide past one another Al-Bender et al. [7], Thomsen and Fidin [92], where the erratic behaviour is because of stick-slip oscillations. At large scales, the rumble of earthquakes is in-part caused by stick-slip phenomena between the tectonic plates [18, 6, 7]. The study of stick-slip phenomena is vast, with a broad literature considering the micro-scales [78] in contrast to the macro-scale which we consider. The micro-scale brings with it greater complexity, such as rough micro-scale surfaces of seemingly smooth surfaces or chemical effects of the atoms Bhushan [14], Bushan [19]. To avoid the unstable nature of stick-slip phenomena Stelter et al. [91] we consider a steady problem with stationary but unknown stick-slip zones.

A brief review of the modelling of stick-slip friction begins with Cattaneo [21] in 1938 who considered an elliptic punch with an inner stick annulus and an outer slip annulus for a monotonically increasing tangential force. Mindlin [66] extended Cattaneo's results to other loading situations, and then both Jäger [48] and Ciavarella [23] generalised Cattaneo's results to any plane contact problem by using integral equations. Proofs of existence and uniqueness for the stick-slip friction law have encountered some difficulties, with no general proof existing in the literature. Nonetheless, Cocu [25] provided a proof of existence which is unique if the coefficient of friction is small. Whereas, Klarbring [58] explores existence and uniqueness for larger coefficients of friction, finding that non-uniqueness is inherent in quasi-static settings. The literature reviewed in this section has focussed on sliding problems, whereas we consider a rolling contact problem, partially in a bid to avoid the difficulties with non-uniqueness by building the history of the process into the problem.

Locating the stick-slip transition points is in itself a broad topic with early consideration taken in Galin and Gladwell [39], who formulated a contact problem with a flat punch. Galin and Gladwell [39] initially sought to locate

the stick-slip transition points by considering a Fuchsian differential equation but could not solve the differential equation and so pursued a conformal mapping instead. However, much later Mossakovskii [70] considered the same Fuchsian differential equation and progressed by solving it numerically to find agreement with Galin's mapping method [103]. A different approach was adopted by Antipov and Arutyunyan [10] who reduced a contact problem to a matrix Riemann–Hilbert problem. Antipov and Arutyunyan [10] then located the stick-slip transition points analytically by imposing finite stress at the transition point. Self-similar solutions were explored by Spence [90], developing an approach for parabolic punches which was solved by applying the Wiener–Hopf technique. Spence [90] finds the stick-slip transition points analytically by requiring that the shear stress is bounded and finite across the stick-slip boundary. The self-similar approach was used by Zhupanska and Ulitko [102], finding a solution by applying a conformal mapping and the scalar Wiener–Hopf technique. Our work differs to the reviewed literature as none consider a rolling problem, nor are asymmetric stick-slip zones considered either. In fact, much of the literature considers a symmetric setting which allows symmetry to be exploited to reduce the complexity of the problem.

The introduction of a central sticking region causes the size of the matrix Wiener–Hopf equation to be 4×4 , as there are four distinct jumps in the boundary conditions. Matrix Wiener–Hopf equations of this size are rarely explored, instead, much attention is given to 2×2 problems but a summary of these techniques may be found in Kisil et al. [57], Rogosin and Mishuris [85]. Jones [51] developed an n -dimensional approach for factorising commutative matrices of a specific structure, their approach was later generalised by [96] for factorising matrices with distinct eigenvalues. A technique for factorising triangular matrices of order n was proposed by Rogosin and Primachuk [86] by using an inductive step. Alternatively, one may pursue a purely numerical approach by formulating a Riemann–Hilbert problem and applying the spectral method developed in Llewellyn Smith and Luca [63], or by considering the unified transform approach developed by Colbrook et al.

[26].

A description of the physical problem and the boundary conditions are given in section 5.2. Considering the different boundary conditions in their domains leads to the construction of the matrix Wiener–Hopf problem in section 5.3. This Wiener–Hopf problem is solved in section 5.4 by using the iterative method outlined in section 3.3.1 with the additional details of the numerical implementation of the Cauchy transforms in section 5.4.1. The details of our approach for tackling the free-boundary problem is presented in section 5.5, illustrated with some numerical results. The results of the analysis and numerics is presented in section 5.6 for a variety of parameters. Finally, in section 5.7, a conclusion is given along with some avenues for future research.

5.2 Model formulation

Consider the system as in the schematic, figure 5.2.1. A cylinder of radius R is pushed into an elastic half-space $y < 0$ with a force \mathbf{F} , resulting in an indentation of depth ϵ and is in contact with the half-space between unknown points $-a$ and d . The cylinder rotates with an angular velocity Ω , and translates in the x -direction across the half-space at a linear velocity V . The points labelled $-b$ and c are the unknown location of where the frictional behaviour transitions from slipping to sticking. The rest of this system is outlined in section 2.1, so please refer there for the definition of terms.

5.2.1 Boundary conditions

In the system above, a cylinder rotates on the surface of an elastic half-space with the cylinder in contact with the surface in the region $-a \leq x \leq d$. The points $-a$ and d are unknown and to be found as part of the solution.

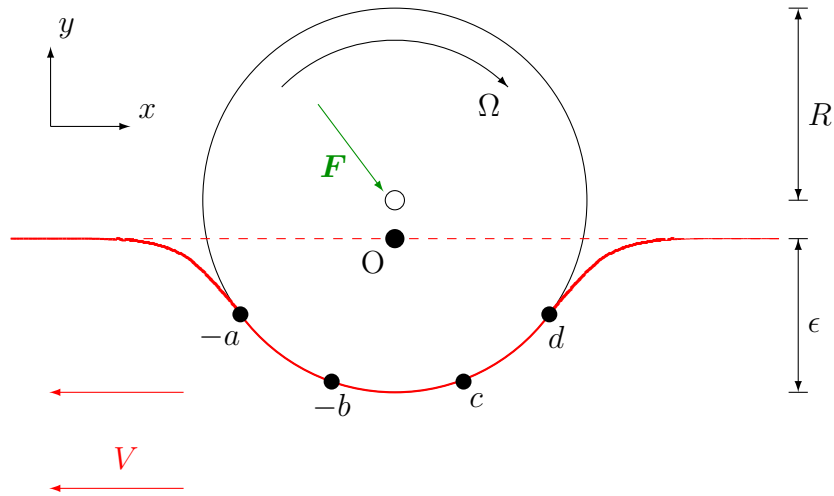


Figure 5.2.1: A schematic of a cylinder rolling along an elastic half-space. A similar setting to 4.2.1 with additional free-boundary points $-b$ and c . The cylinder moves at a linear velocity V in the x -direction along the elastic half-space. The origin of the coordinate system (labelled O) is taken in a frame of reference moving with the cylinder, directly below the centre of the cylinder at the height of the undeformed elastic surface. The cylinder is in contact with the elastic surface between the points $-a$ and d , with and transitions between sticking and slipping behaviour at points $-b$ and c . The cylinder of radius R rolls about its centre axis with angular velocity Ω , and a force \mathbf{F} is applied to the centre of the cylinder, causing the cylinder to be indented by ϵ into the elastic half-space.

The surface of the half-space is displaced by the rigid cylinder and may not penetrate the cylinder. The half-space experiences stick-slip friction due to the cylinder, with sticking in the region $-b \leq x \leq c$ and slipping otherwise. The points $-b$ and c are unknown and are to be found as part of the solution also. Outside of the contact region the surface of the half-space is free from any stress and so traction-free boundary conditions are imposed, as shown in figure 5.2.2. The resultant mathematical problem is a mixed-free-boundary problem, with intricate boundary conditions in each region.

The nonlinear derivation of the boundary conditions from the physical system can be found in section 2.4, with the linearisation of the nonlinear boundary

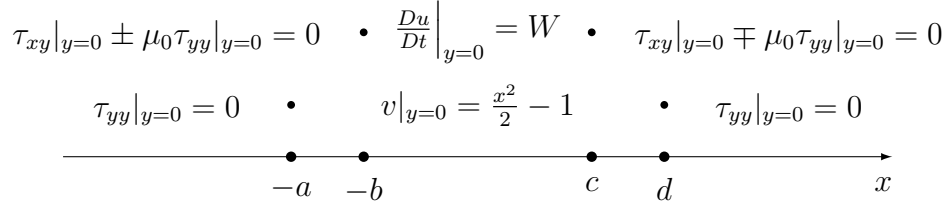


Figure 5.2.2: A diagram of the rearranged stick-slip boundary conditions on the surface of the half-space.

conditions found in section 2.3. A diagram showing the boundary conditions are shown in the schematic 5.2.2. In this chapter the frictional behaviour is stick-slip, which gives the following boundary conditions and domains,

$$\begin{array}{ll}
\text{Contact:} & v(x, 0) = \frac{x^2}{2} - 1, \quad \text{for } -a \leq x \leq d, \\
\text{Stick:} & \frac{Du}{Dt}(x, 0) = W, \quad \text{for } -b \leq x \leq c, \\
\text{Slip:} & \tau_{xy} \mp \mu_0 \tau_{yy}(x, 0) = 0, \quad \text{for } x < -b \ \& \ c < x, \\
\text{Stress-free:} & \tau_{yy}(x, 0) = 0, \quad \text{for } x < -a \ \& \ d < x.
\end{array}$$

We use the convected derivative as

$$\frac{Du}{Dt}(x, 0) = \frac{\partial u}{\partial t}(x, 0) - \frac{\partial u}{\partial x}(x, 0) = W, \quad \text{for } -b \leq x \leq c.$$

Note that the two slip regions may be in forwards (−) or backwards (+) slip and may determine their slip directions independently, but we expect that both regions slip in the same direction.

Thus, there are two boundary conditions in each region and the junctions between each region are the unknown free-boundary points $-a$, $-b$, c and d . The boundary conditions may be reformulated into a matrix Wiener–Hopf equation which we then solve numerically. To locate the free-boundary points a numerical technique is applied to ensure continuity of the solution at each of the junctions.

5.2.2 General solution

As we consider the same governing equations throughout we simply quote the results from section 2.4 and use the same general solution derived there, please refer there for details. We have the following general solution

$$\begin{aligned} u(x, y) &= \frac{1}{2\pi} \int_{-\infty}^{\infty} \left[\hat{A}_1(k) \hat{B}_1(k) e^{y\gamma_1(k)} + A_2(k) e^{y\gamma_2(k)} \right] e^{-ikx} dk, \\ v(x, y) &= \frac{1}{2\pi} \int_{-\infty}^{\infty} \left[\hat{A}_1(k) e^{y\gamma_1(k)} + A_2(k) B_2(k) e^{y\gamma_2(k)} \right] e^{-ikx} dk, \end{aligned}$$

where

$$\begin{aligned} \gamma_1(k) &= \sqrt{k^2 - \frac{\rho V^2}{\lambda + 2\mu} (\omega + k)^2}, & \gamma_2(k) &= \sqrt{k^2 - \frac{\rho V^2}{\mu} (\omega + k)^2} \\ \hat{B}_1(k) &= \frac{-ik}{\gamma_1(k)} = \frac{1}{\sqrt{\frac{\rho V^2 (1 + \frac{\omega}{k})^2}{\lambda + 2\mu} - 1}}, & B_2(k) &= \frac{ik}{\gamma_2(k)} = -\frac{1}{\sqrt{\frac{\rho V^2 (1 + \frac{\omega}{k})^2}{\mu} - 1}}. \end{aligned}$$

with $\hat{A}_1(k)$ and $A_2(k)$ unknown and are to be found as part of our solution.

5.3 Constructing the matrix Wiener—Hopf equation

We may determine the functions $\hat{A}_1(k)$ and $A_2(k)$ by considering the transformed boundary conditions. For this purpose, we write the boundary conditions as the difference of various half-range Fourier transforms, which are detailed in section 3.2.1. Once the boundary conditions are Fourier transformed combine them via the transformed governing equations into a matrix Wiener–Hopf equation.

5.3.1 Transformation of the boundary conditions

Initially an 8×8 matrix Wiener–Hopf equation was derived by considering the two boundary conditions in the intervals between each of the four free-boundary points disjointly, for example the contact boundary condition was split over 3 intervals. The 8×8 matrix Wiener–Hopf problem had singular matrices so the matrix cannot be inverted. In fact, singular matrix Wiener–Hopf problems may suggest that the matrix may be simplified further. This led to the reformulation of the boundary conditions with the aim of minimising the number of disjoint intervals in the boundary conditions. Taking this approach simplified the 8×8 singular matrix Wiener–Hopf equation to the reformulated to a 4×4 non-singular matrix Wiener–Hopf equation.

In figure 5.2.2 the boundary conditions are rearranged to minimise the number of transitions. To minimise the number of transitions, we observe that the stress-free boundary conditions may be arranged to form the slip boundary conditions, extending the slip region to infinity in both directions. Thus, we have reduced the number of transitions to four, and so we should expect to be able to form a 4×4 matrix Wiener–Hopf equation.

Taking a full-range Fourier transform of the vertical displacement, $v(x, 0)$, we find

$$\tilde{v}(k) = e^{ikd}\tilde{v}_+^{(d)}(k) + e^{-ika}\tilde{v}_-^{(-a)}(k) + f(k),$$

where $\tilde{v}_+^{(d)}(k)$ and $\tilde{v}_-^{(-a)}(k)$ are unknown functions to be found as part of the solution and analytic in \mathcal{D}^+ and \mathcal{D}^- respectively. The function

$$f(k) = \frac{e^{-ika}}{ik} \left(1 - \frac{a^2}{2} - \frac{a}{ik} + \frac{1}{k^2} \right) - \frac{e^{ikd}}{ik} \left(1 - \frac{d^2}{2} + \frac{d}{ik} + \frac{1}{k^2} \right)$$

is derived in section 4.3.1.

Taking the full-range Fourier transform of both slip boundary conditions we

find the following,

$$\begin{aligned}\widetilde{\tau_{xy} \pm \mu_0 \tau_{yy}}(k) &= e^{-ikb} \widetilde{\tau_{xy} \pm \mu_0 \tau_{yy_+}}^{(-b)}(k), \\ \widetilde{\tau_{xy} \mp \mu_0 \tau_{yy}}(k) &= e^{ikc} \widetilde{\tau_{xy} \mp \mu_0 \tau_{yy_-}}^{(c)}(k),\end{aligned}$$

where $\widetilde{\tau_{xy} \pm \mu_0 \tau_{yy_+}}^{(-b)}(k)$ and $\widetilde{\tau_{xy} \mp \mu_0 \tau_{yy_-}}^{(c)}(k)$ are unknown functions to be found as part of the solution and analytic in \mathcal{D}^+ and \mathcal{D}^- respectively.

Similarly, the full-range transform of the convective derivative, $\frac{Du}{Dt}(x, 0)$, becomes

$$\widetilde{\frac{Du}{Dt}}(k) = e^{ikc} \widetilde{\frac{Du}{Dt_+}}^{(c)}(k) + e^{-ikb} \widetilde{\frac{Du}{Dt_-}}^{(-b)}(k) + g(k),$$

where $\widetilde{\frac{Du}{Dt_+}}^{(c)}(k)$ and $\widetilde{\frac{Du}{Dt_-}}^{(-b)}(k)$ are unknown functions to be found as part of the solution and analytic in \mathcal{D}^+ and \mathcal{D}^- respectively. The function $g(k)$ is known and derived in the following way

$$g(k) = \int_{-b}^c W e^{ikx} dx = \frac{W e^{ikc}}{ik} - \frac{W e^{-ikb}}{ik}.$$

Finally, as in the full-slip regime, the transformed stress-free boundary conditions become

$$\begin{aligned}\widetilde{\tau_{yy}}(k) &= e^{-ika} \widetilde{\tau_{yy_+}}^{(-a)}(k), \\ &= e^{ikd} \widetilde{\tau_{yy_-}}^{(d)}(k),\end{aligned}$$

where $\widetilde{\tau_{yy_+}}^{(-a)}(k)$ and $\widetilde{\tau_{yy_-}}^{(d)}(k)$ are unknown functions to be found as part of the solution and analytic in \mathcal{D}^+ and \mathcal{D}^- respectively.

5.3.2 Assembling the matrix Wiener–Hopf equation

The strategy is to eliminate the full-range transforms of the boundary conditions by expressing them as a composition of half-range variables. To aid with the assembly of the Wiener–Hopf equations we first relate the full-range transforms to $\widehat{A}_1(k)$ and $A_2(k)$, these relationships are

$$\begin{aligned}\widetilde{\tau}_{yy}(k) &= \left[(\lambda + 2\mu)\gamma_1(k) - ik\lambda\widehat{B}_1(k) \right] \widehat{A}_1(k) \\ &\quad + \left[(\lambda + 2\mu)B_2(k)\gamma_2(k) - ik\lambda \right] A_2(k) \\ &= n_1(k)\widehat{A}_1(k) + n_2(k)A_2(k), \\ \tau_{xy} \widetilde{\pm \mu_0 \tau}_{yy}(k) &= \left[\mu(\widehat{B}_1(k)\gamma_1(k) - ik) \pm \mu_0 n_1(k) \right] \widehat{A}_1(k) \\ &\quad + \left[\mu(\gamma_2(k) - ikB_2(k)) \pm \mu_0 n_2(k) \right] A_2(k) \\ &= m_1^\pm(k)\widehat{A}_1(k) + m_2^\pm(k)A_2(k), \\ \frac{\widetilde{Du}}{Dt}(k) &= i(\omega + k)(\widehat{B}_1(k)\widehat{A}_1(k) + A_2(k)), \\ \widetilde{v}(k) &= \widehat{A}_1(k) + B_2(k)A_2(k), \\ \tau_{xy} \widetilde{\mp \mu_0 \tau}_{yy}(k) &= m_1^\mp(k)\widehat{A}_1(k) + m_2^\mp(k)A_2(k).\end{aligned}$$

To construct the matrix Wiener–Hopf equation we may eliminate $\widehat{A}_1(k)$ and $A_2(k)$ from the equations above and replace the full-range functions with their half-range counterparts. Before we do so, we recall that there is a specific structure that the matrix kernels must have to enable the iterative method to be applied, namely the exponential terms on the non-diagonals must decay in the required half-planes. The only way to ensure this structure is to express $\widehat{A}_1(k)$ and $A_2(k)$ in terms of either $\tau_{xy} \widetilde{\pm \mu_0 \tau}_{yy}(k)$ or $\tau_{xy} \widetilde{\mp \mu_0 \tau}_{yy}(k)$, and $\widetilde{v}(k)$. This gives the following expressions

$$\widehat{A}_1(k) = \frac{m_2^\diamond(k)\widetilde{v}(k)}{m_2^\diamond(k) - B_2(k)m_1^\diamond(k)} - \frac{B_2(k)\tau_{xy} \widetilde{\diamond \mu_0 \tau}_{yy}(k)}{m_2^\diamond(k) - B_2(k)m_1^\diamond(k)}, \quad (5.1)$$

$$A_2(k) = \frac{\tau_{xy} \widetilde{\diamond \mu_0 \tau}_{yy}(k)}{m_2^\diamond(k) - B_2(k)m_1^\diamond(k)} - \frac{m_1^\diamond(k)\widetilde{v}(k)}{m_2^\diamond(k) - B_2(k)m_1^\diamond(k)}, \quad (5.2)$$

5.3. CONSTRUCTING THE MATRIX WIENER–HOPF EQUATION 5.3

where we replace \diamond with either \pm or \mp . Using (5.1) and (5.2) to eliminate $\widehat{A}_1(k)$ and $A_2(k)$ from the remaining full-range transformed functions leads to the equations,

$$\begin{aligned} \widetilde{\tau}_{yy}(k) &= \frac{n_1(k)m_2^\diamond(k) - n_2(k)m_1^\diamond(k)}{m_2^\diamond(k) - B_2(k)m_1^\diamond(k)} \widetilde{v}(k) \\ &+ \frac{n_2(k) - n_1(k)B_2(k)}{m_2^\diamond(k) - B_2(k)m_1^\diamond(k)} \widetilde{\tau}_{xy} \widetilde{\mu_0 \tau_{yy}}(k) \end{aligned} \quad (5.3)$$

$$\begin{aligned} \frac{\widetilde{D}u}{Dt}(k) &= i(\omega + k) \left(\frac{\widehat{B}_1(k)m_2^\diamond(k) - m_1^\diamond(k)}{m_2^\diamond(k) - B_2(k)m_1^\diamond(k)} \widetilde{v}(k) \right. \\ &\left. + \frac{1 - \widehat{B}_1 B_2(k)}{m_2^\diamond(k) - B_2(k)m_1^\diamond(k)} \widetilde{\tau}_{xy} \widetilde{\mu_0 \tau_{yy}}(k) \right). \end{aligned} \quad (5.4)$$

Then substituting in appropriate replacements for \diamond and the half-range functions leads to a system of coupled scalar Wiener–Hopf equations which we assemble in to a matrix Wiener–Hopf equation and rearrange.

There are multiple ways in which the equations may be arranged to attain the Wiener–Hopf matrix. The general format sought here is in the form

$$\mathbf{A}(k)\Phi_+(k) = \mathbf{B}(k)\Phi_-(k) + \mathbf{C}(k),$$

where the unknown functions analytic in \mathcal{D}^+ or \mathcal{D}^- are from section 5.3.1. The upper and lower vectors are therefore

$$\widetilde{\Phi}^+(k) = \begin{pmatrix} \widetilde{v}_+^{(d)}(k) \\ \widetilde{\frac{Du}{Dt}}_+^{(c)}(k) \\ \widetilde{\tau_{xy} \pm \tau_{yy}}_+^{(-b)}(k) \\ \widetilde{\tau_{yy}}_+^{(-a)}(k) \end{pmatrix}, \quad \widetilde{\Phi}^-(k) = \begin{pmatrix} \widetilde{\tau_{yy}}_-^{(d)}(k) \\ \widetilde{\tau_{xy} \mp \tau_{yy}}_-^{(c)}(k) \\ \widetilde{\frac{Du}{Dt}}_-^{(-b)}(k) \\ \widetilde{v}_-^{(-a)}(k) \end{pmatrix}.$$

The unknowns were chosen in this order so that the matrices will be of triangular format in the matrix Wiener–Hopf equation. We note that the asymptotic behaviour of the plus and minus functions may be found by considering

5.3. CONSTRUCTING THE MATRIX WIENER–HOPF EQUATION 5.3

the following edge conditions

$$\begin{aligned} \lim_{x \rightarrow d^+} v(x, 0) &= \frac{d^2}{2} - 1, & \lim_{x \rightarrow -a^-} v(x, 0) &= \frac{a^2}{2} - 1, \\ \lim_{x \rightarrow c^+} \frac{Du}{Dt}(x, 0) &= W, & \lim_{x \rightarrow -b^-} \frac{Du}{Dt}(x, 0) &= W, \\ \lim_{x \rightarrow d^-} \tau_{yy}(x, 0) &= 0, & \lim_{x \rightarrow -a^+} \tau_{yy}(x, 0) &= 0, \\ \lim_{x \rightarrow c^-} \tau_{xy} \pm \mu_0 \tau_{yy}(x, 0) &= 0, & \lim_{x \rightarrow -b^+} \tau_{xy} \pm \mu_0 \tau_{yy}(x, 0) &= 0. \end{aligned}$$

These give quadratic decay in the complex plane for the edge conditions which tend to zero and linear decay otherwise.

To generate the matrix Wiener–Hopf equation we substitute in appropriate replacements to \diamond and the transformed boundary condition into equations (5.3) and (5.4). To construct each scalar Wiener–Hopf equation we consider the two boundary conditions at each transition point and the single boundary condition which holds over the same transition point. Then we may arrange the coupled scalar Wiener–Hopf equations into a matrix format and rearrange to find the following,

$$A(k) = \begin{pmatrix} 1 & 0 & 0 & 0 \\ \frac{-i(\omega+k)(m_1^{\mp} - \hat{B}_1 m_2^{\mp})}{B_2 m_1^{\mp} - m_2^{\mp}} \times e^{ik(d-c)} & 1 & 0 & 0 \\ \frac{i(\omega+k)(m_1^{\pm} - \hat{B}_1 m_2^{\pm})}{B_2 m_1^{\pm} - m_2^{\pm}} \times e^{ik(b+d)} & \frac{-B_2 m_1^{\pm} - m_2^{\pm}}{B_2 m_1^{\pm} - m_2^{\pm}} \times e^{ik(b+c)} & \frac{i(B_2 \hat{B}_1 - 1)(\omega+k)}{B_2 m_1^{\pm} - m_2^{\pm}} & 0 \\ \frac{-(n_1 m_2^{\pm} - n_2 m_1^{\pm})}{(n_1 m_2^{\mp} - n_2 m_1^{\mp})} \times e^{ik(a+d)} & 0 & \frac{(B_2 n_1 - n_2)}{(n_1 m_2^{\pm} - n_2 m_1^{\pm})} \times e^{ik(a-b)} & \frac{m_2^{\pm} - B_2 m_1^{\pm}}{(n_1 m_2^{\pm} - n_2 m_1^{\pm})} \end{pmatrix},$$

$$\mathbf{B}(k) = \begin{pmatrix} \frac{m_2^\mp - B_2 m_1^\mp}{n_1 m_2^\mp - n_2 m_1^\mp} & \frac{(B_2 n_1 - n_2)}{n_1 m_2^\mp - n_2 m_1^\mp} \times e^{ik(c-d)} & 0 & \frac{-(n_1 m_2^\mp - n_2 m_1^\mp)}{n_1 m_2^\mp - n_2 m_1^\mp} \times e^{-ik(a+d)} \\ 0 & \frac{i(B_2 \hat{B}_1 - 1)(\omega + k)}{B_2 m_1^\mp - m_2^\mp} & \frac{-B_2 m_1^\mp - m_2^\mp}{B_2 m_1^\mp - m_2^\mp} \times e^{-ik(b+c)} & \frac{i(\omega + k)(m_1^\mp - \hat{B}_1 m_2^\mp)}{B_2 m_1^\mp - m_2^\mp} \times e^{-ik(a+c)} \\ 0 & 0 & 1 & \frac{-i(\omega + k)(m_1^\pm - \hat{B}_1 m_2^\pm)}{B_2 m_1^\pm - m_2^\pm} \times e^{ik(b-a)} \\ 0 & 0 & 0 & 1 \end{pmatrix},$$

$$\mathbf{C}(k) = \begin{pmatrix} \frac{-(n_1 m_2^\mp - n_2 m_1^\mp)}{n_1 m_2^\mp - n_2 m_1^\mp} e^{-ikd} f(k) \\ \frac{i(\omega + k)(m_1^\mp - \hat{B}_1 m_2^\mp)}{B_2 m_1^\mp - m_2^\mp} e^{-ikc} f(k) - \frac{B_2 m_1^\mp - m_2^\mp}{B_2 m_1^\mp - m_2^\mp} e^{-ikc} g(k) \\ \frac{-i(\omega + k)(m_1^\pm - \hat{B}_1 m_2^\pm)}{B_2 m_1^\pm - m_2^\pm} e^{ikb} f(k) + \frac{B_2 m_1^\pm - m_2^\pm}{B_2 m_1^\pm - m_2^\pm} e^{ikb} g(k) \\ \frac{(n_1 m_2^\pm - n_2 m_1^\pm)}{(n_1 m_2^\mp - n_2 m_1^\mp)} e^{ika} f(k) \end{pmatrix}.$$

We have constructed a (4×4) matrix Wiener–Hopf equation which is not singular and has the required analyticity of the exponential factors to apply the iterative method, which has been outlined in section 3.3.1. In the following section we discuss the application of the iterative method to approximate the stick-slip solution.

5.4 Application of the iterative method

The physical model has now been reduced to a 4×4 matrix Wiener–Hopf equation with the required structure to apply the iterative method. The exponential terms allows one to apply an iterative method, similar to 4.4, in which the non-diagonals are first approximated to be zero. The approximation decouples each scalar equation in the system and so each scalar equation may be treated as a scalar Wiener–Hopf equation which may be solved numerically.

To aide with the application of the iterative method, we define the functions $A_{33}(k)$, $A_{34}(k)$, $A_{44}(k)$, $B_{11}(k)$, $B_{21}(k)$, $B_{22}(k)$, $K_1(k)$ and $K_2(k)$ as the entries of the 4×4 matrix Wiener–Hopf equation we have constructed in the stick-slip regime,

$$A(k) = \begin{pmatrix} 1 & 0 & 0 & 0 \\ -K_1(k) & 1 & 0 & 0 \\ \times e^{ik(d-c)} & & & \\ K_2(k) & -1 & A_{33}(k) & 0 \\ \times e^{ik(b+d)} & \times e^{ik(b+c)} & & \\ -1 & 0 & A_{34}(k) & A_{44}(k) \\ \times e^{ik(a+d)} & & \times e^{ik(a-b)} & \end{pmatrix},$$

$$\mathbf{B}(k) = \begin{pmatrix} B_{11}(k) & B_{21}(k) & 0 & -1 \\ & \times e^{ik(c-d)} & & \times e^{-ik(a+d)} \\ 0 & B_{22}(k) & -1 & K_1(k) \\ & & \times e^{-ik(b+c)} & \times e^{-ik(a+c)} \\ 0 & 0 & 1 & -K_2(k) \\ & & & \times e^{ik(b-a)} \\ 0 & 0 & 0 & 1 \end{pmatrix},$$

$$\mathbf{C}(k) = \begin{pmatrix} -e^{-ikd} f(k) \\ K_1(k)e^{-ikc} f(k) - e^{-ikc} g(k) \\ -K_2(k)e^{ikb} f(k) + e^{ikb} g(k) \\ e^{ika} f(k) \end{pmatrix}.$$

To arrive at the initial approximations we approximate all of the exponential terms in the matrices to zero, multiplicatively split the scalar kernel functions, and additively split the resulting forcing term. The initial decoupled scalar equations are

$$\begin{aligned} \widetilde{v}_+^{(d)0}(k) &= B_{11}(k) \widetilde{\tau}_{yy-}^{(d)}(k) - e^{-ikd} f(k) \\ \frac{\widetilde{D}u}{Dt_+}^{(c)0}(k) &= B_{22}(k) \widetilde{\tau}_{xy} \mp \widetilde{\tau}_{yy-}^{(c)0}(k) + e^{-ikc} (K_1(k)f(k) - g(k)) \\ A_{33}(k) \widetilde{\tau}_{xy} \pm \widetilde{\tau}_{yy+}^{(-b)0}(k) &= \frac{\widetilde{D}u}{Dt_-}^{(-b)0}(k) + e^{ikb} (g(k) - K_2(k)f(k)) \\ A_{44}(k) \widetilde{\tau}_{yy+}^{(-a)}(k) &= \widetilde{v}_-^{(-a)}(k) + e^{ika} f(k). \end{aligned}$$

To find the initial solution only Wiener–Hopf splittings are required on the equations above. Once the Wiener–Hopf splittings are completed, rearranging to upper and lower components is sought, then by analytic continuation one may find entire functions which may be set to zero by applications of Liouville’s theorem by the asymptotic behaviour of the half-range functions. The initial approximation of the unknowns are then

$$\begin{aligned}
\widetilde{v}_+^{(d)0}(k) &= B_{11+}(k) \left[-\frac{e^{-ikd} f(k)}{B_{11+}(k)} \right]^+, \\
\widetilde{\tau}_{yy-}^{(d)0}(k) &= -\frac{1}{B_{11-}(k)} \left[-\frac{e^{-ikd} f(k)}{B_{11+}(k)} \right]^-, \\
\widetilde{\frac{Du}{Dt}}_+^{(c)0}(k) &= B_{22+}(k) \left[\frac{e^{-ikc} (K_1(k)f(k) - g(k))}{B_{22+}(k)} \right]^+, \\
\widetilde{\tau}_{xy} \mp \tau_{yy-}^{(c)0}(k) &= -\frac{1}{B_{22-}(k)} \left[\frac{e^{-ikc} (K_1(k)f(k) - g(k))}{B_{22+}(k)} \right]^-, \\
\widetilde{\tau}_{xy} \pm \tau_{yy+}^{(-b)0}(k) &= \frac{1}{A_{33+}(k)} \left[\frac{e^{ikb} (g(k) - K_2(k)f(k))}{A_{33-}(k)} \right]^+, \\
\widetilde{\frac{Du}{Dt}}_-^{(-b)0}(k) &= -A_{33-}(k) \left[\frac{e^{ikb} (g(k) - K_2(k)f(k))}{A_{33-}(k)} \right]^-, \\
\widetilde{\tau}_{yy+}^{(-a)0}(k) &= \frac{1}{A_{44+}(k)} \left[\frac{e^{ika} f(k)}{A_{44-}(k)} \right]^+, \\
\widetilde{v}_-^{(-a)0}(k) &= -A_{44-}(k) \left[\frac{e^{ika} f(k)}{A_{44-}(k)} \right]^-.
\end{aligned}$$

Finally, by following the same approach as 3.3.1 and 4.4, the scalar equations within the matrix Wiener–Hopf are considered with the exponential terms reintroduced. Then we proceed by iteratively updating the n -th equations,

which are

$$\begin{aligned}
\widetilde{v}_+^{(d)n}(k) &= B_{11}(k)\widetilde{\tau}_{yy-}^{(d)n}(k) - e^{-ik(a+d)}\widetilde{v}_-^{(-a)n-1}(k) \\
&\quad + B_{21}(k)e^{ik(c-d)}\widetilde{\tau}_{xy} \mp \widetilde{\tau}_{yy-}^{(c)n-1}(k) - e^{-ikd}f(k), \\
\frac{\widetilde{Du}}{\widetilde{Dt}_+}^{(c)n}(k) &= B_{22}(k)\widetilde{\tau}_{xy} \mp \widetilde{\tau}_{yy-}^{(c)n}(k) - e^{-ik(b+c)}\frac{\widetilde{Du}}{\widetilde{Dt}_-}^{(-b)n-1}(k) \\
&\quad + K_1(k)\left(e^{-ik(a+c)}\widetilde{v}_-^{(-a)n-1}(k) + e^{ik(d-c)}\widetilde{v}_+^{(d)n}(k)\right) \\
&\quad + e^{-ikc}(K_1(k)f(k) - g(k)), \\
A_{33}(k)\widetilde{\tau}_{xy} \pm \widetilde{\tau}_{yy+}^{(-b)n}(k) &= \frac{\widetilde{Du}}{\widetilde{Dt}_-}^{(-b)n}(k) + e^{ik(b+c)}\frac{\widetilde{Du}}{\widetilde{Dt}_+}^{(c)n}(k) \\
&\quad - K_2(k)\left(e^{ik(b-a)}\widetilde{v}_-^{(-a)n-1}(k) + e^{ik(b+d)}\widetilde{v}_+^{(d)n}(k)\right) \\
&\quad + e^{ikb}(g(k) - K_2(k)f(k)), \\
A_{44}(k)\widetilde{\tau}_{yy+}^{(-a)n}(k) &= \widetilde{v}_-^{(-a)n}(k) - A_{34}(k)e^{ik(a-b)}\widetilde{\tau}_{xy} \pm \widetilde{\tau}_{yy+}^{(-b)n}(k) \\
&\quad + e^{ik(a+d)}\widetilde{v}_+^{(d)n}(k) + e^{ika}f(k).
\end{aligned}$$

We find the solutions by treating the reintroduced terms as a forcing and applying the Wiener–Hopf splittings outlined in sections 3.2.2, 4.4.1, and 5.4.1. The solutions to the n -th iteration are thus

$$\begin{aligned}
\widetilde{v}_+^{(d)n}(k) &= B_{11+}(k)\left[\frac{-e^{-ik(a+d)}\widetilde{v}_-^{(-a)n-1}}{B_{11+}(k)}\right. \\
&\quad \left. + \frac{B_{21}(k)e^{ik(c-d)}\widetilde{\tau}_{xy} \mp \widetilde{\tau}_{yy-}^{(c)n-1} - e^{-ikd}f(k)}{B_{11+}(k)}\right]^+, \\
\widetilde{\tau}_{yy=0-}^{(d)n}(k) &= -\frac{1}{B_{11-}(k)}\left[\frac{-e^{-ik(a+d)}\widetilde{v}_-^{(-a)n-1}}{B_{11+}(k)}\right. \\
&\quad \left. + \frac{B_{21}(k)e^{ik(c-d)}\widetilde{\tau}_{xy} \mp \widetilde{\tau}_{yy-}^{(c)n-1} - e^{-ikd}f(k)}{B_{11+}(k)}\right]^-,
\end{aligned}$$

$$\begin{aligned}
\frac{\widetilde{Du}^{(c)n}}{Dt_+}(k) &= B_{22+}(k) \left[\frac{K_1(k) \left(e^{-ik(a+c)} \widetilde{v}_-^{(-a)n-1} + e^{ik(d-c)} \widetilde{v}_+^{(d)n} \right)}{B_{22+}(k)} \right. \\
&\quad \left. + \frac{-e^{-ik(b+c)} \frac{\widetilde{Du}^{(-b)n-1}}{Dt_-} + e^{-ikc} (K_1(k)f(k) - g(k))}{B_{22+}(k)} \right]^+, \\
\widetilde{\tau_{xy} \mp \tau_{yy-}}^{(c)n}(k) &= -\frac{1}{B_{22-}(k)} \left[\frac{K_1(k) \left(e^{-ik(a+c)} \widetilde{v}_-^{(-a)n-1} + e^{ik(d-c)} \widetilde{v}_+^{(d)n} \right)}{B_{22+}(k)} \right. \\
&\quad \left. + \frac{-e^{-ik(b+c)} \frac{\widetilde{Du}^{(-b)n-1}}{Dt_-} + e^{-ikc} (K_1(k)f(k) - g(k))}{B_{22+}(k)} \right]^-, \\
\widetilde{\tau_{xy} \pm \tau_{yy+}}^{(-b)n}(k) &= \frac{1}{A_{33+}(k)} \left[\frac{-K_2(k) \left(e^{ik(b-a)} \widetilde{v}_-^{(-a)n-1} + e^{ik(b+d)} \widetilde{v}_+^{(d)n} \right)}{A_{33-}(k)} \right. \\
&\quad \left. + \frac{e^{ik(b+c)} \frac{\widetilde{Du}^{(c)n}}{Dt_+} + e^{ikb} (g(k) - K_2(k)f(k))}{A_{33-}(k)} \right]^+, \\
\frac{\widetilde{Du}^{(-b)n}}{Dt_-}(k) &= -A_{33-}(k) \left[\frac{-K_2(k) \left(e^{ik(b-a)} \widetilde{v}_-^{(-a)n-1} + e^{ik(b+d)} \widetilde{v}_+^{(d)n} \right)}{A_{33-}(k)} \right. \\
&\quad \left. + \frac{e^{ik(b+c)} \frac{\widetilde{Du}^{(c)n}}{Dt_+} + e^{ikb} (g(k) - K_2(k)f(k))}{A_{33-}(k)} \right]^-, \\
\widetilde{\tau_{yy+}}^{(-a)n}(k) &= \frac{1}{A_{44+}(k)} \left[\frac{-A_{34}(k) e^{ik(a-b)} \widetilde{\tau_{xy} \pm \tau_{yy+}}^{(-b)n}}{A_{44-}(k)} \right. \\
&\quad \left. + \frac{e^{ik(a+d)} \widetilde{v}_+^{(d)n} + e^{ika} f(k)}{A_{44-}(k)} \right]^+, \\
\widetilde{v}_-^{(-a)n}(k) &= -A_{44-}(k) \left[\frac{-A_{34}(k) e^{ik(a-b)} \widetilde{\tau_{xy} \pm \tau_{yy+}}^{(-b)n}}{A_{44-}(k)} \right. \\
&\quad \left. + \frac{e^{ik(a+d)} \widetilde{v}_+^{(d)n} + e^{ika} f(k)}{A_{44-}(k)} \right]^-.
\end{aligned}$$

In the implementation, more iterations have been necessary than the full-slip limit but convergence to at least $1e - 8$ occurs typically in less than eight iterations. We do note that the first and last row of the matrix Wiener–Hopf equation is very similar to the two equations in the full-slip limit, allowing

the same Wiener–Hopf splittings to solve the equations. The central two rows require further consideration and the additional details for the splittings required for them is discussed in the following section.

5.4.1 Wiener–Hopf splittings

We follow the same numerical procedures for computing the Cauchy transforms as we did in section 4.4.1 but shall include details on the additional terms and intricacies in this more complicated setting.

5.4.1.1 Wiener–Hopf factorisation

To compute the Wiener–Hopf factorisations we use the same approach outlined in section 4.4.1.1 but will outline the additional factorisations required. We note that functions $B_{11}(k)$ and $A_{44}(k)$ are the same as $K(k)$ so we may compute their factorisations in the same way. However, to compute the factorisation of $B_{22}(k)$ and $A_{33}(k)$ we analytically factorise the $(k + \omega)$ term to the lower component and then compute the factorisation of the remaining function with the same approach as section 4.4.1.1. Explicitly factorising the functions $\widehat{B}_{22}(k)$ and $\widehat{A}_{33}(k)$ where,

$$B_{22}(k) = (k + \omega)\widehat{B}_{22}(k), \quad A_{33}(k) = (k + \omega)\widehat{A}_{33}(k).$$

Then we proceed to numerically factorise $\widehat{B}_{22}(k)$ and $\widehat{A}_{33}(k)$ in the exact same way we factorised $K(k)$.

5.4.1.2 Wiener–Hopf decomposition

To compute the Wiener–Hopf decompositions we use the same approach as section 4.4.1.2 but take care when computing the decomposition of terms with exponential growth in both \mathcal{D}^+ and \mathcal{D}^- . To avoid the exponential

growth we consider each exponent separately, so for a general forcing $f(k)$,

$$f(k) = e^{ikL} f_1(k) + e^{-ikL} f_2(k)$$

where $f_{1,2}(k)$ are analytic in the strip \mathcal{D} . We consider the additive decomposition of the terms $e^{ikL} f_1(k)$ and $e^{-ikL} f_2(k)$ separately to avoid the exponential growth of considering both together. Then we may proceed as section 4.4.1.2 by deforming to the steepest descent contour and applying the spectral method outlined in 4.4.1.

In general we take the above approach to compute the decompositions of the forcing with oscillatory behaviour in both \mathcal{D}^+ and \mathcal{D}^- but in the cases where $f_{1,2}(k)$ are not analytic in the strip we proceed in the following way. This occurs when we take the decomposition of the terms

$$\begin{aligned} e^{-ikc} f(k) &= \frac{e^{-ik(a+c)}}{ik} \left(1 - \frac{a^2}{2} - \frac{a}{ik} + \frac{1}{k^2} \right) - \frac{e^{ik(d-c)}}{ik} \left(1 - \frac{d^2}{2} + \frac{d}{ik} + \frac{1}{k^2} \right) \\ e^{ikb} f(k) &= \frac{e^{-ik(a-b)}}{ik} \left(1 - \frac{a^2}{2} - \frac{a}{ik} + \frac{1}{k^2} \right) - \frac{e^{ik(d+b)}}{ik} \left(1 - \frac{d^2}{2} + \frac{d}{ik} + \frac{1}{k^2} \right) \end{aligned}$$

the LHS is analytic in the strip but by considering the exponential terms separately we find singularities at the origin. Instead, we may subtract the singularities without changing the functions,

$$\begin{aligned} e^{-ikc} f(k) &= \frac{e^{-ik(a+c)}}{ik} \left(1 - \frac{a^2}{2} - \frac{a}{ik} + \frac{1}{k^2} \right) - \left(1 - \frac{c^2}{2} - \frac{c}{ik} + \frac{1}{k^2} \right) \\ &\quad + \left(1 - \frac{c^2}{2} - \frac{c}{ik} + \frac{1}{k^2} \right) - \frac{e^{ik(d-c)}}{ik} \left(1 - \frac{d^2}{2} + \frac{d}{ik} + \frac{1}{k^2} \right), \\ e^{ikb} f(k) &= \frac{e^{-ik(a-b)}}{ik} \left(1 - \frac{a^2}{2} - \frac{a}{ik} + \frac{1}{k^2} \right) - \left(1 - \frac{b^2}{2} + \frac{b}{ik} + \frac{1}{k^2} \right) \\ &\quad + \left(1 - \frac{b^2}{2} + \frac{b}{ik} + \frac{1}{k^2} \right) - \frac{e^{ik(d+b)}}{ik} \left(1 - \frac{d^2}{2} + \frac{d}{ik} + \frac{1}{k^2} \right). \end{aligned}$$

Thus, we have arrived at a form where we may apply the quadratic additive decomposition procedure outlined in section 4.4.1.2 to calculate the splitting.

5.5 Free-boundary problem

As in the full-slip regime, we do not know the location of the junction points $-a$, $-b$, c and d and need to determine their location as part of the solution. In section 4.5 we were able to determine the location of the contact points $-a$ and d by ensuring continuity of the solution at the points $-a$ and d so we seek to apply the same technique to locate the stick-slip transition points $-b$ and c also. A note on stick-slip friction based on the literature is that it is unclear what determines the transition but it is assumed that within the stick region, the tangential force is insufficient for causing stick,

$$|\tau_{xy}(x)| \leq \mu_0 |\tau_{yy}(x)| \Rightarrow |\tau_{xy} \mp \mu_0 \tau_{yy}(x)| \leq 2\mu_0 |\tau_{yy}(x)|, \quad \forall x \in (-b, c) \quad (5.5)$$

We continue by applying the method used in section 4.5, determining the location of $-a$, $-b$, c and d through the conditions $\tau_{yy}(-a) = 0$, $\tau_{xy} \pm \mu_0 \tau_{yy}(-b) = 0$, $\tau_{xy} \mp \mu_0 \tau_{yy}(c) = 0$ and $\tau_{yy}(d) = 0$ respectively. In this more complicated setting it is not clear whether framing the minimisation problem as a multivariate minimisation problem or whether multiple independent minimisation problems is more appropriate. In our implementation of both systems we found that a multivariate approach, Broyden's method [17], was less stable than applying independent secant methods. Thus, we applied the secant method to each free-boundary point independently. To formulate the minimisation problem more formally,

$$\mathbf{min}_{\chi^j} \|\tau_{yy}^j(\chi^j, 0)\|, \quad \mathbf{min}_{\chi^j} \|\tau_{xy} \diamond \mu_0 \tau_{yy}^j(\chi^j, 0)\|,$$

where we define the initial and j -th iteration junction points and corresponding solution as

$$\begin{aligned} \chi^0 &= (a^0, b^0, c^0, d^0), & \tau^0(x) &= \tau_{yy}^0(x, 0), & \psi^0(x) &= \tau_{xy} \diamond \mu_0 \tau_{yy}^0(x, 0), \\ \chi^j &= (a^j, b^j, c^j, d^j), & \tau^j(x) &= \tau_{yy}^j(x, 0), & \psi^j(x) &= \tau_{xy} \diamond \mu_0 \tau_{yy}^j(x, 0). \end{aligned}$$

To find an initial solution, we take two initial guesses of the junction points, χ^0, χ^1 and find the corresponding solutions $\tau_{yy}^0(x, 0), \tau_{yy}^1(x, 0)$ and $\psi^0(x, 0), \psi^1(x, 0)$. Then we find the next iteration of junction point by implementing a secant method. We may find the $j + 1$ -th iteration of junction points, χ^{j+1} , by solving the following equations

$$\begin{aligned} a^{j+1} &= a^j - \tau^j(-a^j) \times \left(\frac{a^j - a^{j-1}}{\tau^j(-a^j) - \tau^{j-1}(-a^{j-1})} \right) \\ b^{j+1} &= b^j - \psi^j(-b^j) \times \left(\frac{b^j - b^{j-1}}{\psi^j(-b^j) - \psi^{j-1}(-b^{j-1})} \right) \\ c^{j+1} &= c^j - \psi^j(c^j) \times \left(\frac{c^j - c^{j-1}}{\psi^j(c^j) - \psi^{j-1}(c^{j-1})} \right) \\ d^{j+1} &= d^j - \tau^j(d^j) \times \left(\frac{d^j - d^{j-1}}{\tau^j(d^j) - \tau^{j-1}(d^{j-1})} \right). \end{aligned}$$

This procedure is iterated until successive iterations are below a tolerance,

$$\|\chi^j - \chi^{j-1}\| \leq \text{tol}.$$

Once converged, the final χ^j will give a solution where the junction points are accurately estimated and ensure continuity of the solution.

This approach works well for large ω as shown in figure 5.5.1 and the figures in section 5.6.2 however for smaller values of ω there is some oscillatory behaviour which occurs which may be related to Gibbs Phenomena, see 5.6.3 for more discussion on these instabilities and [93] for more on Gibbs Phenomena. We note that there is a strict ordering of the junction points

$$-a < -b < c < d \tag{5.6}$$

and breaking this ordering would lead to an incorrect structure in the matrix Wiener–Hopf equation but we note this could indicate an alternative arrangement of the stick-slip zones may be necessary. The ordering of the transition points gives conditions which must be satisfied by the minimisation method and as shown in 4.6 the contact points $-a$ and d are related to

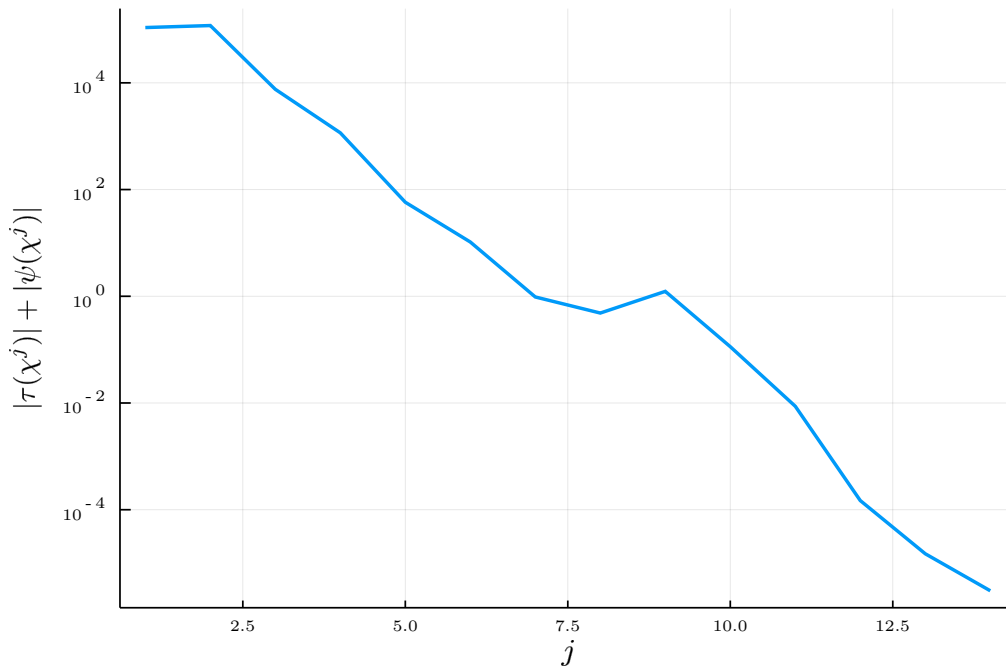


Figure 5.5.1: A plot of the error for the free-boundary method at each iteration until the solution has converged. The parameter values are those in table 5.1.

the value of ω and the same applies here. Thus, to ensure that the ordering holds we may simultaneously vary ω and W to find a solution. Physically a large positive W would correspond to full-slip in one direction and a large negative W would correspond to full-slip in the opposing direction.

In the following sections we outline an analytical approach for locating the free-boundary points and discuss the difficulties in implementing them here. The free-boundary method applied here is the secant method outlined, but include the analysis of the large k behaviour as a discussion point.

5.5.1 Large k limit

To understand more about the behaviour at the free-boundary points we consider the half-range functions in the limit $k \rightarrow \infty$. An asymptotic expansion may be derived from repeated use of integration by parts, which then

relates the behaviour at the free-boundary point to the large k asymptotic behaviour of the half-range function.

To begin with, recall the following half-range variables which were derived from the transformation of the boundary conditions

$$\begin{aligned} \widetilde{v}_+^{(d)}(k), \widetilde{\frac{Du}{Dt}}_+^{(c)}(k), \widetilde{\tau_{xy} \pm \tau_{yy}}_+^{(-b)}(k), \widetilde{\tau_{yy}}_+^{(-a)}(k) \\ \widetilde{\tau_{yy}}_-^{(d)}(k), \widetilde{\tau_{xy} \mp \tau_{yy}}_-^{(c)}(k), \widetilde{\frac{Du}{Dt}}_-^{(-b)}(k), \widetilde{v}_-^{(-a)}(k). \end{aligned}$$

By considering the definition of these half-range variables in the limit as $k \rightarrow \infty$, the asymptotic behaviour of the variables may be related to the behaviour of the spatial variables at the free-boundary point.

To illustrate the relationship between the solution at the free-boundary points and the asymptotic behaviour of the half-range variables an example with $\widetilde{\tau_{yy}}_+^{(-a)}(k)$ is considered. Recalling the definition and applying a repeated use of integration by parts gives the following,

$$\begin{aligned} \widetilde{\tau_{yy}}_+^{(-a)}(k) &= \int_{-a}^{\infty} \tau_{yy}(x, 0) e^{ik(x+a)} dx \\ &= \left[-\tau_{yy}(x, 0) \frac{e^{ik(x+a)} i}{k} \right]_{-a}^{\infty} + \int_{-a}^{\infty} \frac{\partial \tau_{yy}}{\partial x}(x, 0) \frac{ie^{ik(x+a)}}{k} dx \\ &= \left[\tau_{yy}(-a, 0) \frac{(i)}{k} \right] + \sum_{n=1}^{\infty} \left[\frac{\partial^n \tau_{yy}}{\partial x^n}(-a, 0) \frac{(i)^{n+1}}{k^{n+1}} \right]. \end{aligned}$$

Then by imposing a condition on the value of $\tau_{yy}(-a, 0)$ from the boundary conditions, the asymptotic behaviour of the transformed variable $\widetilde{\tau_{yy}}_+^{(-a)}(k)$ as $k \rightarrow \infty$ may be found. In this example the condition imposed and the corresponding asymptotic behaviour would be

$$\tau_{yy}(-a, 0) = 0, \quad \widetilde{\tau_{yy}}_+^{(-a)}(k) \sim \frac{\tau(-a)}{k^2}, \text{ as } |k| \rightarrow \infty,$$

where $\tau(-a)$ is a constant.

Applying the same argument as above suggests the large k asymptotic behaviour for all the half-range variables to be

$$\begin{aligned} \widetilde{v}_+^{(d)}(k) &\sim \frac{1}{ik} \left(\frac{d^2}{2} - 1 \right), & \widetilde{v}_-^{(-a)}(k) &\sim -\frac{1}{ik} \left(\frac{a^2}{2} - 1 \right), \\ \widetilde{\frac{Du}{Dt}}_+^{(c)}(k) &\sim \frac{W}{ik}, & \widetilde{\frac{Du}{Dt}}_-^{(-b)}(k) &\sim -\frac{W}{ik}, \\ \widetilde{\tau}_{yy-}^{(d)}(k) &\sim \frac{\tau(d)}{k^2}, & \widetilde{\tau}_{yy+}^{(-a)}(k) &\sim \frac{\tau(-a)}{k^2}, \\ \widetilde{\tau_{xy} \mp \tau_{yy-}}^{(c)}(k) &\sim \frac{\psi(c)}{k^2}, & \widetilde{\tau_{xy} \pm \tau_{yy+}}^{(-b)}(k) &\sim \frac{\psi(-b)}{k^2}. \end{aligned}$$

Thus, instead of the previous method of iterating the entire Wiener–Hopf solution based on re-estimating $-a, -b, c$ and d , only the large k behaviour of the half-range variables may be considered. However, as discussed in section 4.5, it is difficult to derive the large k asymptotic behaviour of the half-range functions as they have been approximated numerically.

5.6 Results

In this section we discuss the preliminary results for the stick-slip friction model. These results are preliminary as the small ω limit causes instabilities in our solution and it is not clear yet if this invalidates the results in the large ω limit. However, we include results for both the large and small ω limits to illustrate the differences. Furthermore, we analyse the stick-slip configurations in the large ω limit and give an explanation on the relationship of the slip directions and the parameter W . Finally, we shall give a brief discussion on the small ω limit.

To find the full solution we invert the Fourier transformed variables by using a Gaussian quadrature method as discussed in section 4.6. We note that there are some additional half-range functions $\widetilde{\frac{Du}{Dt}}_+^{(c)}(k)$, $\widetilde{\tau_{xy} \pm \tau_{yy+}}^{(-b)}(k)$, $\widetilde{\tau_{xy} \mp \tau_{yy-}}^{(c)}(k)$ and $\widetilde{\frac{Du}{Dt}}_-^{(-b)}(k)$, which are to be inverted via quadrature also.

For completeness we state the integrals which are to be computed

$$\tau_{xy} \diamond \tau_{yy}(x, 0) = \frac{1}{2\pi} \int_{-\infty}^{\infty} \widetilde{\tau_{xy} \diamond \tau_{yy}}(k, 0) e^{-ikx} dk,$$

$$\frac{Du}{Dt}(x, 0) = \frac{1}{2\pi} \int_{-\infty}^{\infty} \frac{\widetilde{Du}^{(c)}}{Dt_+}(k) e^{ik(c-x)} + \frac{\widetilde{Du}^{(-b)}}{Dt_-}(k) e^{-ik(b+x)} + g(k) e^{-ikx} dk.$$

5.6.1 Parameters

In the parameter study in section 4.6 we state that any parameter set is valid provided they satisfy the inequality $V^2 < \frac{\mu}{\rho}$, and the condition is required here too, to ensure that a strip on analyticity remains. This inequality persists in the stick-slip case because the same convected elastic half-space is considered, and so the general solution is the same. As shown in section 4.6, solutions may be found for Alternative parameter values, however, only the parameter values for structural steel (see table 5.1) will be considered here.

Parameter	Value	Dimensions
λ	210000	MPa
μ	81000	MPa
μ_0	0.3	-
ρ	7850	kg m ⁻³
V	1	-
ω	-8i	-

Table 5.1: The parameter values for structural steel [11], which are used for the plots shown in this section.

5.6.2 Stick-slip configuration

The analysis of the stick-slip configurations will be investigated here, with a focus to understand how the directions of slip changes the solution and the

parameter W . We expect that the slipping directions should always be in the same direction and that the value of W determines the slip configurations. As an example, consider the case $W > 0$, where the cylinder is rotating slower than the convection speed and so a particle on the surface of the elastic media must reduce its speed before the stick region and then increase its speed after the stick region. In this case, the speed of a particle on the surface of the elastic media is greater than the cylinder's in both slip regions, so one would expect the same direction of slip on both sides. In this example, the resulting configuration is backward-slip in both slip regions. We note that for $W < 0$ one would expect the opposite to occur and so only forward-slip should be present in both slip regions.

All of the possible stick-slip configurations forward-stick-forward, forward-stick-backward, backward-stick-forward, and backward-stick-backward are shown in figures 5.6.1 , 5.6.2, 5.6.3, and 5.6.4 respectively. These figures agree with the expectation that the slip directions and W are linked as the forward-stick-forward and backward-stick-backward configurations have a negative and positive value of W respectively. Additionally, we note that in the remaining configurations (forward-stick-backward and backward-stick-forward) the correct locations of $-a$, $-b$, c and d could not be found but some values were chosen to illustrate the solution in these two cases. The correct locations could not be found as the located points did not satisfy the ordering in equation (5.6). Furthermore, we observe the sharpness in the plots of $u(x, 0)$ for the forward-stick-backward and backward-stick-forward configurations, which suggests that these may not be physically realisable. Therefore, we deduce that stick-slip friction with a roller speed close to its convected speed yields configurations where both slip regions have the same direction however we require further study of the small ω limit for conclusive evidence.

Forward-stick-forward

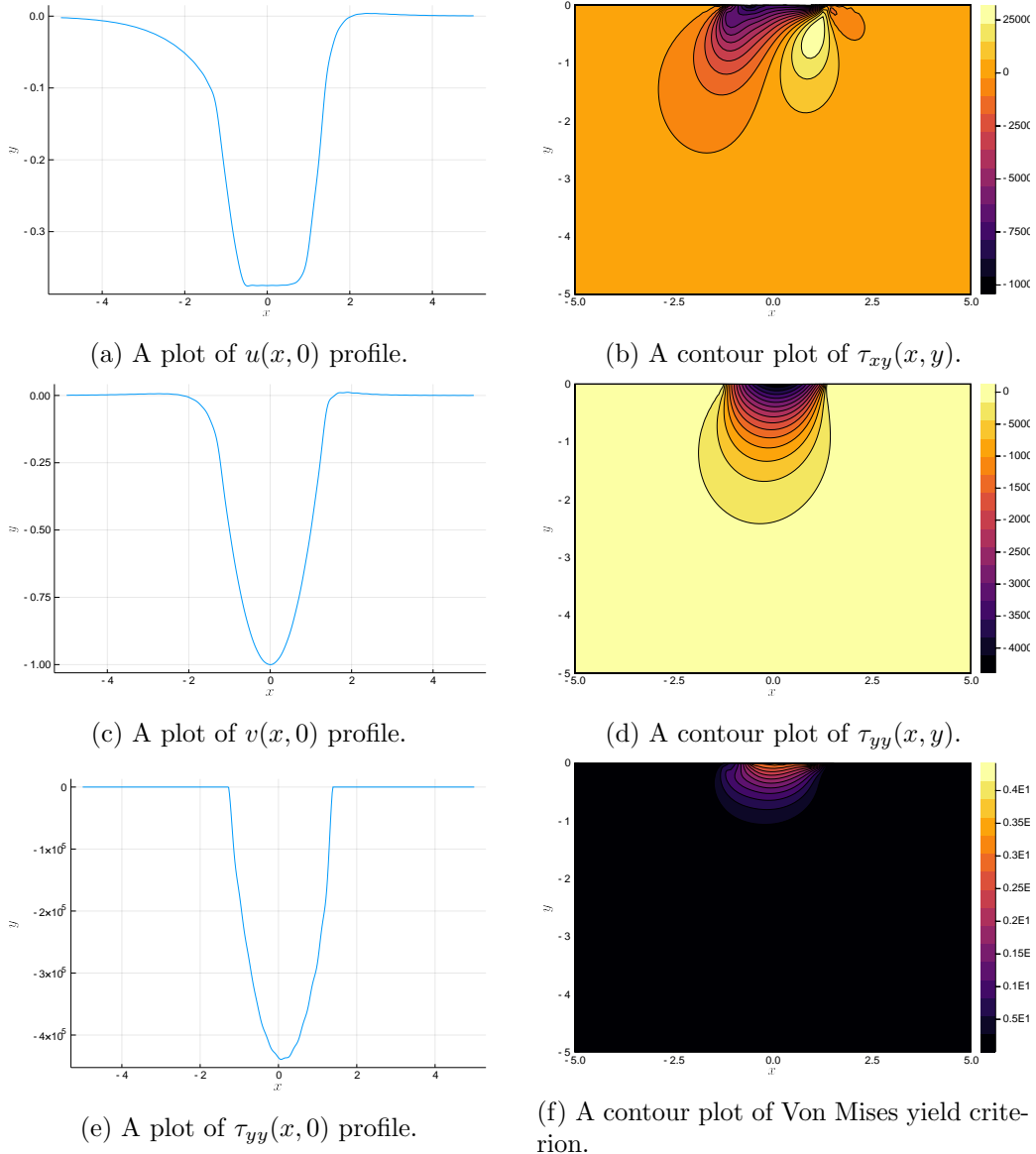
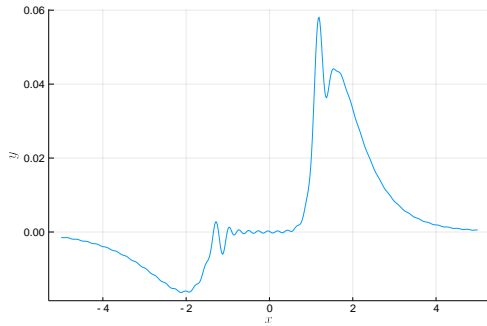
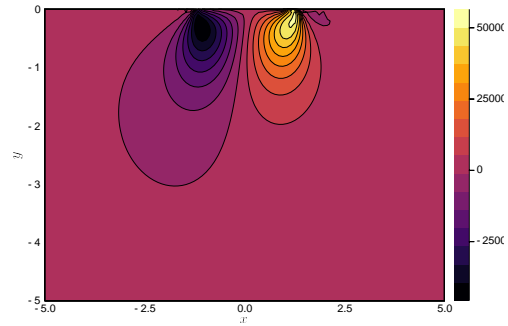


Figure 5.6.1: Plots of the solution for the forward-stick-forward configuration. The angular velocity of the cylinder is taken to be $W = -3$ and the junction points were found to be $a = 1.27, b = 0.58, c = 1.07, d = 1.39$.

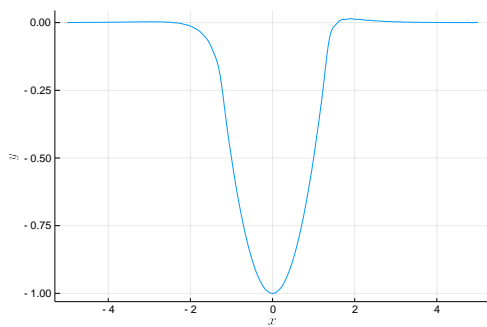
Forward-stick-backward



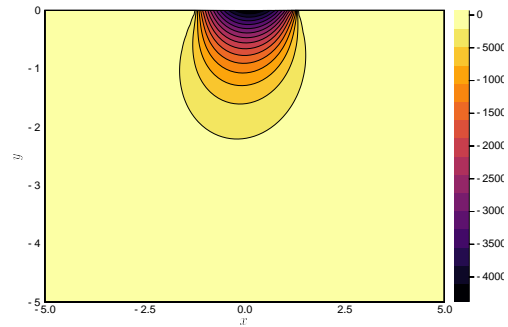
(a) A plot of $u(x, 0)$ profile.



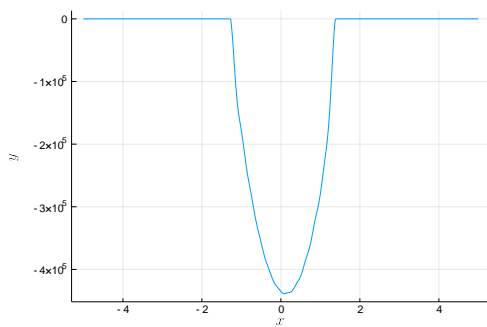
(b) A contour plot of $\tau_{xy}(x, y)$.



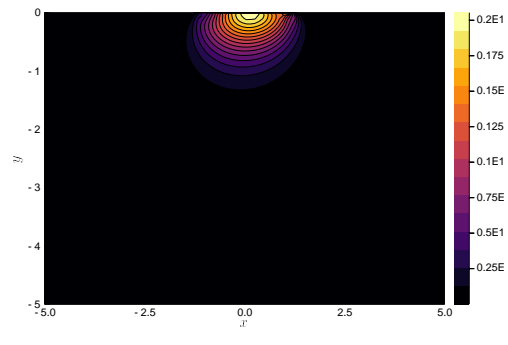
(c) A plot of $v(x, 0)$ profile.



(d) A contour plot of $\tau_{yy}(x, y)$.



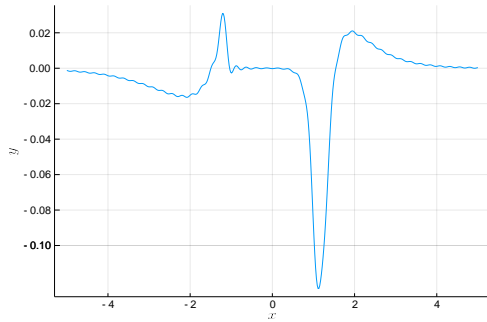
(e) A plot of $\tau_{yy}(x, 0)$ profile.



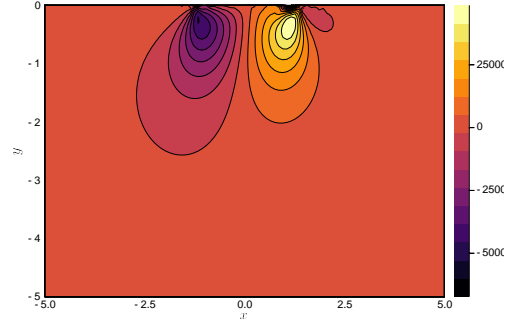
(f) A contour plot of Von Mises yield criterion.

Figure 5.6.2: Plots of the solution for the forward-stick-backward configuration. The angular velocity of the cylinder is taken to be $W = 0$ and the junction points were found to be $a = 1.28, b = 1.09, c = 1.12, d = 1.38$.

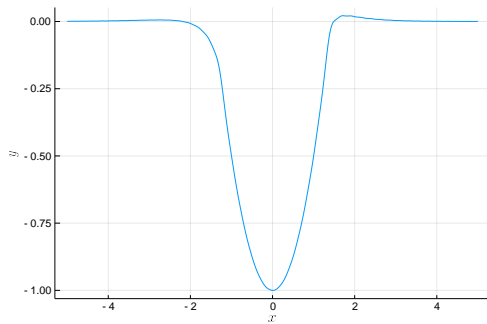
Backward-stick-forward



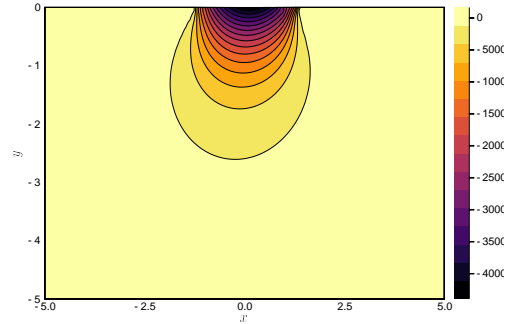
(a) A plot of $u(x, 0)$ profile.



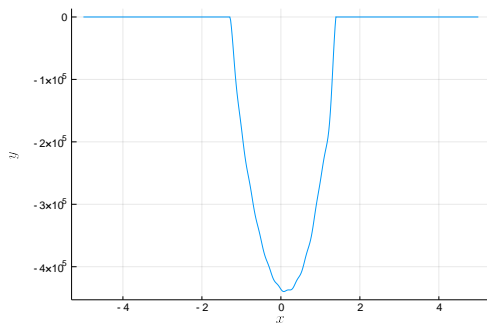
(b) A contour plot of $\tau_{xy}(x, y)$.



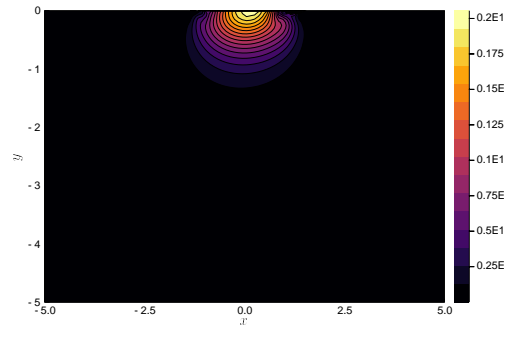
(c) A plot of $v(x, 0)$ profile.



(d) A contour plot of $\tau_{yy}(x, y)$.



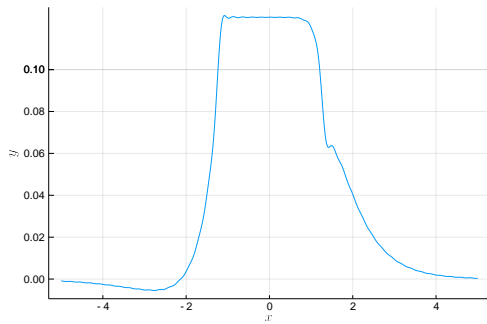
(e) A plot of $\tau_{yy}(x, 0)$ profile.



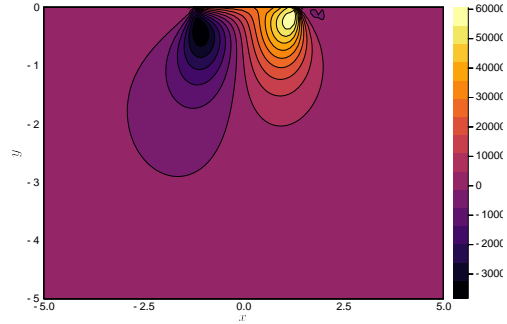
(f) A contour plot of Von Mises yield criterion.

Figure 5.6.3: Plots of the solution for the backward-stick-forward configuration. The angular velocity of the cylinder is taken to be $W = 0$ and the junction points were found to be $a = 1.28, b = 1.1, c = 1.02, d = 1.39$.

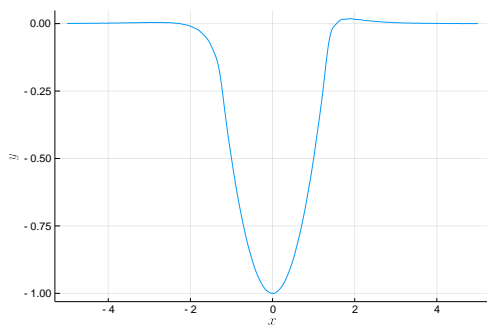
Backward-stick-backward



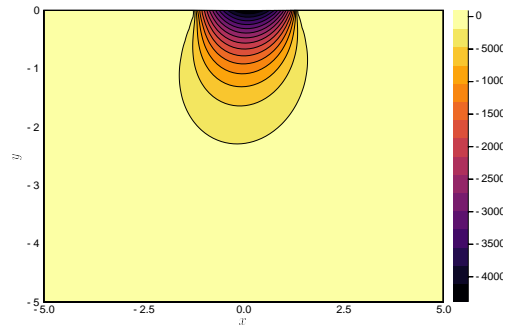
(a) A plot of $u(x, 0)$ profile.



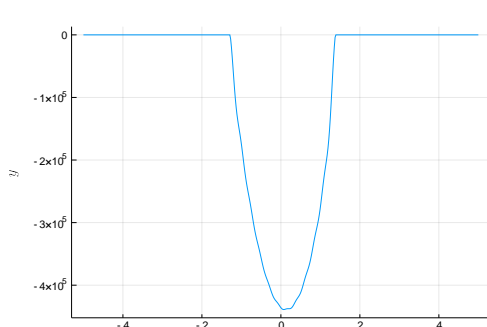
(b) A contour plot of $\tau_{xy}(x, y)$.



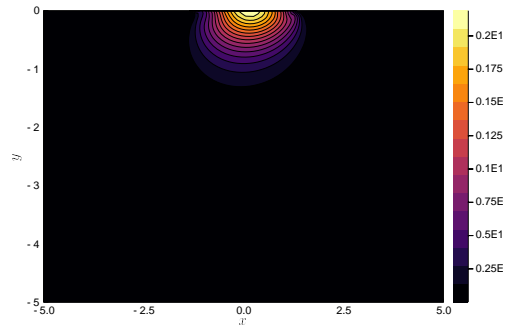
(c) A plot of $v(x, 0)$ profile.



(d) A contour plot of $\tau_{yy}(x, y)$.



(e) A plot of $\tau_{yy}(x, 0)$ profile.



(f) A contour plot of Von Mises yield criterion.

Figure 5.6.4: Plots of the solution for the backward-stick-backward configuration. The angular velocity of the cylinder is taken to be $W = 1$ and the junction points were found to be $a = 1.28, b = 1.14, c = 1.27, d = 1.38$.

5.6.3 Discussion

Finally, we discuss the instabilities which occur in the small ω case. The figure 5.6.5 shows a converged free-boundary method for $\omega = -0.5i$ and the figures 5.6.6 show the corresponding plots of the solution. Despite locating the free-boundary points, the solutions in 5.6.6 show a much more oscillatory solution than the large ω case, it is unclear whether this is a physical effect or an outcome of the numerical methods used. We analyse if a higher spectral resolution is required in figures 5.6.7 but see that the instabilities persist, which suggests that the instabilities are more inherent than the numerical methods. In the iterative method some variables are found directly from the Cauchy transform whereas others are found by using the additive relation and taking the difference, meaning that there is some dependency of the variables and that there is an ordering to finding the solution of each half-range variable. The ordering for finding each variable is $\tilde{v}(k)$, $\frac{\tilde{D}u}{\tilde{D}t}(k)$, $\tau_{xy} \diamond \mu_0 \tau_{yy}(k)$ and finally $\tilde{\tau}_{yy}(k)$. We observe that the oscillatory behaviour initially occurs in the plot of $\frac{Du}{Dt}(x)$ and influences the dependent solutions, which suggests that there is a discontinuity in $\frac{Du}{Dt}(x)$ which causes the Gibbs Phenomena in $\frac{Du}{Dt}(x)$ and its dependencies. However, when we instead frame the free-boundary method for locating $-b$ and c such that there are no discontinuities in $\frac{Du}{Dt}(x)$ we are no longer able to find a solution that satisfies the ordering (5.6). To summarise, the free-boundary method locates the roots as intended but there is some instability in the small ω case which leads us to believe that these roots may not be the correct locations of $-a, -b, c$ and d , or there is a more intricate problem in the small ω limit.

This leads us to question if there is an alternative approach which may be more suitable in the small ω case. One's intuition of the physics of the problem would suggest that there may be a critical limit of the normal force or W which leads to stick but no discussion of this is made in the literature. Alternatively, we could pursue the large k asymptotic approach in section 5.5.1 which relates the asymptotic behaviour of the half-range functions to the edge conditions, however, this has been tricky to impose numerically.

Instead, we pose determining the location of the stick-slip transition points in the small ω limit as a topic for further study.

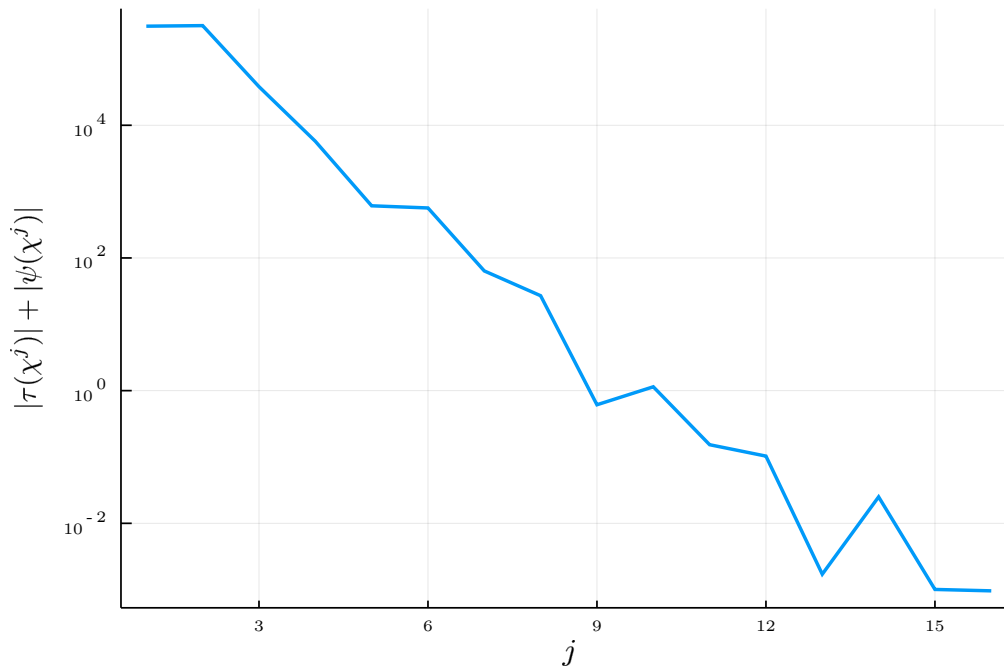


Figure 5.6.5: A plot of the error for the free-boundary method at each iteration until the solution has converged. The parameter values are those in table 5.1, with $\omega = -0.5i$.

5.7 Conclusion

The derivation of the model of an elastic half-space being deformed by a rigid roller under a stick-slip friction law has been presented. The additional central sticking region has expanded the matrix Wiener–Hopf equation from the full-slip setting to a 4×4 matrix Wiener–Hopf equation, this more complex equation retains similar structure to the full-slip case allowing an application of the iterative method outlined in chapter 3 to find a solution. The final complication from the stick-slip model is the addition of two free-boundary points, $-b$ and c , which are the stick-slip transition points.

Small ω

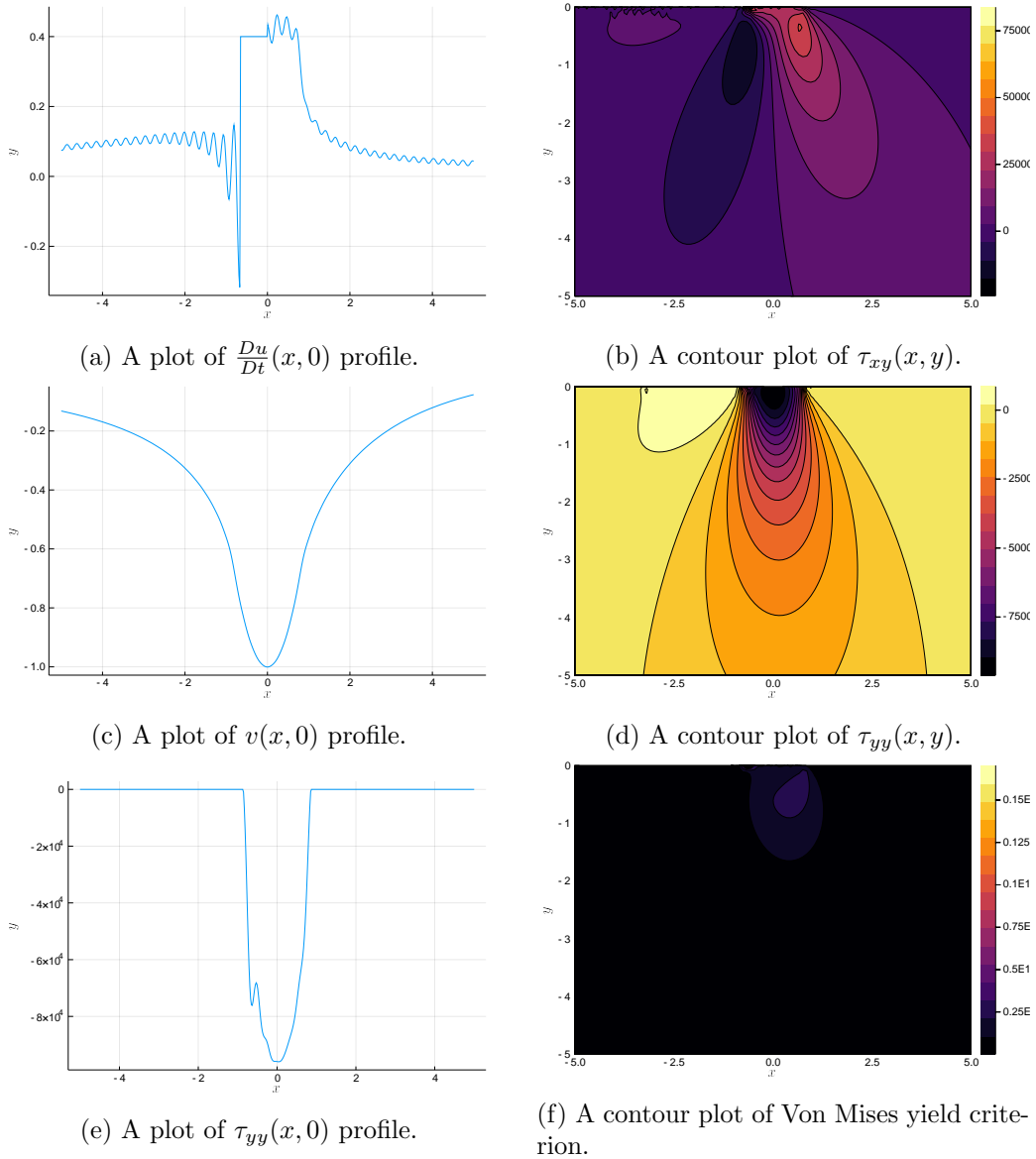
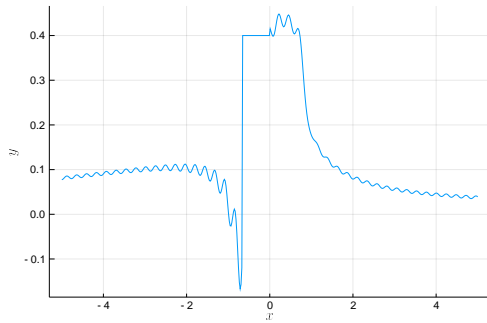


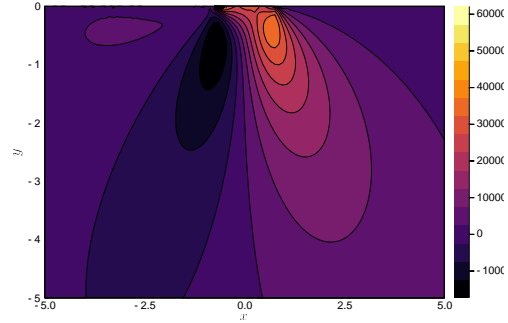
Figure 5.6.6: Plots of the solution with $\omega = -0.5i$ and the backward-stick-backward configuration.

The angular velocity of the cylinder is taken to be $W = 0.4$ and the junction points were found to be $a = 0.86, b = 0.67, c = 0.0059, d = 0.86$.

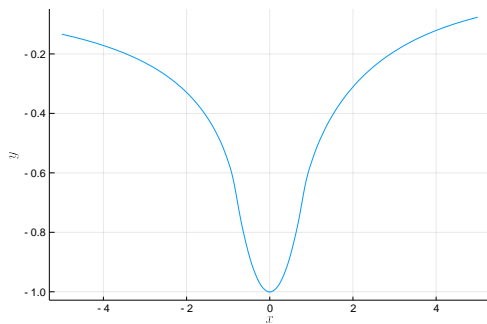
High spectral resolution



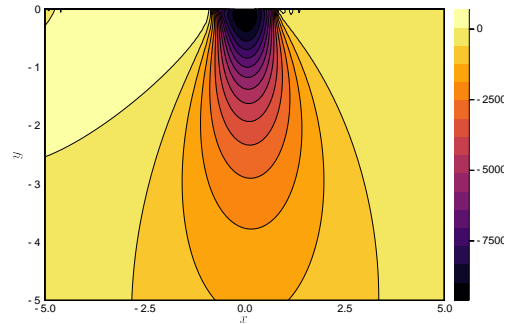
(a) A plot of $\frac{Du}{Dt}(x, 0)$ profile.



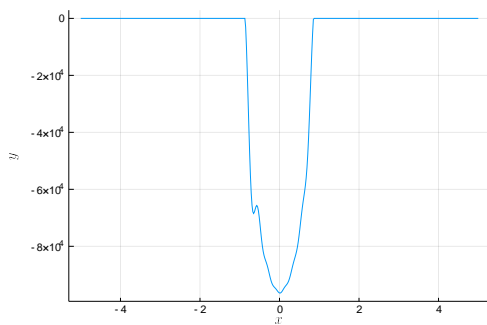
(b) A contour plot of $\tau_{xy}(x, y)$.



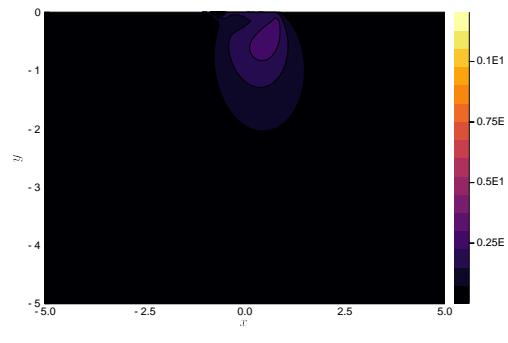
(c) A plot of $v(x, 0)$ profile.



(d) A contour plot of $\tau_{yy}(x, y)$.



(e) A plot of $\tau_{yy}(x, 0)$ profile.



(f) A contour plot of Von Mises yield criterion.

Figure 5.6.7: Plots of the solution of the small ω case with a higher spectral resolution.

All other parameters are the same as figure 5.6.6.

The application of the iterative method and locating the stick-slip transition points follows straightforwardly in the large ω case but for smaller values of ω some instabilities arise. Initial thoughts on the source of the instabilities is that the spectral resolution was too low but further investigation shows it not to be the case. The instabilities being present in $\frac{Du}{Dt}(x, 0)$ suggests that despite the free-boundary method locating roots, these roots are not the location of the stick-slip transition points.

Further work is required to locate the stick-slip transition points in the small ω case. An alternative analytical approach has been outlined in section 5.5 however it is difficult to implement in a numerical setting. Experiments have been made to the condition which determines the location of the stick-slip transition, such as determining it from $\frac{Du}{Dt}(x, 0)$ or the inequality (5.5) but neither of these approaches offers an improvement to our existing method.

Chapter 6

Outlook

In this thesis we have derived an analytical model of a rolling contact problem for a cylindrical indenter with full-slip and stick-slip friction laws. The Wiener–Hopf technique was then discussed and the iterative matrix Wiener–Hopf technique was outlined and applied to the full-slip and stick-slip contact problems. Finally, a method for locating the contact points and the stick-slip transition points was developed but requires some further work in locating the stick-slip transition points in the small ω limit.

Chapter 1 explained why lower CO₂ emissions are necessary and how the efficient use of metal enables lower emissions. A metal sheet spinning machine [71] was invented for this purpose but it is yet to be used in industry due to the computational constraints. We reduce one of the physical problems the machine faces to a fundamental rolling contact problem and examined it in detail. Thus, we propose and analyse a mathematical model of an elastic half-space in frictional contact with a rolling rigid cylinder.

In chapter 2 a mathematical model for the deformation of an elastic half-space by a rolling cylinder under a stick-slip friction law was derived. Then by considering the cylinder’s angular velocity relative to the convection speed of the half-space we derive a simplifying limit of full-slip, these friction regimes

may be characterised in the following way

$$\text{Friction regime} = \begin{cases} \text{Full-slip} & |\Omega| \gg |V| \text{ or } |\Omega| \ll |V|, \\ \text{Stick-slip} & |\Omega| \approx |V|. \end{cases}$$

In chapter 3 the scalar Wiener–Hopf technique was introduced in the context of contact mechanics by considering a highly simplified problem. The technique was then generalised to the matrix Wiener–Hopf technique and the iterative method [81] was presented.

The analysis of an elastic half-space being deformed by a rigid roller is the main result of this research, with the full-slip friction law considered in chapter 4 and the stick-slip friction law in chapter 5. The mixed boundary value problem in chapter 4 is formulated into a 2×2 matrix Wiener–Hopf equation, where we progress by assuming the location of the contact points and apply an inverse method to locate them numerically. The analysis in chapter 4 showed that provided $V^2 < \frac{\mu}{\rho}$ then any parameter values are valid, with plots included to demonstrate this in section 4.6. In particular, chapter 4 presented a converged solution in the limit $\omega \rightarrow 0$; showing a steady state model of a cylinder rolling on an elastic half-space under a full-slip friction law. The mixed boundary value problem in chapter 5 is formulated into a 4×4 matrix Wiener–Hopf equation, and similarly assumes the location of the contact and stick-slip transition points to facilitate progress. However, in the analysis of the results in chapter 5 we see that in the limit $\omega \rightarrow 0$ there is more work that is required, as discussed in section 5.6.3. For larger values of ω the value of W determines the direction of slip, or vice versa, with both slip regions taking the same direction of slip which fits in line with our physical intuition. To conclude, we have presented a mathematical model an elastic half-space deformed by a rigid roller under two friction regimes, with the magnitude of the angular velocity of the roller determining the friction regime. The models were solved by developing a matrix Wiener–Hopf framework and applying the iterative method to approximate the solution, but note that additional consideration is required in the limit $\omega \rightarrow 0$ for the

stick-slip friction regime.

6.1 Small omega limit

The first extension to the thesis is to locate the correct stick-slip transition points in the limit $\omega \rightarrow 0$ and to understand what causes the instabilities. In the full-slip regime, increasing the number of spectral and quadrature points was required to reduce the oscillatory behaviour in the limit $\omega \rightarrow 0$ but in the stick-slip case the oscillatory behaviour persists as shown in figure 5.6.7. The oscillatory behaviour may be due to the Gibbs Phenomena caused by a discontinuity in the solution, so analytically locating the transition points may eradicate the instabilities. A method for analytically locating the stick-slip transition points has been discussed in section 5.5, which examines the asymptotic behaviour of the half-range functions. Otherwise, approaches imposing boundedness and continuity conditions across the boundary ala Antipov and Arutyunyan [10] or Spence [90] may be sought.

6.2 Full-stick

The mathematical model and corresponding matrix Wiener–Hopf equation is presented in appendix B. The matrix Wiener–Hopf equation does not exhibit the structure to enable the iterative method to be applied directly but it is very similar so it may be applied after some adaptations. Namely, the difficulty in the full-stick regime is the lack of exponential terms in some of the non-diagonal matrix entries. This means that the scalar Wiener–Hopf equations are still coupled after the initial approximation and therefore solving them as scalar equations is not immediately possible. Further progress may be made by incorporating another matrix Wiener–Hopf technique into the method or by re-framing the mixed boundary value problem to reduce the number of junctions.

6.3 General framework for rolling problems

We propose that formulating the contact problem into a matrix Wiener–Hopf equation and applying the iterative method gives a general framework for solving contact problems. Several changes may be made to the model we have considered without changing the general approach, such as the profile of the roller, number of rollers, or the thickness of the elastic media. For example, a two roller system with the same convection speeds under a full-slip friction law would lead to a 4×4 matrix Wiener–Hopf equation, due to the four junctions between boundary conditions. In this example the iterative method would still be applicable as the exponential factors have the correct analyticity, please see appendix C for more details.

6.4 Plasticity

An important extension is to consider plastic deformation in the model too so in the regions where the Von Mises yield criterion is met the half-space will have elastic-weakly-plastic deformation. Let us consider a setting where a single rigid cylinder is rolling along the metal media, with elastic-weakly-plastic behaviour considered.

In modelling the elastic-plastic media, we expect the deformation to be largely elastic, with a small amount of plastic deformation. Thus we expect the problem to be formulated as

$$\mathcal{L}_e \mathbf{u} + \epsilon \mathcal{L}_p \mathbf{u} = \mathbf{f}, \quad (6.1)$$

which has a differential operator describing elasticity \mathcal{L}_e , another operator describing plasticity \mathcal{L}_p , displacement $\mathbf{u}(\mathbf{x}, t)$, and body forces \mathbf{f} . Note the ϵ in-front of the plastic operator representing the weakness in the plastic behaviour. Then considering an asymptotic expansion of the displacement

vector,

$$\mathbf{u} = \mathbf{u}_0 + \epsilon \mathbf{u}_1 + O(\epsilon^2).$$

Taking the asymptotic expansion, substituting into (6.1) and equating coefficients of ϵ gives the solution,

$$\begin{aligned} O(1) : & \quad \mathcal{L}_e \mathbf{u}_0 = \mathbf{f}, \\ O(\epsilon) : & \quad \mathcal{L}_e \mathbf{u}_1 + \mathcal{L}_p \mathbf{u}_0 = \mathbf{0}. \end{aligned}$$

Thus, we have outlined an approach to account for the plastic deformation whilst allowing the matrix Wiener–Hopf technique to continue to be applied.

6.5 Closing remarks

The subject of this thesis has been motivated by an industrial problem in metal sheet spinning. The mathematical modelling of metal forming is an under-researched area, leading to industry relying on numerical simulation to model processes, with potentially large errors and expensive computational costs. The research in this thesis provides a foundation for metal sheet spinning models and presents an approach for the open problem of analytically modelling the process. Another extension is expanding the current framework to model contact problems with other geometries or with multiple rollers.

A results of this thesis is a constructive approach of modelling and solving contact problems. The steady state rolling contact problem in the full-slip limit has been found and the distribution of the yield criterion has been analysed, showing the regions where one would expect plastic deformation to occur. The rolling contact problem in the stick-slip limit has been studied for large ω values, and our intuition on stick-slip configurations has been verified. However, further study is required of the stick-slip problem for small values of ω as outlined.

Appendix A

Some useful definitions and theorems

In this appendix we state some definitions and theorems which may be useful to the reader but for more details on complex analysis see Ablowitz and Fokas [1], the Wiener–Hopf technique see Noble [74], or computing Cauchy transforms see Trogon and Olver [95].

Definition 1. (*Analytic*) The complex function $f : \mathbb{C} \rightarrow \mathbb{C}$ is analytic at point k_0 if $f(k)$ is differentiable in a neighbourhood of k_0 . See page 37 of [1].

Definition 2. (*Regular*) The complex function $f : \mathbb{C} \rightarrow \mathbb{C}$ is regular or holomorphic in a region $\mathbb{C}_0 \subset \mathbb{C}$ if it is analytic at every point in \mathbb{C}_0 , i.e. $f(k)$ is differentiable in a neighbourhood of $k \forall k \in \mathbb{C}_0$. See page 38 of [1].

Definition 3. (*Entire*) The complex function $f : \mathbb{C} \rightarrow \mathbb{C}$ is entire if it is regular over all \mathbb{C} i.e. $f(k)$ is differentiable in a neighbourhood of $k \forall k \in \mathbb{C}$. See page 38 of [1].

Theorem 1. (*Liouville's theorem*) If the complex function $f : \mathbb{C} \rightarrow \mathbb{C}$ is entire and bounded then $f(k)$ is constant. See page 95 of [1].

Theorem 2. (*Extended Liouville's theorem*) If the complex function $f : \mathbb{C} \rightarrow \mathbb{C}$ is entire and $|f(k)| < C|k|^n$ as $|k| \rightarrow \infty$ then $f(k)$ is a polynomial of degree

at most n , where C and n are constants. See page 6 of [74].

Theorem 3. (*Plemelj's lemma on the interval*) We state an alternative form of Plemelj's lemma. Suppose $\phi(k)$ satisfies the following properties:

1. analytic off $[a, b]$,
2. has weaker than pole singularities,
3. decays at infinity,
4. satisfies the jump condition

$$\phi^+(x) - \phi^-(x) = f(x) \quad \text{for } a < x < b.$$

Then $\phi(z) = \mathcal{C}_{[a,b]}f(k)$. See [95, 1] for further details.

Theorem 4. (*Three-term recurrence relationship for weighted orthogonal polynomials*) The weighted orthogonal polynomial basis satisfies a classical three-term recurrence relationship, so there exists constants $a_j, b_j, c_j \neq 0$ such that

$$\begin{aligned} kp_0(k) &= a_0p_0(k) + b_0p_1(k), \\ kp_j(k) &= c_jp_{j-1}(k) + a_jp_j(k) + b_jp_{j+1}(k). \end{aligned}$$

See page 164 of [93] or [95] for more details.

Appendix B

Matrix Wiener–Hopf for the full-stick regime

We briefly present the boundary conditions and the resulting matrix Wiener–Hopf equation in the limit of full-stick. Notably, the limit of full-stick does not simplify the problem like in the limit of full-slip as we are unable to eradicate the jumps in the boundary conditions. In fact, the resulting matrix Wiener–Hopf problem in this case may not be solved by a direct application of the iterative method in 3 since there is not always an exponential factor multiplying the non-diagonal terms in the matrices.

We do imagine that the resulting matrix Wiener–Hopf equation may be solved by either adaptations to the iterative method, or by reformulating the boundary conditions into another form. Despite several ideas on further steps that may be taken to approximate the solution, it has not been explored here.

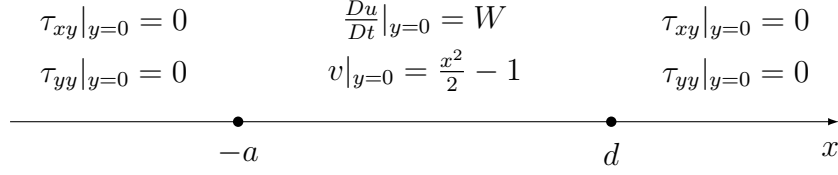


Figure B.1.1: A diagram showing the full-stick boundary conditions and the regions where they hold.

B.1 Boundary conditions

We consider the setting in chapter 2 with a purely sticking contact region between the cylinder and elastic half-space.

The nonlinear derivation of the boundary conditions from the physical system can be found in section 2.4, with the linearisation of the nonlinear boundary conditions found in section 2.3. A diagram showing the boundary conditions are shown in the schematic B.1.1. In this section we consider the full-stick regime, which gives the following boundary conditions and domains,

$$\begin{array}{ll}
 \text{Contact:} & v(x, 0) = \frac{x^2}{2} - 1, \quad \text{for } -a \leq x \leq d, \\
 \text{Stick:} & \frac{Du}{Dt}(x, 0) = W, \quad \text{for } -a \leq x \leq d, \\
 \text{Stress-free:} & \tau_{xy}(x, 0) = \tau_{yy}(x, 0) = 0, \quad \text{for } x < -a \text{ \& } d < x.
 \end{array}$$

We use the convected derivative as

$$\frac{Du}{Dt}(x, 0) = \frac{\partial u}{\partial t}(x, 0) - \frac{\partial u}{\partial x}(x, 0) = W, \quad \text{for } -a \leq x \leq d.$$

In summary, there are two boundary conditions in each region with the junctions between these regions being the unknown free-boundary points $-a$ and d . The boundary conditions may be reformulated into a matrix Wiener–Hopf problem which may not be solved by a direct application of the iterative method.

B.2 Matrix Wiener–Hopf equation

There are multiple ways in which the equations may be arranged to attain the matrix. The general format sought here is in the form

$$\mathbf{A}(k)\Phi_+(k) = \mathbf{B}(k)\Phi_-(k) + \mathbf{C}(k).$$

From this equation, it is hoped that it will be possible to apply the iterative method by treating each row of the linear system as a scalar equation. We shall retain each of the unknowns from the boundary conditions which we stated previously. In vector format we will take them to be:

$$\tilde{\Phi}^+(k) = \begin{pmatrix} \widetilde{v}_+^{(d)}(k) \\ \widetilde{\frac{Du}{Dt}}_+^{(d)}(k) \\ \widetilde{\tau_{xyy=0}}_+^{(-a)}(k) \\ \widetilde{\tau_{yyy=0}}_+^{(-a)}(k) \end{pmatrix}, \quad \tilde{\Phi}^-(k) = \begin{pmatrix} \widetilde{\tau_{yyy=0}}_-^{(d)}(k) \\ \widetilde{\tau_{xyy=0}}_-^{(d)}(k) \\ \widetilde{\frac{Du}{Dt}}_-^{(-a)}(k) \\ \widetilde{v}_-^{(-a)}(k) \end{pmatrix}.$$

The unknowns were chosen in this order so that the matrices will be of triangular format in the matrix Wiener–Hopf.

To generate the matrix Wiener–Hopf, we seek to eliminate the full-range transforms, $\hat{A}_1(k)$ and $A_2(k)$ and only find the unknown functions from above and some functions of k . We may arrange a matrix Wiener–Hopf, which has exponential factors of the correct analyticity, to be

$$\mathbf{A}(k) = \begin{pmatrix} (n_1n_4 - n_2n_3) & 0 & 0 & 0 \\ (n_4 - B_2n_3) & i(\omega + k)(n_3 - B_1n_4) & 0 & 0 \\ -(n_4 - B_2n_3) & -i(\omega + k)(n_3 - B_1n_4) & i(\omega + k)(1 - B_1B_2) & 0 \\ \times e^{ik(a+d)} & \times e^{ik(a+d)} & & \\ -(n_1n_4 - n_2n_3) & 0 & (\hat{B}_1n_1 - n_2) & (n_4 - B_2n_3) \\ \times e^{ik(a+d)} & & & \end{pmatrix},$$

$$\mathbf{B}(k) = \begin{pmatrix} (n_4 - B_2 n_3) & (\hat{B}_1 n_1 - n_2) & 0 & -(n_1 n_4 - n_2 n_3) \\ & & & \times e^{-ik(a+d)} \\ 0 & i(\omega + k)(1 - B_1 B_2) & -i(\omega + k)(n_3 - B_1 n_4) & -(n_4 - B_2 n_3) \\ & & \times e^{-ik(a+d)} & \times e^{-ik(a+d)} \\ 0 & 0 & i(\omega + k)(n_3 - B_1 n_4) & (n_4 - B_2 n_3) \\ 0 & 0 & 0 & (n_1 n_4 - n_2 n_3) \end{pmatrix},$$

$$\mathbf{C}(k) = \begin{pmatrix} -(n_1 n_4 - n_2 n_3) e^{-ikd} f(k) \\ -(n_4 - B_2 n_3) e^{-ikd} f(k) - i(\omega + k)(n_3 - B_1 n_4) e^{-ikd} g(k) \\ (n_4 - B_2 n_3) e^{ika} f(k) + i(\omega + k)(n_3 - B_1 n_4) e^{ika} g(k) \\ (n_1 n_4 - n_2 n_3) e^{ika} g(k) \end{pmatrix}.$$

We define the functions $n_3(k)$ and $n_4(k)$ from the full-range transform

$$\widetilde{\tau}_{xy}(k) = n_3(k) \widehat{A}_1(k) + n_4(k) A_2(k).$$

We briefly note a few details on the matrix Wiener-Hopf equation which we have arrived at. The arrangement of a triangular format is not unique, as both the stick and contact, and the shear and normal stresses are interchangeable without disrupting the structure. A second note is the absence of an exponential factor in some parts of the matrices, which means one may not apply the iterative method directly. However, some adaptations, such as taking an initial approximation by setting all the non-diagonal entries in the matrices to zero, may be made to estimate the solution in this case.

Appendix C

Matrix Wiener–Hopf for two rollers in the full-slip regime

We present the boundary conditions and resulting matrix Wiener–Hopf equation for two similar rollers, both undergoing full-slip in the same direction. In this case we derive a 4×4 matrix Wiener–Hopf equation which may be directly solved by applying the iterative method. As the frictional behaviour is full-slip, the scalar kernel to be factorised is the same as the one considered in chapter 4. In fact, the resultant matrix Wiener–Hopf equation in this setting may be simpler to solve than the one in chapter 5.

C.1 Boundary conditions

We consider the setting in chapter 4, instead with two cylinders in contact with the elastic half-space.

The nonlinear derivation of the boundary conditions from the physical system can be found in section 2.4, with the linearisation of the nonlinear boundary conditions found in section 2.3. This model expands on the one developed

in chapter 4 by considering two similar rollers located between $[x_1, x_2]$ and $[x_3, x_4]$; both rollers have the exact same angular and linear velocities. In this chapter the frictional behaviour is full-slip, which gives the following boundary conditions and domains,

$$\begin{aligned}
 \text{Cylinder A:} \quad & v(x, 0) = \frac{x^2}{2} - 1, & \text{for } x_1 \leq x \leq x_2, \\
 \text{Cylinder B:} \quad & v(x, 0) = \frac{(x - L)^2}{2} - 1, & \text{for } x_3 \leq x \leq x_4, \\
 \text{Slip:} \quad & \tau_{xy} \mp \mu_0 \tau_{yy}(x, 0) = 0, & \text{for } -\infty \leq x \leq \infty, \\
 \text{Stress-free:} \quad & \tau_{yy}(x, 0) = 0, & \text{for } x < x_1, x \in [x_2, x_3], x > x_4.
 \end{aligned}$$

Here L is the center of Cylinder B and Cylinder A centered at $x = 0$.

In summary, there are two boundary conditions in each region with the junctions between these regions being the unknown free-boundary points x_1, x_2, x_3 and x_4 . The boundary conditions may be reformulated into a matrix Wiener–Hopf problem which is in a form where the iterative method may be applied.

C.2 Transformation of the boundary conditions

To derive the Wiener–Hopf problem the unknown variables will be defined from the half-range transforms of $v(x, 0)$ and $\tau_{yy}(x, 0)$. The full-range transforms of the contact boundary conditions gives

$$\begin{aligned}
 \tilde{v}(k) &= e^{ikx_2} \tilde{v}_+^{(x_2)}(k) + e^{ikx_1} \tilde{v}_-^{(x_1)}(k) + f_1(k), \\
 &= e^{ikx_4} \tilde{v}_+^{(x_4)}(k) + e^{ikx_3} \tilde{v}_-^{(x_3)}(k) + f_2(k),
 \end{aligned}$$

where the functions $f_{1,2}(k)$ are defined as

$$\begin{aligned} f_1(k) &= \frac{e^{ikx_1}}{ik} \left(1 + \frac{x_1^2}{2} + \frac{x_1}{ik} + \frac{1}{k^2} \right) - \frac{e^{ikx_2}}{ik} \left(1 - \frac{x_2^2}{2} + \frac{x_2}{ik} + \frac{1}{k^2} \right), \\ f_2(k) &= \frac{e^{ikx_3}}{ik} \left(1 + \frac{(x_3 - L)^2}{2} + \frac{x_3 - L}{ik} + \frac{1}{k^2} \right) \\ &\quad - \frac{e^{ikx_4}}{ik} \left(1 - \frac{(x_4 - L)^2}{2} + \frac{x_4 - L}{ik} + \frac{1}{k^2} \right). \end{aligned}$$

Similarly, the full-range transform of the stress-free boundary conditions are

$$\begin{aligned} \widetilde{\tau}_{yy}(k) &= e^{ikx_4} \widetilde{\tau}_{yy-}^{(x_4)}(k) = e^{ikx_1} \widetilde{\tau}_{yy+}^{(x_1)}(k), \\ &= e^{ikx_3} \widetilde{\tau}_{yy+}^{(x_3)}(k) + e^{ikx_2} \widetilde{\tau}_{yy-}^{(x_2)}(k). \end{aligned}$$

These scalar Wiener–Hopf equations shall then be manipulated to form the matrix Wiener–Hopf equation.

C.3 Matrix Wiener–Hopf equation

There are multiple ways in which the equations may be arranged to attain the matrix. The general format sought here is in the form

$$\mathbf{A}(k)\Phi_+(k) = \mathbf{B}(k)\Phi_-(k) + \mathbf{C}(k).$$

From this equation, it is hoped that it will be possible to apply the iterative method by treating each row of the linear system as a scalar equation. We shall retain each of the unknowns from the boundary conditions which we stated previously. In vector format we will take them to be:

$$\widetilde{\Phi}^+(k) = \begin{pmatrix} \widetilde{v}_+^{(x_4)}(k) \\ \widetilde{\tau}_{yy+}^{(x_3)}(k) \\ \widetilde{v}_+^{(x_2)}(k) \\ \widetilde{\tau}_{yy+}^{(x_1)}(k) \end{pmatrix}, \quad \widetilde{\Phi}^-(k) = \begin{pmatrix} \widetilde{\tau}_{yy-}^{(x_4)}(k) \\ \widetilde{v}_-^{(x_3)}(k) \\ \widetilde{\tau}_{yy-}^{(x_2)}(k) \\ \widetilde{v}_-^{(x_1)}(k) \end{pmatrix}.$$

The unknowns were chosen in this order so that the matrices will be of triangular format in the matrix Wiener–Hopf.

To generate the matrix Wiener–Hopf, we seek to eliminate the full-range transforms, $\hat{A}_1(k)$ and $A_2(k)$ and only find the unknown functions from above and some functions of k . We may arrange a matrix Wiener–Hopf, which has exponential factors of the correct analyticity, to be

$$\mathbf{A}(k) = \begin{pmatrix} 1 & 0 & 0 & 0 \\ -e^{ik(x_4-x_3)} & K(k) & 0 & 0 \\ 0 & -K(k)e^{ik(x_3-x_2)} & 1 & 0 \\ 0 & 0 & -e^{ik(x_2-x_1)} & K(k) \end{pmatrix},$$

$$\mathbf{B}(k) = \begin{pmatrix} K(k) & -e^{ik(x_3-x_4)} & 0 & 0 \\ 0 & 1 & -K(k)e^{ik(x_2-x_3)} & 0 \\ 0 & 0 & K(k) & -e^{ik(x_1-x_2)} \\ 0 & 0 & 0 & 1 \end{pmatrix},$$

$$\mathbf{C}(k) = \begin{pmatrix} -e^{-ikx_4} f_2(k) \\ e^{-ikx_3} f_2(k) \\ -e^{-ikx_2} f_1(k) \\ e^{-ikx_1} f_1(k) \end{pmatrix},$$

where we define the functions $K(k)$ from chapter 4

$$K(k) = \frac{n(k) + B_2(k)}{n_1(k)n(k) + n_2(k)}, \quad \text{with } K(k) = O\left(\frac{1}{|k|}\right) \text{ as } |k| \rightarrow \infty.$$

Note the iterative method may be applied directly to this matrix Wiener–Hopf equation and it may even be considered a simpler problem to the stick-slip matrix Wiener–Hopf, considered in chapter 5. This may be because we have constructed this problem to as two coupled full-slip problems, leading to many similarities to the matrix Wiener–Hopf equation derived in chapter

4.

Bibliography

- [1] M. J. Ablowitz and A. S. Fokas. *Complex Variables: Introduction and Applications*. Cambridge Texts in Applied Mathematics. Cambridge University Press, 2 edition, 2003. doi:[10.1017/CBO9780511791246](https://doi.org/10.1017/CBO9780511791246).
- [2] I. Abrahams. Radiation and scattering of waves on an elastic half-space; a non-commutative matrix wiener-hopf problem. *Journal of the Mechanics and Physics of Solids*, 44(12):2125–2154, 1996.
- [3] I. D. Abrahams. On the solution of Wiener–Hopf problems involving noncommutative matrix kernel decompositions. *SIAM Journal on Applied Mathematics*, 57(2):541–567, 1997.
- [4] I. D. Abrahams. The application of padé approximants to Wiener–Hopf factorization. *IMA Journal of Applied Mathematics*, 65(3):257–281, 2000.
- [5] K. Addi, H. Antes, and G. Stavroulakis. On solving a rolling frictional contact problem using bem and mathematical programming. *International Journal of Applied Mathematical Sciences*, 1, 01 2004.
- [6] A. Akay. Acoustics of friction. *The Journal of the Acoustical Society of America*, 111(4):1525–1548, 2002. doi:[10.1121/1.1456514](https://doi.org/10.1121/1.1456514). URL <https://doi.org/10.1121/1.1456514>.
- [7] F. Al-Bender, V. Lampaert, and J. Swevers. Modeling of dry sliding friction dynamics: From heuristic models to physically motivated

- models and back. *Chaos: An Interdisciplinary Journal of Nonlinear Science*, 14(2):446–460, 2004. doi:[10.1063/1.1741752](https://doi.org/10.1063/1.1741752). URL <https://doi.org/10.1063/1.1741752>.
- [8] J. Allwood, J. Cullen, M. Carruth, and U. of Cambridge. Engineering Department. *Sustainable Materials with Both Eyes Open*. Gabriel Thoumi sustainability collection. UIT Cambridge Limited, 2012. ISBN 9781906860073. URL <https://books.google.co.uk/books?id=GGaHtQAACAAJ>.
- [9] J. M. Allwood, J. M. Cullen, and R. L. Milford. Options for achieving a 50% cut in industrial carbon emissions by 2050. *Environmental Science and Technology*, 44(6):1888–1894, 2010. doi:[10.1021/es902909k](https://doi.org/10.1021/es902909k). URL [10.1021/es902909k](https://doi.org/10.1021/es902909k).
- [10] Y. A. Antipov and N. K. Arutyunyan. Contact problems of the theory of elasticity with friction and adhesion. *Journal of Applied Mathematics and Mechanics*, 55(6):887–901, 1991.
- [11] E. Applied. Table of material properties for structural steel s235, s275, s355, s420, May 2005. URL <https://eurocodeapplied.com/design/en1993/steel-design-properties>.
- [12] J. Barber. *Contact Mechanics*. Solid Mechanics and Its Applications. Springer International Publishing, 2018. ISBN 9783319709390. URL <https://books.google.co.uk/books?id=4GNLDwAAQBAJ>.
- [13] A. D. Berman, W. A. Ducker, and J. N. Israelachvili. Origin and characterization of different stickslip friction mechanisms. *Langmuir*, 12(19):4559–4563, 1996. doi:[10.1021/la950896z](https://doi.org/10.1021/la950896z). URL <https://doi.org/10.1021/la950896z>.
- [14] B. Bhushan. *Modern Tribology Handbook*, volume 2 of *Mechanics and Materials Science*. CRC Press, 2000. ISBN 9780849377877. URL <https://books.google.co.uk/books?id=h6X0NM7ME8IC>.

- [15] F. M. Borodich and B. A. Galanov. Self-similar problems of elastic contact for non-convex punches. *Journal of the Mechanics and Physics of Solids*, 50(11):2441–2461, 2002.
- [16] F. M. Borodich and L. M. Keer. Contact problems and depth-sensing nanoindentation for frictionless and frictional boundary conditions. *International Journal of Solids and Structures*, 41(9-10):2479–2499, 2004.
- [17] C. G. Broyden. A class of methods for solving nonlinear simultaneous equations. *Mathematics of Computation*, 19(92):577–593, 1965. ISSN 00255718, 10886842. URL <http://www.jstor.org/stable/2003941>.
- [18] R. Burridge and L. Knopoff. Model and theoretical seismicity. *Bulletin of the Seismological Society of America*, 57(3):341–371, 06 1967. ISSN 0037-1106. doi:[10.1785/BSSA0570030341](https://doi.org/10.1785/BSSA0570030341). URL <https://doi.org/10.1785/BSSA0570030341>.
- [19] B. Bushan. *Handbook of Micro/Nano Tribology*. Mechanics and materials science series. CRC Press, 2020. ISBN 9781420050493. URL <https://books.google.co.uk/books?id=KwEHEAAAQBAJ>.
- [20] F. Carter. The electric locomotive (including appendix and plate at back of volume). In *Minutes of the Proceedings of the Institution of Civil Engineers*, volume 201, pages 221–252. Thomas Telford-ICE Virtual Library, 1916.
- [21] C. Cattaneo. Sulla torsione di due sfere elastiche a contatto. *Annali della Scuola Normale Superiore di Pisa-Classe di Scienze*, 6(1-2):1–16, 1952.
- [22] C. J. Cawthorn, J. J. Minton, and E. J. Brambley. Asymptotic analysis of cold sandwich rolling. *Int. J. Mech. Sci.*, 106:184–193, 2016. doi:[10.1016/j.ijmecsci.2015.12.012](https://doi.org/10.1016/j.ijmecsci.2015.12.012).
- [23] M. Ciavarella. The generalized Cattaneo partial slip plane contact problem. I — theory. *International Journal of solids and structures*, 35(18):2349–2362, 1998.

- [24] C. J. Cleaver, M. R. Arthington, S. Mortazavi, and J. M. Allwood. Ring rolling with variable wall thickness. *CIRP Annals*, 65(1):281–284, 2016. ISSN 0007-8506. doi:<https://doi.org/10.1016/j.cirp.2016.04.002>. URL <https://www.sciencedirect.com/science/article/pii/S0007850616300026>.
- [25] M. Cocu. Existence of solutions of signorini problems with friction. *International Journal of Engineering Science*, 22(5):567–575, 1984. ISSN 0020-7225. doi:[https://doi.org/10.1016/0020-7225\(84\)90058-2](https://doi.org/10.1016/0020-7225(84)90058-2). URL <https://www.sciencedirect.com/science/article/pii/0020722584900582>.
- [26] M. J. Colbrook, L. J. Ayton, and A. S. Fokas. The unified transform for mixed boundary condition problems in unbounded domains. *Proceedings of the Royal Society A: Mathematical, Physical and Engineering Sciences*, 475(2222):20180605, 2019. doi:[10.1098/rspa.2018.0605](https://doi.org/10.1098/rspa.2018.0605). URL <https://royalsocietypublishing.org/doi/abs/10.1098/rspa.2018.0605>.
- [27] E. T. Copson. On an integral equation arising in the theory of diffraction. *The Quarterly Journal of Mathematics*, os-17(1):19–34, 01 1946. ISSN 0033-5606. doi:[10.1093/qmath/os-17.1.19](https://doi.org/10.1093/qmath/os-17.1.19). URL <https://doi.org/10.1093/qmath/os-17.1.19>.
- [28] R. Craster. The solution of a class of free boundary problems. *Proceedings of the Royal Society of London. Series A: Mathematical, Physical and Engineering Sciences*, 453(1958):607–630, 1997.
- [29] V. Daniele. *The Wiener-Hopf Method in Electromagnetics*. ISMB series. Institution of Engineering and Technology, 2014. ISBN 9781680154139. URL <https://books.google.co.uk/books?id=rdg3jwEACAAJ>.
- [30] V. Daniele and G. Lombardi. Fredholm factorization of Wiener–Hopf scalar and matrix kernels. *Radio Science*, 42(6), 2007. doi:[10.1029/2007RS003673](https://doi.org/10.1029/2007RS003673). URL <https://agupubs.onlinelibrary.wiley.com/doi/abs/10.1029/2007RS003673>.

- [31] E. Dlugokencky and P. Tans. Trends in atmospheric carbon dioxide – NOAA/GML, 2021. URL https://gml.noaa.gov/ccgg/trends/gl_data.html. [Online; accessed 17-November-2021].
- [32] R. Doney. On wiener-hopf factorisation and the distribution of extrema for certain stable processes. *The Annals of Probability*, pages 1352–1362, 1987.
- [33] C. M. Elliott and J. R. Ockendon. *Weak and variational methods for moving boundary problems*, volume 59. Pitman Publishing, 1982.
- [34] EPA. Climate change indicators: Atmospheric concentrations of greenhouse gases. URL <https://www.epa.gov/climate-indicators/climate-change-indicators-atmospheric-concentrations-greenhouse-gases#tab-5>.
- [35] G. Fichera. *Problemi elastostatici con vincoli unilaterali: il problema di Signorini con ambigue condizioni al contorno*. Accademia nazionale dei Lincei, 1964.
- [36] J. Fourier. *Remarques Generales sur les Temperatures Du Globe Terrestre et des Espaces Planetaires*. Number v. 27 in Annales de chimie et de physique. Annales de chimie et de physique, 1824. URL <https://books.google.co.uk/books?id=1Jg5AAAAcAAJ>.
- [37] H. Fromm. Berechnung des schlupfes beim rollen deformierbarer scheiben. *ZAMM-Journal of Applied Mathematics and Mechanics/Zeitschrift für Angewandte Mathematik und Mechanik*, 7(1):27–58, 1927.
- [38] G. Fusai, I. D. Abrahams, and C. Sgarra. An exact analytical solution for discrete barrier options. *Finance and Stochastics*, 10(1):1–26, 2006.
- [39] L. Galin and G. Gladwell. *Contact Problems: The legacy of L.A. Galin*. Solid Mechanics and Its Applications. Springer Netherlands, 2008. ISBN 9781402090431. URL <https://books.google.co.uk/books?id=oGXGtXNBPKQC>.

- [40] L. E. Goodman. Contact Stress Analysis of Normally Loaded Rough Spheres. *Journal of Applied Mechanics*, 29(3):515–522, 09 1962. ISSN 0021-8936. doi:[10.1115/1.3640599](https://doi.org/10.1115/1.3640599). URL <https://doi.org/10.1115/1.3640599>.
- [41] T. G. Gutowski, S. Sahni, J. M. Allwood, M. F. Ashby, and E. Worrell. The energy required to produce materials: constraints on energy-intensity improvements, parameters of demand. *Philosophical Transactions of the Royal Society A: Mathematical, Physical and Engineering Sciences*, 371(1986):20120003, 2013.
- [42] B. Hall. *The Matrix Exponential*, pages 31–48. Springer International Publishing, Cham, 2015. ISBN 978-3-319-13467-3. doi:[10.1007/978-3-319-13467-3_2](https://doi.org/10.1007/978-3-319-13467-3_2). URL https://doi.org/10.1007/978-3-319-13467-3_2.
- [43] A. E. Heins. Systems of wiener–hopf equations. In *Proceedings of Symposia in Applied Mathematics II. McGraw-Hill*, pages 76–81, 1950.
- [44] H. Hertz. Über die berührung fester elastischer körper (on the contact of elastic solids). In D. E. Jones and G. A. Schott, editors, *Miscellaneous papers by H. Hertz*. Macmillan, 1896. Originally in *J. Reine Angew. Math.* 92, 1881.
- [45] F. Heslot, T. Baumberger, B. Perrin, B. Caroli, and C. Caroli. Creep, stick-slip, and dry-friction dynamics: Experiments and a heuristic model. *Phys. Rev. E*, 49:4973–4988, Jun 1994. doi:[10.1103/PhysRevE.49.4973](https://doi.org/10.1103/PhysRevE.49.4973). URL <https://link.aps.org/doi/10.1103/PhysRevE.49.4973>.
- [46] P. Howell, G. Kozyreff, and J. Ockendon. *Applied Solid Mechanics*. Cambridge Texts in Applied Mathematics. Cambridge University Press, 2008. ISBN 9780521671095. URL <https://books.google.co.uk/books?id=JkJBHAAACAAJ>.
- [47] S. D. Howison, J. D. Morgan, and J. R. Ockendon. A class of codimension-two free boundary problems. *SIAM Review*, 39(2):

- 221–253, 1997. doi:[10.1137/S0036144595280625](https://doi.org/10.1137/S0036144595280625). URL [10.1137/S0036144595280625](https://doi.org/10.1137/S0036144595280625).
- [48] J. Jäger. Half-planes without coupling under contact loading. *Archive of Applied Mechanics*, 67:247–259, 1997.
- [49] K. L. Johnson. *Contact Mechanics*. Cambridge University Press, 1985. doi:[10.1017/CBO9781139171731](https://doi.org/10.1017/CBO9781139171731).
- [50] D. S. Jones. A simplifying technique in the solution of a class of diffraction problems. *The Quarterly Journal of Mathematics*, 3(1): 189–196, 01 1952. ISSN 0033-5606. doi:[10.1093/qmath/3.1.189](https://doi.org/10.1093/qmath/3.1.189). URL <https://doi.org/10.1093/qmath/3.1.189>.
- [51] D. S. Jones. Commutative wiener-hopf factorization of a matrix. *Proceedings of the Royal Society of London. A. Mathematical and Physical Sciences*, 393(1804):185–192, 1984. doi:[10.1098/rspa.1984.0053](https://doi.org/10.1098/rspa.1984.0053). URL <https://royalsocietypublishing.org/doi/abs/10.1098/rspa.1984.0053>.
- [52] J. J. Kalker. *Three-dimensional elastic bodies in rolling contact*, volume 2. Springer Science & Business Media, 2013.
- [53] A. Kisil and L. J. Ayton. Aerodynamic noise from rigid trailing edges with finite porous extensions. *Journal of Fluid Mechanics*, 836:117–144, 2018. doi:[10.1017/jfm.2017.782](https://doi.org/10.1017/jfm.2017.782).
- [54] A. V. Kisil. A constructive method for an approximate solution to scalar wiener–hopf equations. *Proceedings of the Royal Society A: Mathematical, Physical and Engineering Sciences*, 469(2154):20120721, 2013.
- [55] A. V. Kisil. The relationship between a strip Wiener–Hopf problem and a line Riemann–Hilbert problem. *IMA Journal of Applied Mathematics*, 80(5):1569–1581, 05 2015. ISSN 0272-4960. doi:[10.1093/imamat/hxv007](https://doi.org/10.1093/imamat/hxv007). URL [10.1093/imamat/hxv007](https://doi.org/10.1093/imamat/hxv007).

- [56] A. V. Kisil. An iterative Wiener–Hopf method for triangular matrix functions with exponential factors. *SIAM Journal on Applied Mathematics*, 78(1):45–62, 2018.
- [57] A. V. Kisil, I. D. Abrahams, G. Mishuris, and S. V. Rogosin. The wiener-hopf technique, its generalizations and applications: constructive and approximate methods. *Proceedings of the Royal Society A: Mathematical, Physical and Engineering Sciences*, 477(2254):20210533, 2021. doi:[10.1098/rspa.2021.0533](https://doi.org/10.1098/rspa.2021.0533). URL <https://royalsocietypublishing.org/doi/abs/10.1098/rspa.2021.0533>.
- [58] A. Klarbring. Examples of non-uniqueness and non-existence of solutions to quasistatic contact problems with friction. *Ingenieur-Archiv*, 60:529–541, 1990.
- [59] D. Lannes. On the dynamics of floating structures. *Annals of PDE*, 3(1):11, 2017.
- [60] T. A. Laursen and I. Stanciulescu. An algorithm for incorporation of frictional sliding conditions within a steady state rolling framework. *Communications in Numerical Methods in Engineering*, 22(4):301–318, 2006. doi:<https://doi.org/10.1002/cnm.815>. URL <https://onlinelibrary.wiley.com/doi/abs/10.1002/cnm.815>.
- [61] J. B. Lawrie and I. D. Abrahams. A brief historical perspective of the wiener–hopf technique. *Journal of Engineering Mathematics*, 59(4):351–358, 2007.
- [62] P. Livasov and G. Mishuris. Numerical factorization of a matrix-function with exponential factors in an anti-plane problem for a crack with process zone. *Philosophical Transactions of the Royal Society A: Mathematical, Physical and Engineering Sciences*, 377(2156):20190109, 2019. doi:[10.1098/rsta.2019.0109](https://doi.org/10.1098/rsta.2019.0109). URL <https://royalsocietypublishing.org/doi/abs/10.1098/rsta.2019.0109>.

- [63] S. G. Llewellyn Smith and E. Luca. Numerical solution of scattering problems using a Riemann–Hilbert formulation. *Proc. Roy. Soc. A*, 475:20190105, 2019. doi:[10.1098/rspa.2019.0105](https://doi.org/10.1098/rspa.2019.0105).
- [64] D. Lüthi, M. Le Floch, B. Bereiter, T. Blunier, J.-M. Barnola, U. Siegenthaler, D. Raynaud, J. Jouzel, H. Fischer, K. Kawamura, et al. High-resolution carbon dioxide concentration record 650,000–800,000 years before present. *nature*, 453(7193):379–382, 2008.
- [65] P. Meijers. The contact problem of a rigid cylinder on an elastic layer. *Applied Scientific Research*, 18(1):353–383, 1968.
- [66] R. D. Mindlin. Compliance of elastic bodies in contact. *J. Appl. Mech.*, 16, 1949.
- [67] J. J. Minton and E. J. Brambley. Meta-analysis of curvature trends in asymmetric rolling. *Procedia Engng*, 207:1355–1360, 2017. doi:doi.org/10.1016/j.proeng.2017.10.896. (presented at ICTP 2017).
- [68] J. J. Minton, C. J. Cawthorn, and E. J. Brambley. An asymptotic approach to asymmetric rolling. *Int. J. Mech. Sci.*, 113:36–48, 2016. doi:[10.1016/j.ijmecsci.2016.03.024](https://doi.org/10.1016/j.ijmecsci.2016.03.024).
- [69] J. F. Mitchell. The “greenhouse” effect and climate change. *Reviews of Geophysics*, 27(1):115–139, 1989.
- [70] V. Mossakovskii. Compression of elastic bodies under conditions of adhesion (axisymmetric case). *Journal of Applied Mathematics and Mechanics*, 27(3):630 – 643, 1963. ISSN 0021-8928. doi:[10.1016/0021-8928\(63\)90150-3](https://doi.org/10.1016/0021-8928(63)90150-3). URL <http://www.sciencedirect.com/science/article/pii/0021892863901503>.
- [71] O. Music and J. M. Allwood. Flexible asymmetric spinning. *CIRP Annals*, 60(1):319 – 322, 2011. ISSN 0007-8506. doi:[10.1016/j.cirp.2011.03.136](https://doi.org/10.1016/j.cirp.2011.03.136). URL <http://www.sciencedirect.com/science/article/pii/S0007850611001375>.

- [72] O. Music, J. Allwood, and K. Kawai. A review of the mechanics of metal spinning. *Journal of Materials Processing Technology*, 210(1):3 – 23, 2010. ISSN 0924-0136. doi:[10.1016/j.jmatprotec.2009.08.021](https://doi.org/10.1016/j.jmatprotec.2009.08.021). URL <http://www.sciencedirect.com/science/article/pii/S0924013609003094>.
- [73] N. Muskhelishvili. *Singular integral equations: boundary problems of function theory and their application to mathematical physics*.
- [74] B. Noble. *Methods Based on the Wiener–Hopf Technique for the Solution of Partial Differential Equations*. AMS Chelsea Publishing Series. Pergamon Press, 1958. URL <https://books.google.co.uk/books?id=RvNQAAAAMAAJ>.
- [75] S. Olver. Computing the Hilbert transform and its inverse. *Mathematics of computation*, 80(275):1745–1767, 2011.
- [76] T. C. O’Sullivan and R. B. King. Sliding Contact Stress Field Due to a Spherical Indenter on a Layered Elastic Half-Space. *Journal of Tribology*, 110(2):235–240, 04 1988. ISSN 0742-4787. doi:[10.1115/1.3261591](https://doi.org/10.1115/1.3261591). URL [10.1115/1.3261591](https://doi.org/10.1115/1.3261591).
- [77] J. M. Papakonstantinou and R. A. Tapia. Origin and evolution of the secant method in one dimension. *The American Mathematical Monthly*, 120(6):500–517, 2013. doi:[10.4169/amer.math.monthly.120.06.500](https://doi.org/10.4169/amer.math.monthly.120.06.500). URL <https://www.tandfonline.com/doi/abs/10.4169/amer.math.monthly.120.06.500>.
- [78] B. N. J. Persson and E. Tosatti. *Physics of sliding friction*. 1996.
- [79] J. A. Polyblank and J. M. Allwood. Parametric toolpath design in metal spinning. *CIRP Annals*, 64(1):301 – 304, 2015. ISSN 0007-8506. doi:[10.1016/j.cirp.2015.04.077](https://doi.org/10.1016/j.cirp.2015.04.077). URL <http://www.sciencedirect.com/science/article/pii/S0007850615000852>.
- [80] V. L. Popov. *Coulomb’s Law of Friction*, pages 133–154. Springer Berlin Heidelberg, Berlin, Heidelberg, 2010. ISBN 978-3-642-10803-

7. doi:[10.1007/978-3-642-10803-7_10](https://doi.org/10.1007/978-3-642-10803-7_10). URL [10.1007/978-3-642-10803-7_10](https://doi.org/10.1007/978-3-642-10803-7_10).
- [81] M. J. Priddin, A. V. Kisil, and L. J. Ayton. Applying an iterative method numerically to solve $n \times n$ matrix Wiener–Hopf equations with exponential factors. *Philosophical Transactions of the Royal Society A*, 378(2162):20190241, 2020.
- [82] B. Rentsch, N. Manopulo, and P. Hora. On the role of anisotropy and bauschinger-effect in sheet metal spinning. *Journal of Physics: Conference Series*, 896:012042, sep 2017. doi:[10.1088/1742-6596/896/1/012042](https://doi.org/10.1088/1742-6596/896/1/012042). URL <https://doi.org/10.1088/1742-6596/896/1/012042>.
- [83] O. Reynolds. On rolling-friction. *Philosophical Transactions of the Royal Society of London*, 166:155–174, 1876. ISSN 02610523. URL <http://www.jstor.org/stable/109190>.
- [84] D. J. K. F. S. e. a. Rogelj, J.; Shindell. *Chapter 2: Mitigation Pathways Compatible with 1.5°C in the Context of Sustainable Development*. Intergovernmental Panel on Climate Change, 2018. URL https://www.ipcc.ch/site/assets/uploads/sites/2/2019/05/SR15_Chapter2_High_Res.pdf.
- [85] S. Rogosin and G. Mishuris. Constructive methods for factorization of matrix-functions. *IMA Journal of Applied Mathematics*, 81(2):365–391, 2016.
- [86] S. Rogosin and L. Primachuk. Factorization of triangular matrix-functions of an arbitrary order. 2018.
- [87] A. C. Serrenho, Z. S. Mourão, J. Norman, J. M. Cullen, and J. M. Allwood. The influence of uk emissions reduction targets on the emissions of the global steel industry. *Resources, Conservation and Recycling*, 107:174–184, 2016. ISSN 0921-3449. doi:<https://doi.org/10.1016/j.resconrec.2016.01.001>. URL <https://www.sciencedirect.com/science/article/pii/S0921344916300015>.

- [88] R. M. Slevinsky and S. Olver. A fast and well-conditioned spectral method for singular integral equations. *Journal of Computational Physics*, 332:290–315, 2017.
- [89] A. Sommerfeld. *Mathematische Theorie der Diffraction*. B.G. Teubner, 1896. URL <https://books.google.co.uk/books?id=pDxtHQAACAAJ>.
- [90] D. Spence. Self similar solutions to adhesive contact problems with incremental loading. *Proc. R. Soc. Lond. A*, 305(1480):55–80, 1968.
- [91] K. K. Stelter, P. Thompson, J. M. Tutill, and P. Gray. Stick-slip vibrations and chaos. *Philosophical Transactions of the Royal Society of London. Series A: Physical and Engineering Sciences*, 332(1624):89–105, 1990. doi:10.1098/rsta.1990.0102. URL <https://royalsocietypublishing.org/doi/abs/10.1098/rsta.1990.0102>.
- [92] J. J. Thomsen and A. Fidlin. Analytical approximations for stick–slip vibration amplitudes. *International Journal of Non-Linear Mechanics*, 38(3):389–403, 2003. ISSN 0020-7462. doi:[https://doi.org/10.1016/S0020-7462\(01\)00073-7](https://doi.org/10.1016/S0020-7462(01)00073-7). URL <https://www.sciencedirect.com/science/article/pii/S0020746201000737>.
- [93] L. Trefethen. *Approximation Theory and Approximation Practice*. Other Titles in Applied Mathematics. SIAM, 2013. ISBN 9781611972405. URL <https://books.google.co.uk/books?id=h80N5JHm-u4C>.
- [94] T. Trogdon. Rational approximation, oscillatory Cauchy integrals, and Fourier transforms. *Constructive Approximation*, 43(1):71–101, 2016.
- [95] T. Trogdon and S. Olver. *Riemann–Hilbert problems, their numerical solution, and the computation of nonlinear special functions*, volume 146. Siam, 2015.
- [96] B. H. Veitch and I. David Abrahams. On the commutative factorization of $n \times n$ matrix wiener-hopf kernels with distinct eigenvalues. *Proceedings of the Royal Society A: Mathematical, Physical and Engineering*

- Sciences*, 463(2078):613–639, 2007. doi:[10.1098/rspa.2006.1780](https://doi.org/10.1098/rspa.2006.1780). URL <https://royalsocietypublishing.org/doi/abs/10.1098/rspa.2006.1780>.
- [97] Z.-J. Wang, W.-Z. Wang, H. Wang, D. Zhu, and Y.-Z. Hu. Partial Slip Contact Analysis on Three-Dimensional Elastic Layered Half Space. *Journal of Tribology*, 132(2), 03 2010. ISSN 0742-4787. doi:[10.1115/1.4001011](https://doi.org/10.1115/1.4001011). URL [10.1115/1.4001011](https://doi.org/10.1115/1.4001011). 021403.
- [98] G. H. Wannier. *Statistical physics*. Courier Corporation, 1987.
- [99] N. Wiener. Über eine klasse singularer integralgleichungen. *Sitz. Ber. Preuss. Akad. Wiss., Phys.-Math.*, 1:696–706, 1931.
- [100] H. Yoshizawa and J. Israelachvili. Fundamental mechanisms of interfacial friction. 2. stick-slip friction of spherical and chain molecules. *The Journal of Physical Chemistry*, 97(43):11300–11313, 1993. doi:[10.1021/j100145a031](https://doi.org/10.1021/j100145a031). URL <https://doi.org/10.1021/j100145a031>.
- [101] O. Zhupanska. Adhesive full stick contact of a rigid cylinder with an elastic half-space. *International Journal of Engineering Science*, 55:54 – 65, 2012. ISSN 0020-7225. doi:[10.1016/j.ijengsci.2012.02.002](https://doi.org/10.1016/j.ijengsci.2012.02.002). URL <http://www.sciencedirect.com/science/article/pii/S0020722512000328>.
- [102] O. Zhupanska and A. Ulitko. Contact with friction of a rigid cylinder with an elastic half-space. *Journal of the Mechanics and Physics of Solids*, 53(5):975 – 999, 2005. ISSN 0022-5096. doi:[10.1016/j.jmps.2005.01.002](https://doi.org/10.1016/j.jmps.2005.01.002). URL <http://www.sciencedirect.com/science/article/pii/S0022509605000177>.
- [103] O. I. Zhupanska. On the analytical approach to galin’s stick-slip problem. a survey. *Journal of Elasticity*, 90:315–333, 2008.